Faculty of Science and Engineering
Department of Petroleum Engineering

Elastic and Elastoplastic Finite Element Simulations of Injection into Porous Reservoirs

Amin Chamani

This thesis is presented for the Degree of
Doctor of Philosophy
of
Curtin University

July 2013

Declaration

'To the best of my knowledge and belief this thesis contains no material previously published by any other person except where due acknowledgement has been made. This thesis contains no material which has been accepted for the award of any other degree or diploma in any university.'

Amin Chamani

Abstract

Underground gas injection has attracted remarkable attention for natural gas storage and carbon dioxide (CO_2) geologic sequestration applications. Injection of natural gas into depleted hydrocarbon reservoirs is the most popular storage method. CO_2 geologic sequestration plays a vital role in alleviating global warming and climate change issues related to the significant release of CO_2 as one of the major greenhouse gases produced from the combustion of fossil fuels.

The injection of gas into underground geologic formations builds up the fluid pore pressure, which changes the effective stress, i.e. the stress applied to the rock skeleton. The deformation due to change of stresses could result in various geomechanics related issues across the reservoir interval and over/under burden rocks such as fault or fracture reactivation, collapse of casings, wellbore instabilities and ground uplift. To simulate injection of gas into porous formations and investigate subsequent stress induced events finite element (FE) modelling has been used in the past. This numerical method is suitable for continuum media, similar to porous formations considered for injections.

In this study a three-dimensional (3D) finite element program was developed for simulations of gas injection into a porous medium. Both isotropic linear elastic and elasto-plastic behaviours (including von Mises, Mohr-Coulomb and Drucker-Prager yield criteria) were assumed for geomaterials. The program applies isoparametric formulation using 3D 8-noded hexahedron elements and supports different types of loading including those due to body (gravity) force and tractions on outer boundary. The effective stress concept and Biot's theory were integrated in the fundamental formulations in order to account for the gas injection modelling.

The developed code was applied to model some typical elastic examples for which analytical solutions exist: this allowed validation of the program. Thereafter several simulations of porous formations carried out to study the injection induced stress and displacements within the injection zone and surrounding formations with horizontal and curved structures. The results indicated the change in the state of stress regime due to injection and its variation at different locations in a non-horizontal structure.

The results of elasto-plastic models were also validated against some simple cases with known responses. The model then applied to simulate the development of

plastic zone around a porous formation due to gas injection. The results of sensitivity analysis showed how the plastic zone expands when the formation exhibits less strength properties, i.e. cohesion.

The 3D FE program was finally applied to study a real case in which injection into a sandstone formation was studied. The stress and displacements before and after injection were estimated considering both isotropic linear elastic and elasto-plastic behaviours for the formation. This allowed estimation of ground uplift and the development of the plastic zone around the injection area.

Published papers from this research thesis

Chamani, A., and Rasouli, V., 2013. Wellbore associated problems due to gas injection into non-horizontal structures, Journal of Mining & Environment.

Chamani, A., and Rasouli, V., 2011. A 3D numerical study on Geomechanical response of a structural reservoir due to gas injection, GeoProc2011, July 6-9, Perth, Western Australia

Chamani, A., and Rasouli, V., 2011. Simulation of depletion-induced surface subsidence in a coal seam, The 3rd Asia Pacific Coalbed Methane Symposium, APCBM 2011, May 3-6, Brisbane, Australia

Chamani, A., and Rasouli, V., 2011. 3D numerical simulation of injection into a porous natural gas storage, Australian Petroleum Production Exploration Association Limited, APPEA Journal 2011

Acknowledgments

I would like to express my gratitude to all those who help and support me during this research.

Firstly, I would like to acknowledge the Department of Petroleum Engineering for providing me with the Curtin International Postgraduate Research Scholarship (CIPRS) which was a great financial support towards my studied.

I am greatly indebted to my supervisor, Associate Professor Vamegh Rasouli, for his instructions at every step during this research, and also for his valuable comments on the final draft of the thesis.

I would like to offer my gratitude to Professor Vahid Lotfi who introduced me to the interesting concepts of finite element method and gave me many hints in this subject and Dr Seyed Youssef Ahmady-Broghani who shared with me his knowledge in the area of continuum mechanics.

I express my thanks to my close friends, Mr. Ahmadreza Younessi and Mr. Seyed Hasan Fallahzadeh for their support during my PhD studies.

I wish to express my great appreciation to my family for their valuable help and support especially during my research abroad.

To the memory of Professor Zienkiewicz

Contents

Page

Chapter 6 Conclusions and recommendations

List of Figures

Page

List of Tables

Page

1 Geomechanics simulation of porous reservoirs

1.1 Introduction

Since 1990's a revolution emerged with regards to the impact of geomechanical behavior of the reservoir formation or/and its surrounding media (e.g. overburden, sideburden and underburden) when studying producing reservoirs. The main reason for such a need in a reservoir engineering study is the fact that numerous hydrocarbon reservoirs locate in challenging geological environments (Fredrich and Fossum, 2002). Reservoir formations with high porosity and low degree of consolidation (e.g. poorly consolidated sands) or formations of poor geomechanical condition (e.g. evaporates with low strength) or formation with proved time-dependent behavior (such as creeping salt bed and shale) are good instances of these challenging environments. Such miscellany problematic aspects lead in expensive experiences and events during the course of reservoir production including well casing collapse, remarkable change of porosity and permeability of the reservoir formations, reactivation of preexisting sliding planes such as fractures at different scales, surface movements and subsidence. These and other similar incidences have been repeatedly reported in major hydrocarbon fields all around the globe (Ekofisk, South Belridge, Groningen, Bolivar Coast, Inglewood, Wilmington and Valhalla) in a wide spectrum of rocks like as highly porous chalk and sandstones with different degrees of consolidation and creeping media (Ruddy et al., 1988; Smlts and Waal, 1988; Waal and Smlts, 1988; Chase and Dietrich, 1989; Abdulraheem et al., 1994; Eiksund et al., 1995; Hansen et al., 1995; Dudley et al., 1998; Rhett, 1998; Schutjens et al., 1998; Fredrich et al., 2000; Hettema et al., 2000).

At any point inside a porous formation the total stress is taken by the rock skeleton and the fluid inside the pores. The stress applied to the rock grains is known as the effective stress, whereas the portion taken by fluid equals the pore pressure. According to this if the pore pressure changes the portion of the total stress field

sustained by the solid skeleton will change. For example, inside a producing porous reservoir during the depletion phase where the reservoir fluid pressure decreases the solid skeleton experiences more compression. Contrary to this during the course of injection, when the fluid pressure builds up, the solid skeleton compression inside the reservoir horizon decreases. This indicates the need for simultaneous consideration of fluid flow and rock responses.

During the last two decades numerous approaches have been proposed for studying this concept. The main difference between the proposed approaches is with respect to the degree of coupling which basically governs the mathematical difficulty and computational costs involved in each method (David and Ravalec-dupin, 2007). These methods cover a spectrum from uni-directional coupling algorithm at one end to fully coupled algorithm at another end while the more accepted loose coupling (or partially coupled) algorithm exists somewhere between the two extremes (Minkoff et al., 2003). While the fully coupled algorithm is the most comprehensive mathematically developed approach, the other two approaches has gained more attractions because of their simplicity, less mathematical complexity and computational costs. However, in this Chapter it will be shown that in some especial conditions the fully coupled nature of the governing equations describing the fluid flow and geomechanical behavior of formation can be decoupled and this will highly increase the validity of uni-directional and loosely coupled approaches. In these types of analysis the governing equations of fluid flow and geoemchanical behavior are handled separately with different simulators and at certain time lags the results are exchanged. As an example, the fluid flow simulator is used to determine the fluid pressure field throughout the reservoir and the given pressure is used as an input data in the geomechanical simulator. The interested readers may refer to Settari and Mourits (1998) and Settari and Walters (2001), and Minkoff et al. (2003) for further studying this concept. Settari and Mourits (1998) used the partially coupled algorithm in order to simultaneously combine the results of three different analysis of two-dimensional reservoir simulator, three-dimensional stress simulator (geomechanical model) and two-dimensional fracture simulator in a cyclic steam injection scenario. In the geomechanical simulator they considered the linear elastic behavior and hyperbolic elastic behavior for geometerials. Fredrich et al. (2000) used the uni-directional approach and input the pore pressure field determined by three-dimensional fluid flow simulator (Black oil version of MORE®) in a nonlinear

geomechanical simulator (JAS3D quasi-static finite element code of Sandia National Laboratories). The main goal of their study was the verification of the effect of production and injection induced stress changes on casing damages in Belridge diatomite field, California. They considered the plastic behavior based on Drucker-Prager cap model for geomaterials and pore pressure was an independent input load in the geomechanical simulator. Settari and Walters (2001) developed the study initiated by Settari and Mourits (1998) in order to consider the nonlinear plastic constitutive model of the geomaterial based on Drucker-Prager cap plasticity model to study the effect of compaction during production and used the algorithm of loose coupling to investigate the geomechanical response of the reservoir horizon and surrounding media during the period of 20 years in a gas field where the depletion resulted in decreasing gas pore pressure from 3400 psi to 1800 psi. They also considered the thermal effects by some formulation from thermoporoelasticity. In another sophisticated study, Minkoff et al. (2004) combined the fluid flow simulator (IPARS which was developed at Texas University) and a geomechanical simulator (JAS3D) in a loosely coupled approach. They used fluid flow simulator to determine the pressure field and applied this pore pressure field in the geomechanical simulator. They determined the changes in porosity and permeability based on the geomechanical simulator results using two empirical relationships and then updated these parameters in the reservoir simulator on a continuous basis. The field of their study is the same as that of Fredrich et al. (2000).

While a more comprehensive literature review about different simulation methods will be given in Chapter 2, the above examples indicate the importance of geomechanical simulations of porous reservoirs and the need to expand the knowledge in different areas of reservoir geomechanics. The stresses and displacement changes due to injection into a porous reservoir is one of the specific areas which has attracted a large attention within the past decades. This is due to the need for gas injection into depleted reservoirs for storage purposes as well as carbon dioxide geologic sequestration. The subsequent section will expand on this subject, as this is the research topic of this Thesis.

1.2 Injection-induced stress analysis

During the last decades a growing dependency of countries on natural gas as a source of energy has taken place in both domestic consumers and infrastructure. Natural gas has some especial features that enhance the need of available storage for it in parallel to its direct production or import. At first, there are remarkable seasonal and even daily fluctuations in its demand. During the winter it reaches the peak of annual demand and also even during the 24 hours period its consumption experiences remarkable change mostly depended on the temperature fluctuation. Secondly, due to some dangerous potential of entering air into the pipelines it needs a stable continuity of supply. Finally, in many countries the gas producing hubs are far from the major gas consumer zones and considering relatively slow transport of the gas inside the pipeline accentuate the need of natural gas storage locally near the consumers' zones rather than countless regulating the production in order to maintain the supply-demand balance (Havard and French, 2009). There are three main types of natural gas storage: storage in depleted hydrocarbon reservoirs, storage in aquifers and storage in leached salt caverns. However, short terms gas storage are also needed in coal seam gas (CSG) projects where the CSG is fed into the LNG plant, for example the Galilee basin in Queensland, Australia (Holland et al., 2008). Also, limited cases are available where storage in caverns made of hard rocks are reported. Plaat (2009) presented a comprehensive review on different types of natural gas storage and outlined their advantages and disadvantages. According to Table 1.1 storage in depleted hydrocarbon reservoirs is the most popular storage type worldwide currently.

Table 1.1 Existing worldwide underground gas storage facilities (after Plaat, 2009)

Area	Number of underground gas storage facilities			
	Depleted oil/gas fields	**Aquifers**	**Salt caverns**	**Other**
Europe	68	23	29	3
Former Soviet Union	36	13	1	----
USA	318	45	26	1
Canada	45	----	9	----
South America	2	----	----	----
Asia	5	----	----	----
Australia	4	----	----	----
Total	478	81	65	4

The history of underground gas storage activities goes back to the storage operation in a depleted gas reservoir in Welland County, Ontario (Canada) in 1915 (Evans, 2009). Afterward until the 1950s almost all gas storage activities were undertaken in the depleted gas reservoirs and currently nearly 81.6 % of all worldwide activities are in depleted hydrocarbon reservoirs (Davidson, 2009). The majority of the past storage cases are in depleted gas fields instead of depleted oil fields (Davidson, 2009).

The main goal of this study is to address the geomechanical features of injection into a depleted reservoir for natural gas storage purposes or carbon dioxide geologic sequestration.

In this study a three-dimenional finite element (FE) numerical code has been developed to study the changes in stresses and displacements in a complete isotropic elastic as well as elasto-plastic media due to gas injection into porous reservoirs. The numerical code was used to simulate the injection-induced stresses and displacements in a hypothetical reservoir with an embedded porous formation. Finally the developed three-dimensional finite element programs were used to investigate the geomechanical effects of underground carbon dioxide sequestration in a real case considering both linear elastic and elasto-plastic behaviours of formations.

Therefore the main focus in terms of simulations would be on equations which include the effect of the structure of the body as well as pore pressure: these equations will be presented in the next section. To develop the equations, we assume a constant fluid pressure field inside the storage space and then do the structural analysis of the effects and influences of injection into the reservoir as well as the surrounding formations. For situations where the assumption of constant pressure for fluid is not a valid or a close approximation, the fluid pressure field can be simulated and determined using conventional reservoir simulators and is used by this FE structural simulator. The decoupled nature of the corresponding equations supports the authenticity and validity of such a decoupled routine. The following section presents the governing equations of two-phase porous media where the effect of pore pressure (i.e. the fluid effect) is integrated in structural analysis of the formation.

1.3 Two-phase porous media

The subject of solid skeleton deformation associated with pore fluid motion is of vital importance in many branches of engineering such as soil mechanics (e.g. earthquake and consolidation problems), petroleum engineering (e.g. coupled porous reservoir analysis), and biomechanics (e.g. fluid circulating through bones) (Zienkiewicz and Shiomi, 1984). Such studies concern the interaction between pore fluid and solid skeleton which can be described in its simplest form as effective stress concept where

$$\dot{\sigma}_{ij} = \dot{\sigma}''_{ij} - \alpha\delta_{ij}\dot{p} \tag{1.1}$$

In this equation $\dot{\sigma}_{ij}$ is the rate of total Cauchy stress tensor, $\dot{\sigma}''_{ij}$ is that part of the rate of total stress tensor which is responsible for all deformation of solid skeleton, δ_{ij} is the Kronecker delta, $\dot{p}$ is the rate of pore fluid pressure, and α is Biot's constant of the porous media which is defined as:

$$\alpha = 1 - \frac{\delta_{ij} D_{ijkl} \delta_{kl}}{3K_s} \tag{1.2}$$

In which D_{ijkl} is the tangential stiffness matrix of the bulk solid skeleton, and K_s is the average bulk modulus of the solid grains. In above equation α is close to unity for soil-like material whereas for rock-like material it may reduce as low as 0.5. When $\alpha = 1.0$, $\dot{\sigma}''_{ij}$ becomes the rate of so-called effective stress tensor which is conventionally referred to in soil mechanics (Zienkiewicz and Shiomi, 1984).

The incremental form of equation (1.1) can be presented as:

$$d\sigma_{ij} = d\sigma''_{ij} - \alpha\delta_{ij}dp \tag{1.3}$$

In addition we may consider the matrix notation form of the above equation which is more convenient in finite element discussion. This is written as:

$$d\sigma = d\sigma'' - \alpha m dp \tag{1.4}$$

Due to the symmetric characteristic of stress and strain tensors, we can use the contract form of stress and strain tensor and then m can be defined as:

$$m^T = \begin{pmatrix} 1 & 1 & 1 & 0 & 0 & 0 \end{pmatrix} \tag{1.5}$$

The problem of equilibrium state of a two-phase porous media consisting of solid skeleton phase and fluid phase that occupies the pores was comprehensively

discussed by Zienkiewicz (1982). He concluded that the motion and deformation of both phases in fully dynamic analysis can be described by six sets of equations as:

$$d\varepsilon = Ldu \tag{1.6-a}$$

$$d\sigma = Dd\varepsilon - \alpha m dp \tag{1.6-b}$$

$$d\theta = \alpha m^T d\varepsilon + \frac{1}{Q} dp \tag{1.6-c}$$

$$L^T \sigma + \rho b = \rho \ddot{u} + \rho_f \ddot{w} \tag{1.6-d}$$

$$-\nabla p + \rho_f b = \rho_f \ddot{u} + \rho_f \frac{\ddot{w}}{n} + \rho_f \frac{b}{K} \dot{w} \tag{1.6-e}$$

$$\nabla^T \dot{w} + \dot{\theta} = 0 \tag{1.6-f}$$

In the above equations:

ε : strain matrix,

L : Linear strain operator for small strain theory,

u : displacements field of solid skeleton phase,

D : tangential stiffness matrix,

θ : fluid volume stored per unit volume of solid skeleton phase,

Q : a constant related to Biot's constant, fluid compressibility, solid grains compressibility and porosity,

b : body forces per unit mass of the solid skeleton,

w : relative displacements field of fluid with respect to solid phase,

p : fluid pressure filed,

ρ_f : density of the fluid,

n : porosity,

K : permeability coefficient for isotropic porous media,

∇ : divergence operator vector as $\left(\partial/\partial x \quad \partial/\partial y \quad \partial/\partial z\right)^T$

In fact equations (1.6-a) to (1.6-f) describe respectively the "strain-displacement equation, effective stress equation, storability change due to change of stress field, dynamic equilibrium equation of porous media, dynamic equilibrium equation of fluid phase alone, and finally fluid inflow to the storage" (Zienkiewicz, 1982). A complete solution of a deforming porous media with moving fluids can be obtained by solving simultaneously all equations (1.6-a) to (1.6-f) throughout the space and

time domains considering the particular boundary and initial conditions of an especial case; however, there are some cases where these sets of simultaneous equations are reduced to simpler forms. As an instance, if the motion of the solid skeleton is too small then all dynamic terms carrying dynamic forces in these equations can be discarded. As another example, if the relative displacement of fluids with respect to solid skeleton is too small we can ignore all terms having the derivatives of w with respect to time since in such case the velocity and acceleration of fluid particles are negligible. Such assumptions and approximations are not very far from the reality. The former is a very good assumption for the case of consolidating porous media especially in the field of civil and petroleum engineering since the velocity of deformation is negligible in particular in long term consideration. The latter case complies with the fluid flow throughout porous media with low permeability (Zienkiewicz, 1982).

Zienkiewicz (1982) discussed comprehensively all possible assumptions and approximates for equation (1.6) regarding engineering applications. He also showed that the set of equations (1.6) in drained static condition with slow consolidation (such as production from a reservoir) can be decomposed or decoupled into four major sets of equations as below:

$$-\nabla^T\left(\frac{K}{\rho g}\right)\nabla p+\nabla^T\left(\frac{K}{\rho g}\right)\rho_f b=0 \tag{1.7-a}$$

$$d\sigma = Dd\varepsilon - \alpha m dp \tag{1.7-b}$$

$$L^T\sigma+\rho b=0 \tag{1.7-c}$$

$$d\varepsilon = Ldu \tag{1.7-d}$$

Here, the first equation describes the well-known three-dimensional Darcy flow equation. The last three equations in (1.7) describe the effective stress concept, the static equilibrium equation, and strain-displacement relationship of a continuum, respectively. Because of the decoupled nature of these equations the first equation can be modeled or solved independently from the other three equations in order to obtain the fluid pressure field. Afterwards, the pressure field can be accounted for through equation (1.7-b) and three equations (1.7-b) to (1.7-d) can be solved simultaneously by using an appropriate method. Solving these three equations is a routine process in a standard finite element analysis considering their continuum

nature. The only difference with conventional finite element analysis of structures is the role of effective stress rather than total stress which is taken into account through equation (1.7-b).

1.4 Objectives of this thesis

Based on the statement of the problem briefly addressed in the previous sections the objectives of this Thesis can be summarized as follows:

- Present a comprehensive review of literature to state the past and latest developments in geomechanical simulations of porous reservoirs.

- State the strength and shortcoming of different geomechanical numerical modeling methods, hence present the most appropriate method to simulate the gas injection into porous reservoirs.

- Develop a three-dimensional finite element code in order to simulate gas injection into porous reservoir. The developed code includes isotropic linear elastic analysis as in many situations rocks exhibit elastic behavior. Development of this program which was fully written using FORTRAN language program required an extensive effort but having access to the source code and being able to make any changes for sensitivity analysis of different parameters is the major advantage over using available commercial software.

- Develop the 3D finite element code to capture the elasto-plastic behavior of geomaterial. This is because in many situations rocks exhibit elasto-plastic behavior.

- Validate the results of the developed codes by comparing the results in some simple cases for which analytical solutions exist or the results are known.

- Apply the developed simulator to analyse the effect of gas injection into porous reservoir; at initial stages for hypothetical underground structures and then for a real case of carbon dioxide geologic sequestration in a porous reservoir. This includes simulations of stresses and displacements in reservoir and surrounding rocks, expansion of formations and corresponding uplift effects and development of the plastic zone due to gas injection.

1.5 Significance of this thesis

Reservoir related geomechanics studies have gained intense attention during the last few decades. Numerical simulations are the main approach that has been used for analysis of producing reservoirs and to study the response of a porous formation after injection of gas. The major focus of this Thesis is to study the effect of gas injection into porous media. Based on the discussions presented in the previous section this Thesis is distinguished from other similar work in several ways.

- Despite the significant geomechanical effects of gas injection into a porous formation, this subject has not been adequately studied in the past and there are many areas of potential research exist for further studies. This study initiated considering the lack of enough knowledge in this subject and the results presented in this Thesis will demonstrate the contribution of this study to this important topic.

- Amongst available studies in the area of gas injection into porous formations only a few consider, in particular, the geomechanics of the problem but the main focus is on the reservoir aspects of the gas injection from production point of view. In this study, however, through coupling analysis the concept of effective stress is fully integrated into the formulations and therefore the effect of both aspects is considered simultaneously.

- A comprehensive simulation of gas injection into a porous reservoir requires changing various rock and fluid parameters as well as using yield criteria suitable for formations. Practically, this is not always possible using commercial software as there is no access to the program source code. As a result, and for the purpose of this research a 3D finite element code was developed using FORTRAN language program. The code accounts for both linear elastic and elasto-plastic behaviors for geomaterials. Also, a strong meshing algorithm capable of considering appropriate mesh shape has been developed to perform accurate simulations. The post-processing programming developed in this study allows presenting the output results of simulations. Having access to the source of the code allows any desired change to be made for comparison purposes. The code has been developed in specific to account for applications in oil and gas

industry, in particular for injection into a porous media. This is a clear advantage over existing codes.

- The case studies presented in this Thesis refer to the most practical problems encountered in real field. This is hoped that by reading these examples the importance of geomechanics studies before any injection operation is adequately highlighted. In linear elastic part these include simulation of injection into both horizontal and curved (i.e. an anticline structure) porous reservoir to study the stress field changes, induced deformation field. The results indicate how curved structures result in higher shear induced stresses at the flank.

- In elasto-plastic analysis three well-known constitutive models of von Mises, Drucker-prager and Mohr-Coulomb were considered in order to investigate the development of plastic zone due to injection into porous reservoirs.

- The validity of the developed 3D finite element code was extensively assessed. Only few of these validation examples are presented in this Thesis which shows the accuracy of the results for cases where closed form solutions are available or the model response is well known.

- The 3D FE program was finally applied to study a real potential site for carbon dioxide geologic sequestration. The results of numerical simulation for both isotropic linear elastic and elasto-plastic behaviours of the injected formation were discussed and analysed qualitatively and quantitatively before and after injection for stresses and displacements fields. This data can be used for any related geomechanical studies such as potential for casing collapse in the overburden zone or pre-existing fracture reactivation or cap rock integrity due to gas injection.

1.6 Thesis structure

According to the objectives of this research study which was discussed in Section 1.4 the Thesis structured in six Chapters. A brief review of the Chapters is given below.

In Chapter 2 at first the concept of production-induced effective stress is introduced and discussed. Then the concept of stress-dependency of fluid flow is explained and it is discussed how the production results in reservoir and surrounding

structures to deform and the stress fields to change. Then geomechanics-reservoir coupling algorithms are introduced and it is explained how the loosely coupled algorithm has some advantages over the fully coupled algorithm. Afterward, the concept of constitutive models is introduced and it is demonstrated how it is important in solving classical solid deformation problems. This part is divided into the introduction of elasticity theory and plasticity theory. Then an introduction into numerical methods is given and the advantages of finite element method over other numerical methods for solving continuous problems are discussed. Finally several examples of reservoir geomechanics problems are presented.

In Chapter 3 the features of the developed 3D FE code in this research are presented with a main focus on linear elastic analysis. This is followed by a brief discussion about elasticity theory problems and finite element discretization of an elastic domain and structure. Then several simple case studies for validating the developed 3D FE code results are presented. The first example is related to injection into horizontal porous reservoir and the concepts of stress changes and deformation due to gas injection inside the reservoir as well as surrounding structures. The problem of injection into curved structure (anticline) which is a common structure in the hydrocarbon fields is the next example. Therefore the effect of formation curvature is studied and the results are compared against horizontal layers. Production from a coal layer in coal bed methane (CBM) is the last example presented, which allows comparing the depletion scenario against injection into a formation which is the main topic of this study.

The concept of elasto-plastic behaviour of geomaterials is covered in Chapter 4. At the beginning of this Chapter a brief introduction to mathematical theory of plasticity is given. Then the simulation results are presented for several simple examples for validation purposes. Finally the code is used to investigate the development of plastic zone inside and around the gas injected zone of porous reservoir.

In Chapter 5 the 3D FE program was applied to study a real potential site for carbon dioxide geologic sequestration. The model input including formation mechanical properties were obtained from a log-based analysis. The results of this study, based on the given data, indicated that no considerable plastic zone is expected to develop due to the injection program into the selected potential formation. Also, the amount of expected ground uplift due to gas injection is not significant. The

results also provide various profiles and patterns of stresses and displacements before and after injection.

In Chapter 6 the main concluding remarks of this Thesis are outlined and topics for further research as a continuation of this work are recommended.

A list of all references used in this research is provided at the end of the Thesis.

Figure 1.1 shows the Thesis structure.

Chapter 1 Geomechanics simulation of porous reservoirs

- A brief review on the geomechanical simulation of porous reservoir.
- Describing the objectives and significance of the current study.
- Presenting the layout of the Thesis.

Chapter 2 Numerical simulations in reservoir geomechanics

- A comprehensive discussion on the production-induced effective stresses and coupling algorithms.
- A brief introduction to the rock constitutive models including theories of elasticity and plasticity.
- Example applications.

Chapter 3 Isotropic linear elastic finite element simulations

- Discuss the features of the developed 3D finite element code.
- Introduction to linear finite element discritization.
- Validation examples to verify the correctness of the developed 3D finite element code, isotropic linear elastic behaviour.
- Presenting case study results of gas injection.

Chapter 4 Elasto-plastic finite element simulations

- Introduction to the mathematical theory of plasticity.
- Validation examples to verify the correctness of the developed 3D finite element code, elasto-plastic behaviour.
- Presenting case study results of gas injection.

Chapter 5 Case Study: Analysis of injection into a porous sandstone reservoir

- Presenting case study results of CO_2 injection using the 3D FE code for isotropic linear elastic behaviour of the formations.
- Presenting case study results of CO_2 injection using the 3D FE code for elasto-plastic behaviour of the formations.

Chapter 6 Conclusions and recommendations

References

Figure 1.1 Thesis structure

2 Numerical simulations in reservoir geomechanics

A review of the literature in reservoir engineering within the past few decades reveals the importance of the gomechanical studies as a core part of field development plan and engineering design. The applications of geomechanics are multi-fold and apply during the whole life of the field. Within the context of this research, i.e. the injection induced geomechanical phenomena; in this Chapter we discuss briefly some of the geomechanics related aspects which are fundamentals for further model developments in the next Chapters.

2.1 Production-induced effective stresses

Let's consider an element of a porous formation, i.e. a reservoir rock. Two distinct parts could be distinguished in this element: the rock solid skeleton and the void space which is generally filled with the reservoir fluids (i.e. water, oil and/or gas). At the studied depth this rock element is subjected to stresses due to the weight of overlying layers. The geomechanical equilibrium state requires this total stress to be carried by both rock solid skeleton and fluids phase inside the pore spaces. The portion of stress which is sustained by rock solid skeleton phase is referred to as the effective stress. Mathematically this can be written as (Lewis and Scherefler, 1998):

$$\sigma_{ij}^{effective} = \sigma_{ij} - \delta_{ij}\left(S_w p^w + S_o p^o + S_g p^g\right) \tag{2.1}$$

where $\sigma_{ij}^{effective}$ is the effective stress tensor, σ_{ij} is the total stress tensor applied to the rock element, δ_{ij} is Kronecker Delta, S_w, S_o, S_g are saturation degree of water, oil, and gas, respectively, and p^w, p^o, p^g are the fluid pressure of water, oil, and gas, respectively. In case of one fluid phase (e.g. only oil) or assuming an average fluid phase pressure for different fluids Equation (2.1) will be simplified as

$$\sigma_{ij}^{effective} = \sigma_{ij} - \delta_{ij} p^{fluid} \tag{2.2}$$

Equations 2.1 and 2.2 form the fundamental mathematical description for Biot's theory and the effective stress concept (Lewis and Scherefler, 1998).

Inside any rock element of the reservoir the total stresses, which is resulted from the regional structural geology and plate tectonic conditions, is almost constant during the production life of a reservoir; however, the effective stress is not constant but in general is expected to increase due to production or locally decrease due to injection into a reservoir, for example for storage purposes. This production-induced effective stresses fluctuations cause some important collateral effects such as reservoir rock compaction, deformation in the overburden and sideburden, rock structure yielding and time-independent or time-dependent post-yield deformation, ground subsidence, casing collapse and pre-existing fault reactivation. All of these consequences have been repeatedly reported in major hydrocarbon fields all around the globe (e.g. Ekofisk, South Belridge, Groningen, Bolivar Coast, Ingelwood, Wilmington and Vallhal) in a wide spectrum of rocks such as chalk and well-consolidated, poorly-consolidated, and unconsolidated sandstones (Ruddy et al., 1988; Smlts & Waal, 1988; Waal & Smlts, 1988; Chase & Dietrich, 1989; Abdulraheem et al., 1994; Eiksund et al., 1995; Hansen et al., 1995; Dudley et al., 1998; Rhett, 1998; Schutjens et al., 1998; Fredrich et al., 2000; Hettema et al., 2000).

2.2 Stress dependency of fluid flow

Based upon equation 2.2, fluid pore pressure decreases during production phase resulting in an increase in effective stress, i.e. the stress applied to the solid skeleton of rock element. This will cause compaction of the solid skeleton which corresponds to reduced formation porosity and permeability: this will result in hydrocarbon being pushed out from the pore spaces which enhances the production. This type of compaction is one of the main production mechanisms in most poorly compacted reservoirs like unconsolidated sandstones. As an instance, in the Bachaquero reservoir, Venezuela, half of the production is due to reservoir compaction (David & Ravalec-Dupin, 2007). It is to be noted that an opposite case is during injection process as a means for production enhancement, for natural gas storage in depleted reservoirs, or for CO_2 geologic sequestration purposes the pore pressure will increase.

The change in effective stress also results in rock deformation not only in the reservoir interval but also within the overburden and sideburden horizons. This is

called elastic deformation when it is recoverable whereas referred to as plastic flow if it is irrecoverable. The most eminent effects of such production-induced deformation are ground subsidence and casing deformation or collapse in particular within the overburden sections: such incidences have been reported in many occasions in major hydrocarbon reservoirs around the world (Chan, 2004). The relationship between effective stress and deformation fields is described comprehensively through the concept of constitutive equations and models which will be discussed in more details in Section 2.4.

The above discussion indicates that during production phase while fluid flows within the reservoir interval, various geomechanics related events (e.g. effective stress changes, rock deformation, yield and post-yield flow) occur to the rocks in both reservoir and surrounding media (i.e. overburden and sideburdens). To consider both of these effects simultaneously a coupled multi-physics analysis would be required (Longuemare et al., 2002). Different algorithms have been introduced and discussed in the literature for such coupled analysis accounting for simultaneous effect of two or more different physical attributes and mechanisms. In the next section a brief overview of different algorithms used for coupled analysis of geomechanics related problems in reservoir engineering will be given.

2.3 Coupled algorithms

Independent and dependent (coupled) methods are the two approaches which can be used when studying a multi-physics mechanism, here the interrelationship between fluid flow and geomechanical parameters of a reservoir. In the first method there are two independent sets of partial differential equations (PDE) describing the geomechanical behaviour of rock solid skeleton and flow of reservoir fluids, respectively. However, in a coupled fluid flow-geomechanical analysis of a reservoir these two sets of differential equations will be connected somehow in order to describe the interaction or interrelationship between the two components. We discussed briefly, in the last section, the qualitative interaction between fluid flow and geomechanical responses of a porous formation.

Different coupled algorithms have been introduced since late 1990s in the reservoir related literature which forms a wide spectrum from one-way coupled algorithm in one end to fully coupled algorithm to the other end. Loosely or partially coupled algorithms are those considered within this spectrum (Minkoff et al., 2003).

These types of coupling algorithms have been classified based upon the different level of coupling.

One-way coupled analysis of a reservoir is based on the analysis of governing differential equations for geomechanical behaviour and fluid flow independently in separate simulators. However, the results of one of these analyses will be exported as the input data into the second simulator. The exported data could be the initial state or boundary conditions. This method is called one-way coupled analysis as no feedback data is provided to the first simulator in a reverse way. As an example, modelling fluid flow within the reservoir interval during depletion using conventional reservoir simulators will result in estimation of pore pressure. The pore pressure data can be sent as input data to a geomechanical simulator to study the effects of pore pressure changes on geomechanical behaviour of formations (e.g. stresses, strains and deformations fields). As is seen in this one-way coupled example, the changes in porosity and permeability due to compaction of solid skeleton will not be sent back to the reservoir simulator for any updates for the remaining time of the analysis (Minkoff et al., 2003).

The fully coupling analysis serves the highest coupling level in which the governing partial differential equations of the reservoir including fluid flow and geomechanical behaviour are formed and developed together from the beginning. The end product of this algorithm is one set of partial differential equations which describes the fluid flow and geomechanical governing equations as well as the interaction between them simultaneously. Thus one simulator calculates the fluid flow and geomechanical parameters at each step of its solution. Despite the inherent advantages of using one package for coupled analysis as is served using this method, it is subjected to some disadvantages. Firstly, there is a considerable mathematical complexity in developing partial differential equations which integrate two different mechanisms (i.e. fluid flow and geomechanics) and also takes into account their interaction. This intrinsic complexity resulted in applying simplified assumptions and to analyse only simple cases, for example, considering linear elastic behaviour for solid skeleton or one phase fluid flow. Secondly, in fully coupled analysis the coupled solution is given for each single point over the entire space: this is a computationally expensive and time consuming practice while is unnecessary in many cases (Settari & Walters, 2001). For example, the fluid flow equations are not needed to be solved for points outside the reservoir interval.

The loosely coupled analysis has a coupling level of between the two extreme cases of on-way and fully coupled algorithm and has attracted a large attention during the last decade. In this algorithm the governing partial differential equations of fluid flow and geomechanical behaviour are analysed separately (similar to one-way coupling method) but in a dependent manner. The results of each analysis, i.e. geomechanics or fluid flow, will be sent, as part of the input information, to the other one in a two-way interconnected approach. This algorithm is found to be more advantageous than the two other methods: it is less expensive in terms of computational effort and time than fully coupled model but uses a two-way method to make the connection between the two sets. As an example of the partially coupled algorithm, we can consider the fluid flow through the reservoir interval which can be modelled using a reservoir simulator to determine pore pressure field data corresponding to a certain period of time during production. This information will then be sent to an advanced geomechanical simulator where parameters related to geomechanical behaviour (e.g. compaction and changes of porosity and permeability) are subjected to the production induced stress changes. The results now are fed back into the reservoir simulator to update the values of porosity and permeability (Minkoff et al., 2003).

The above discussions demonstrate the advantages of using partially coupled over one-way or fully coupled algorithms. In particular having two individual simulators for fluid flow and geomechanical analysis is more appropriate for studying complicated problems for example multi-phase fluid flow or advanced constitutive models such as elasto-plastic and time-dependent constitutive models for rock deformation. In addition, the independency of the two simulators allows developing models suitable for different intervals, for example, a fluid flow model for the reservoir interval with an extended geomechanical model for the entire interval under study (Settari & Mourits, 1998).

2.4 Rock constitutive models

According to three-dimensional continuum solid mechanics, there are fifteen unknowns to be determined in any loaded solids: these include three displacements, six strain, and six stress components (Chapter 3). On the other hand, three equilibrium and six compatibility equations define equilibrium state and continuous deformation of a body which are known as field equations. Therefore having just

nine independent equations and fifteen independent unknowns, there should be some more six equations in order to fully and individually solve the equations system corresponding to an individual and defined loaded solid structure.

It is to be noted that the physical properties of the solid are not included in the above mentioned equations (Obert and Duvall, 1967). This would be considered through the constitutive models (equations or relations), which in the case of a loaded solid is the constitutive stress-strain models. These constitutive stress-strain models generally depend on the current state of stress and strain, strain rate, stress history, material properties, and temperature which are the main concerns of elasticity and plasticity theories.

2.4.1 Elasticity theory

A simpler constitutive model is obtained when the effect of stress history and strain rate is ignored: this forms the fundamental of elasticity theory. Therefore in the elasticity theory stress will be mainly a function of strain, material properties, and temperature. An elastic solid will completely recover its original shape and state when removing the entire applied loads. A rather simpler elastic model will be shaped if the stress-strain relations are assumed to be linear which is called a *linear elastic* model (Sadd, 2005).

The linear relationship between Cauchy stress tensor and strain tensor can be expressed easily in tensorial notation in a three-dimensional, 3D, space as

$$\sigma_{ij} = C_{ijkl}\,\varepsilon_{kl} \tag{2.3}$$

where C_{ijkl} is the fourth-order elasticity tensor whose 81 components describe the entire material contribution in the deformations and stresses. Because of the symmetric characteristic of the stress and strain tensors it is simply concluded that 36 components are to be independent. In addition, considering the concept of strain energy from hyper-elasticity domain it is easily proven that C_{ijkl} is symmetric and hence the total independent components will be reduced to 21. It should be mentioned that equation 2.3 with these 21 independent material properties describes the linear elastic model for a completely anisotropic material. The more isotropic the material the smaller the number of independent components will be. In another word, it can be shown that for a monoclinic material (with one symmetry plane), orthotropic material (with three perpendicular symmetry planes), transversely

isotropic material (with invariant elastic potential with respect to rotation angle in a plane), and finally the complete isotropic material (being directionally independent) the elasticity tensor has 13, 9, 5, and 2 independent components, respectively (Cristescu, 1989).

For a complete isotropic material, as mentioned above, the number of independent components in C_{ijkl} reduces to only 2 material properties. This leads in equation 2.3 being simplified as

$$\sigma_{ij} = \lambda \varepsilon_{kk} \delta_{ij} + 2\mu \varepsilon_{ij} \tag{2.4}$$

in which λ and μ are Lame constants. Equation 2.4 is called generalized Hook's law for linear isotropic solid (Landau & Lifshitz, 1970).

It will be discussed later on that the stress-strain relations corresponding to most of materials especially different rock types in engineering applications are more complex than that of explained using linear elastic model. However, this simple model is widely used and the main reasons for this include:

- considerable simplicity in the mathematical development based upon this model,
- provides a good approximation in the first instance on the structure behaviour, and
- the ability in expanding this model to develop more complicated constitutive models such as elasto-plastic and visco-elastic model(Cristescu, 1989).

The concept of linear elasticity theory will be discussed in further details in Chapter 3.

2.4.2 Plasticity theory

If the applied load exceeds a threshold, in some engineering solid materials (such as rocks, soils, clays, concrete, and metals) a permanent deformations is sustained upon removal of the load. This *permanent* deformation is called *plastic* deformation. Studying plastic deformation when the material is assumed to deform independent of the *rate* of loading is the subject of the *rate-independent* (or *time-independent*) *plasticity theory*, which is traditionally referred to as simply “plasticity theory”. The *viscoplasticity theory* studies the material’s deformations when the deformation is load rate dependent.

Different engineering materials show different qualitative mechanical responses under loading but they have some *phenomenological* aspects in common. A wide range of mechanical responses may be expected for a material undergoing plastic deformations due to loading. However, *elastic domain*, *plastic flow*, and *hardening*, are the three important phenomenological properties to be considered: these will be discussed in Chapter 4.

During uniaxial loading, the material sustains plastic deformation when the uniaxial load exceeds a critical value known as *yield* stress. Any applied stress below the onset of *plastic flow* and lower than the yield stress will cause elastic and recoverable deformation. A permanent or plastic deformation remains in the material if the stress is above the uniaxial yield stress. The boundary between purely elastic and *elasto-plastic* deformations in a general three-dimensional stress space is defined through the concept of *yield criterion* also known as *yield function* or *yield surface*. In the general stress space the yield function, $F(\sigma_{ij}, \mathbf{A}) = 0$, is a function of current stress tensor, σ_{ij}, and a set of hardening thermodynamical forces, $\mathbf{A}$; hence it forms generally a hyper surface in the multidimensional stress space (Neto et. al, 2008).

Various yield criteria has been introduced in the literature with a wide range of applications. Some of these criteria are appropriate for applications in materials such as metals whereas others have been developed for geomaterials (rocks and soils). Comprehensive mathematical and phenomenological discussions are given in the context of plasticity theory in terms of advantages and disadvantages as well as applicability of one or class of yield criteria for a particular material or class of materials. The most commonly used yield criteria for the engineering applications are traditionally called *classical yield criteria* or *von Mises-type yield criteria*. This is subdivided into *von Mises*, *Tresca*, *Drucker-Prager*, and *Mohr-Coulomb* criteria. The first two criteria are more suitable for pressure-insensitive materials such as metals whereas the latter two criteria are more applicable for pressure-sensitive materials such as rocks and soils (Neto et. al, 2008).

There are also other yield criteria (e.g. modified Cam-clay, Capped Drucker-Perager) which consider some other important properties of the material. Due to the complex nature of these criteria they are used for especial materials and for specific application purposes (Besson et al., 2010).

After the onset of yielding the deformation will be partly elastic and partly plastic and therefore any *increment* in total strain field could be decomposed into two separate parts which can be written mathematically as:

$$d\varepsilon_{ij} = (d\varepsilon_{ij})^{elastic} + (d\varepsilon_{ij})^{plastic} \tag{2.5}$$

The elastic part of deformation can be calculated from equation 2.3. For the plastic flow it is assumed that the plastic strain increment is determined using *plastic potential* Q as:

$$(d\varepsilon_{ij})^{plastic} = d\lambda \frac{\partial Q}{\partial \sigma_{ij}} \tag{2.6}$$

where $d\lambda$, the *plastic multiplier*, is a material-dependent constant. The above equation is referred to as *flow rule* (Owen & Hinton, 1980).

Experimental results strongly suggest that the elastic domain boundary, or yield stress, depends on the degree of the plastic flow that the material has experienced during its loading history. Generally but not essentially, the more the plastic flow the larger the yield stress will be. Therefore this concept is termed *hardening* and it is one of the most important and mathematically complicated concepts in the theory of plasticity. There are four main classes of hardening rules: these are *perfect plasticity*, *isotropic hardening*, *kinematic hardening* and *mixed* (or *hybrid*) *hardening* (Yu, 2006). These classes describe different ways of changing the yield hyper surface in the multidimensional stress space after yielding and more importantly during the cyclic loading and unloading. The first hardening rule is more relevant for brittle failure in geomaterials which is happening commonly during nearly uniaxial loading conditions. The isotropic hardening uses some simpler mathematics in identifying the yield hyper surface. The first two rules are more frequently quoted for geomechanics applications. The third hardening rule was introduced by Prager (1955) and developed further by Ziegler (1959) in order to account for the Bauschinger effect. This also involves complicated mathematical calculations. The mixed hardening rule is the most complicated one amongst the four rules but integrates the benefits associated with the isotropic and kinematic hardening rules.

Reviewing the literature related to the time or rate-dependent behaviour of geomaterials, it is observed that non porous formations mainly observed in mining and civil engineering applications and porous formations representing most of petroleum reservoirs rocks are studied with special focus. In addition, fundamental

studies have been carried out with respect to the constitutive behaviour of the geomaterial to understand the microphysical phenomena of irreversible deformation of different rocks such as salt (Langer, 1979; Vogler & Blum, 1990; Senseny et al., 1992; Hunsche & Humpel 1999), chalk (Longuemare et al., 2002; Cristescu, 1997) and sandstone (He et al., 2002; Hagin, 2003).

Although the early studies carried out in mining and civil engineering assumed rock as an elastic body (Obert and Duvall, 1967), by the advent and considerable development of the plasticity (Hill, 1950) and viscoplasticity theory (Perzyna, 1967) during the 1950s and 1960s mostly for metals, these concepts were gradually introduced to geomechanics applications. This resulted in foundation of first studies of elasto-plastic behaviour of rock-like materials (Dreyer, 1973; Rice 1975) and soil-rock materials (Schofield & Wroth, 1968). Further attempts were made since then to introduce a more appropriate multidimensional constitutive elasto/viscoplastic models for wide range of rocks with respect to geomechanics applications (Cristescu, 1997). As an example, lab experiments on small scale reservoir rock elements were performed to show the nonlinear irreversible behaviour (plastic, viscoplastic, and creep) of porous reservoir rocks such as sandstones with different level of consolidation (Waal & Smlts, 1988; Baud & Meredith, 1997; Schtjens et al., 1998; Chang & Zoback, 1998; Hettema et al., 1998; Dudley et al., 1998; Hettema et al., 2000; Hagin & Zoback, 2007), chalk (Johnson et al., 1988; Ruddy et al., 1989; Frantziskonis & Abdulraheem, 1992; Rhett, 1998; Collin et al., 2002; Xie & Shoo, 2006), limestone (Hamilton & Shafer, 1991, Coelho et al., 2006), and Shale (Chang & Zoback, 2008; Chang & Zoback, 2009; Chang & Zoback, 2010). Investigating the elasto-plastic behaviour of producing formations at field-scale geomechanical models was further advancement made by other researchers (Smlts & Waal, 1988; Chase & Dietrich, 1989; Abdulraheem et al., 1994; Chin et al., 1994; Hansen et al., 1995; Eiksund et al., 1995; Fredrich et al., 2000; Settari & Walters, 2001; Fredrich & Fossum, 2002; Longuemare et al., 2002; Yale, 2002; Minkoff et al., 2003; Minkoff et al., 2004).

Despite several evidence suggesting time-dependent behaviour (elasto/viscoplastic) of reservoir rocks, for example the lab results mentioned above, time-dependent modelling in reservoir geomechanics applications is not fully developed and requires further research.

2.5 FEM versus other numerical methods

In order to solve any *physical problem* in engineering a *mathematical model* should be built which generally consists of a *set of partial differential equations* (PDE). Within the context of this research work, let's consider a general problem of finding the stress, strain, and deformation fields for an isotropic linear elastic body extended in the space domain Ω with certain boundary conditions applied on its outer boundary, $\partial\Omega$. As mentioned earlier, according to the elasticity theory the stress, strain, and displacement fields are determined using following four major sets of differential equations:

$$\varepsilon_{ij} = (u_{i,j} + u_{j,i})/2 \qquad \text{(six strain-displacement relations)} \qquad (2.7)$$

$$\varepsilon_{ij,kl} + \varepsilon_{kl,ij} - \varepsilon_{ik,jl} - \varepsilon_{jl,ik} = 0 \qquad \text{(six Saint Venant compatibility equations)} \qquad (2.8)$$

$$\sigma_{ij,j} + F_i = 0 \qquad \text{(three equilibrium equations)} \qquad (2.9)$$

$$\sigma_{ij} = \lambda\varepsilon_{kk}\delta_{ij} + 2\mu\varepsilon_{ij} \qquad \text{(six generalized Hooke's law equations)} \qquad (2.10)$$

In above equations, u_i, $F_i, \sigma_{ij}, \varepsilon_{ij}$ are displacement, body force, stress and strain fields, respectively and "," in the subscript implies that the derivative operator as well as the repeated index rule is regarded. There are generally two different types of boundary condition: known loads applied on some part of the outer boundary ($\partial\Omega_L$), and certain displacements applied over the remaining part of the outer boundary ($\partial\Omega_D$). In mathematical sense we have:

$$\partial\Omega_L \cup \partial\Omega_D \equiv \partial\Omega \qquad (2.11)$$

It can be easily realised that obtaining an analytical solution, even for the simple physical problem, is not straightforward. However, in real applications in rock engineering the materials are far more complex: they may have different boundary conditions, be inhomogenous, behave nonlinearly (e.g. elasto-plastic or elasto-viscoplastic) or have certain damage behaviour. Numerical modelling is a strong tool which can be used to find a close approximate answer to the above physical problems. Indeed, the more robust and reliable the mathematical models, the closer the approximation will be. A *comprehensive* mathematical model that is *effective* and *reliable* is generally achieved through the use of a fully non-linear three-dimensional model (Bathe, 1996).

When a physical problem is described by a mathematical model, i.e. a set of partial differential equations, it is defined completely over its entire spatial domain at each single point. Such system is called *continuous* and is formed based on mathematical fiction of infinitesimal and consists of infinite number of points. The answer to such continuous system is found using exact mathematical manipulation. If in this type of problems the answer is defined by only finite number of components it is called a *discrete* problem. The response of a discrete system can be determined following the standard computational procedures. This indicates how we may find an *approximate* answer in a continuous domain (for which obtaining an analytical solution is impractical) by dividing it into finite number of components or *elements* in order to transform it into a discrete system, for which the answer can be found easily through standard computational procedures. This consists of undertaking three main steps. Firstly, the domain and the continuous problem should be divided into finite number of elements whose behaviour can be easily described and understood. Secondly, mathematical model is assigned to each individual element to describe its behaviour. Finally, the behaviour of the structure is rebuilt using the *assemblage* of elements behaviour. It is clear that the more the number of elements or the finer the size of the elements the better and more precise the approximation of the real responses of the structure will be (Zienkiewics & Taylor, 2000). Because the second type of analysis is done using standard computational procedures and indeed by remarkable aid of digital computers, it is called *numerical modelling* or *computational method* in contrast with traditional analytical methods of mathematical modelling.

In order to establish the reasons for why finite element method has been chosen as the numerical and computational method in this study a brief introduction to other numerical methods is given below which allows highlighting the advantages of finite element method over other numerical methods in this research.

Based on the discretisation procedures and the mathematical treatment of the discretised system several numerical techniques were introduced during the second half of the last century. With respect to the structural problems of solid materials these techniques can be classified into two major groups: numerical models for continuous media (e.g. reservoir formation with no major discontinuity such as joints or faults) and discontinuous media (e.g. a rock mass divided into blocks by faults or a fractured reservoir). It is well established that the concept of continuity and

discontinuity of solids is not absolute but relative and scale-dependent. In current study the structure of the reservoir formation is assumed as continuum which may consist of different materials, i.e. different rock layers. The inclusion of any discontinuity into the model is the next step which adds significant complications to the numerical calculations.For a continuous media finite difference method (FDM), boundary element method (BEM), and finite element method (FEM) are the three major numerical techniques being used. FDM is the oldest numerical method for PDEs approximation and is based on the direct discretisation of the partial differential equations. However, the basic FDM is not flexible in its applications for problems including heterogeneity and complex boundary conditions. This is while most of rock engineering related problems are as such. BEM treats a PDE by only discretising the boundary in contrast to FDM and FEM and therefore it is much more effective in terms of computational costs. However, it is based on rather more complicated mathematical manipulations and of course it is not suitable for problems with nonlinearity (such as plasticity and viscoplasticity) and inhomogeniety. BEM is an ideal approach to be used for linearly elastic problems especially in dynamic analysis and modelling far-field domains. FEM, however, is the most commonly used and popular numerical technique in different engineering applications including rock engineering. Its capability and flexibility in treating material inhomogeniety and nonlinearity together with large amount of mathematical development in FEM, which has been of interest to both mathematicians and engineers, has made this numerical method as being the first choice amongst different numerical models in most science and engineering disciplines (Becker, 1992; Zienkiewics & Taylor, 2000). In addition to this, it is important to note that modelling material nonlinearity of elasto-plastic and elasto-viscoplastic behaviour were carried out by FEM initially (Cyr & Teter, 1973; Zienkiewicz & Cormeau, 1974; Cormeau, 1975; Pande at al., 1977; Kanchi et al., 1978; Hughes & Taylor, 1980; Owen & Hinton, 1980).

As a result of the above discussion in current Thesis we have chosen FEM for numerical modelling of nonlinear behaviour of the reservoir formations. The development of the program based on the FEM and its functionalities will be explained in detail in the next Chapters.

2.6 Example applications of reservoir geomechanics

Fluid injection operation has been done through the decades for many purposes such as increasing oil production, storing fluid especially gas underground, CO_2 geologic sequestration, decreasing land subsidence due to remarkable production (Teatini et al., 2010). Fluid injection causes land uplift from millimetres to several centimetres. According to Teatini et al. (2010) the amount and speed of land uplift is depending on geological structure, quantity and distribution of fluid, pore pressure and hydro-geomechanical properties of the injected horizon. Injection used widely from 1950s and according to U.S. Environmental Protection Agency there were 400,000 injection wells just in the United State in 2002 (Teatini et al., 2010). Teatini et al. (2010) also report several case studies from different type of injection.

During the last three decades, reservoir geomechanics drew a remarkable attention especially in the field of coupled analysis of conventional reservoir simulation and geomechanical consideration. In this section we review papers in this field with emphasize on the field-scale geomechanical simulation of reservoirs.

Minkoff et al. (2003) described comprehensively the advantages and disadvantages of fully coupled, loosely coupled and one-way coupled methods between fluid flow and geomechanical set of equations. Despite the perfectness of fully coupled models, they stated that it is extremely hard to set up the set of simultaneous equations for multiphase flow and nonlinear geomechanical behaviour. On the other hand the one-way coupled method does not possess this perfectness of simultaneous solution of fluid flow and geomechanical set of equations but it makes easier to use advanced and sophisticated fluid flow and geomechanical codes to handle the problem. This allows capturing features in advanced problems such as multiphase fluid flow or nonlinear elasto-plastic behaviour of geomaterials. They explained that the loosely coupled method, in between the other two way of coupling, enhances the capability of one-way coupling method since it allows the updated data transfer between two simulators in order to increase the degree of coupling of the solution. On the other side, the loosely coupled method permits the use of highly progressed and advanced simulators since they run independently. The algorithm of loosely coupling method was shown in Figure 2.1.

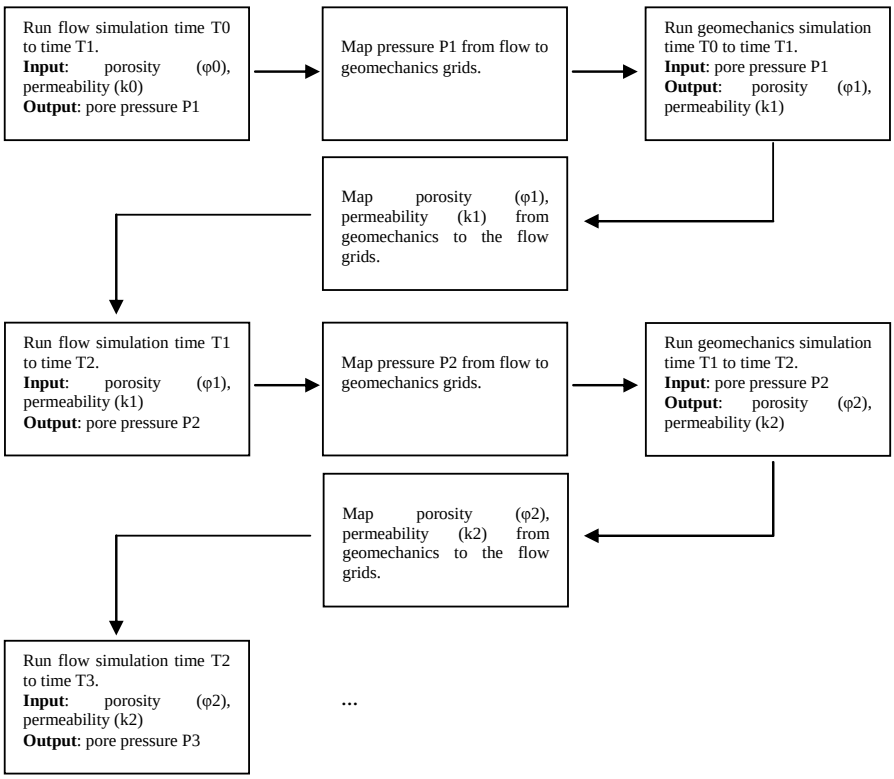

Figure 2.1 The algorithm of loosely coupling method (after Minkoff et al., 2003)

Using the loosely coupled method they coupled two advanced simulators of IPARS as a reservoir simulator, which is capable of handling multiphase flow and faults and JAS3D, an advanced geomechanical simulator, which handles nonlinear complicated constitutive models for geomaterials. In these coupled programs pore pressure is determined using the reservoir simulator and it is applied as an external load to the geomechanical simulator. After some iterations in time reservoir properties (i.e. porosity and permeability) are updated using newly determined stress, strain and displacement fields. Using this approach Minkoff et al. (2003) simulated a single layer of Belridge field, California, where the initial oil in place is estimated at 500 Mm^3. The field contains two reservoirs; one in Tulare sand and another in diatomite layer. The Tulare sand is shallow reservoir but the diatomite reservoir has the extension of about 305 m in depth and is deeper than Tulare sand. The diatomite reservoir has high porosity (40%-70%) but low permeability (0.1 mD), which required the use of hydraulic fracturing to produce economically. In their modelling they focused on the one layer of diatomite reservoir at a depth of 361 m with the initial pore pressure of 3.76 MPa. Their model extends 106 m in *x* and *y* direction and 44 m in *z* direction. The modified Sandler-Rubin cap plasticity constitutive

model was used for the geomaterial behaviour. At the four corners of the model there were four wells. They compared the simulations of flow separately and using loosely coupled between IPARS/JAS3D after five years of production. Their results showed that using the IPARS itself the reservoir pressure changes 40% after five years of production whereas this increases to 50% for the coupled simulation. After five years of production the surface subsidence was calculated to be 0.15 m. Also coupled simulation revealed that the permeability decreased from 0.1 mD to 0.001 mD. The contours of porosity at the end of 25-year of production was shown in Figure 2.2. The production wells are located in front of the model whereas the injection wells are located in the back.

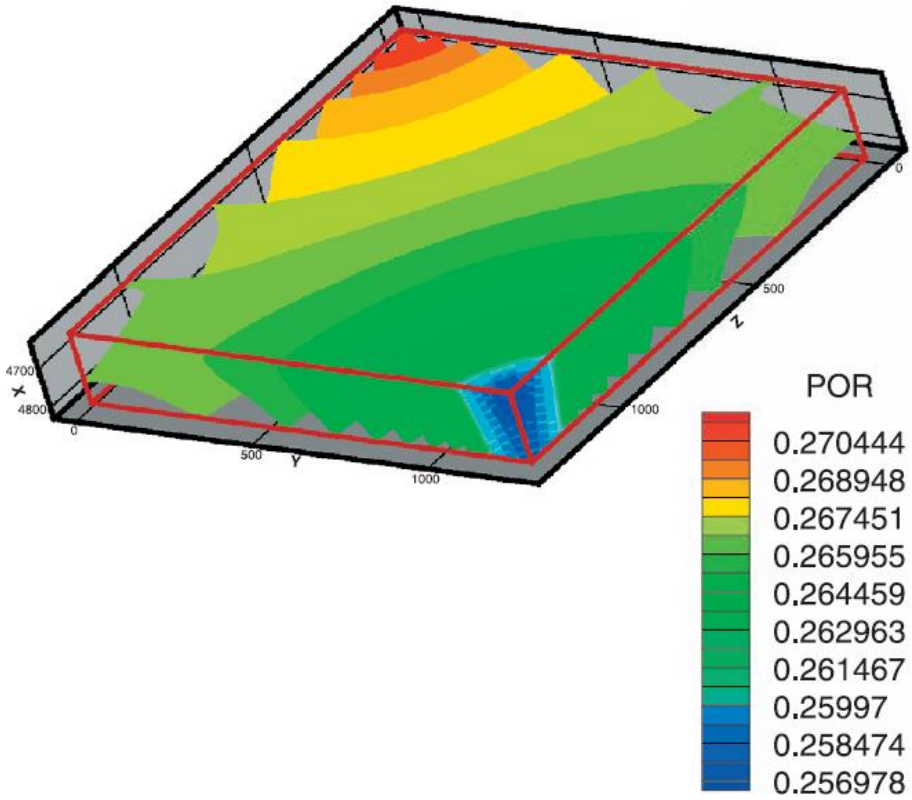

Figure 2.2 Contour plot of porosity for 25-year production (after Minkoff et al., 2003). The initial porosity was 30 %.

Longuemare et al. (2002) discuss the three different type of coupling between reservoir simulator and geomechanical simulator. They selected partially coupling and coupled reservoir simulator ATHOS developed at IFP and geomechanical simulator VISAGE (Figure 2.3). They described reservoir simulator calculate pore pressure, temperature and saturation. These pieces of information are sent to the geomechanical simulator which computes stress and strain fields. These pieces of

information are used to update permeability tensor in each grid cell for the next time step of reservoir simulation. They used this partially coupled procedure to investigate five years production of a limestone reservoir in Middle East. Their investigation shows some faults reach critical state depending on stress and temperature and experienced strain localization.

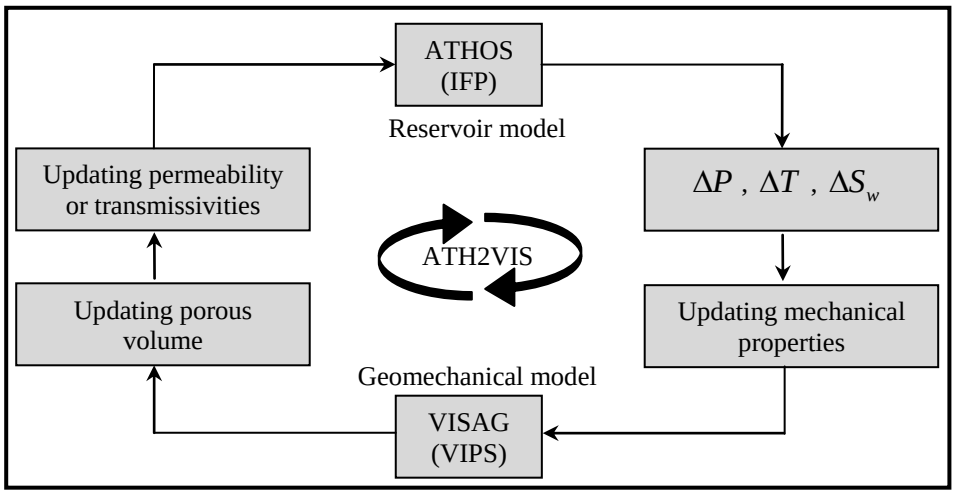

Figure 2.3 Coupling between reservoir and geomechanical simulators (after Longuemare et al., 2002)

In their work the reservoir simulation only consist of reservoir part whereas the geomechanical simulation includes overburden, sideburdens and underburden (Figure 2.4).

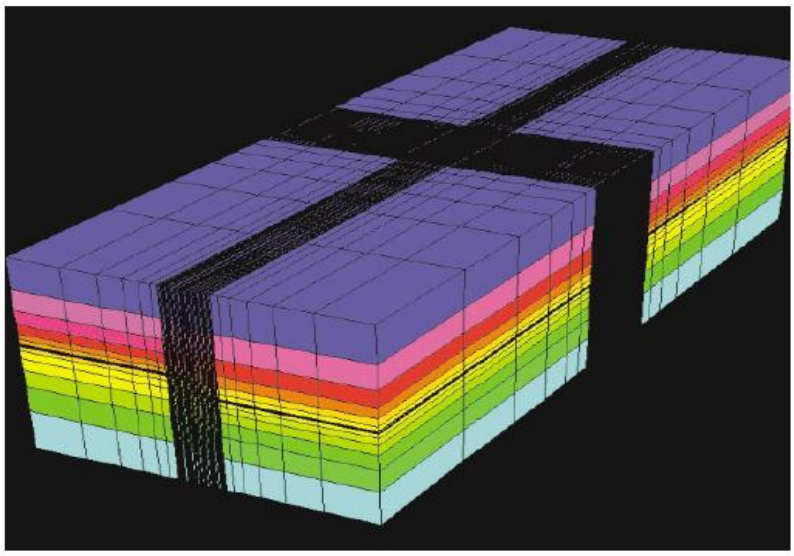

Figure 2.4 Geomechanical model of partially coupled simulation including reservoir, sideburdens, overburden, underburden (after Longuemare et al., 2002)

Settari and Mourits (1998) express the advantages of partially coupled algorithm as researcher can use separated and sophisticated simulators. They discussed the limitations exist in three different field of reservoir simulation, stress models, and fracture propagation models (Figure 2.5).

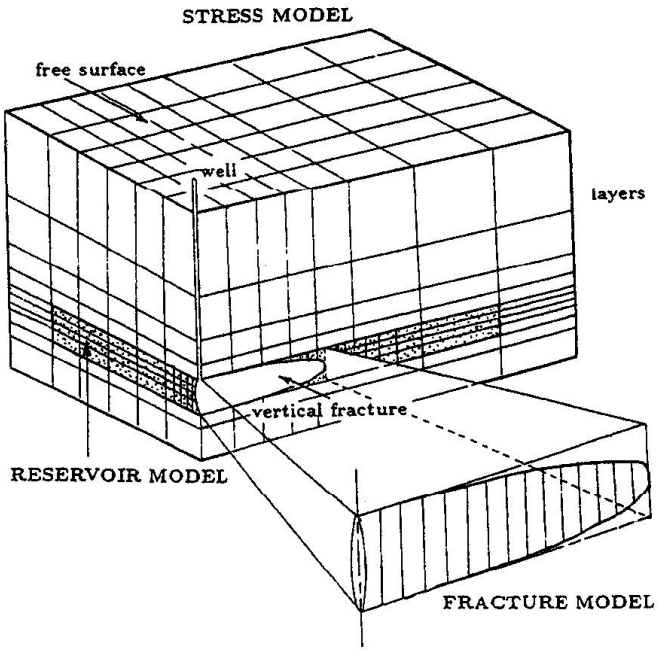

Figure 2.5 Three area of reservoir, stress and fracture models (after Settari and Mourits, 1998)

They developed the formulation for volume coupling between reservoir model and stress model (Figure 2.6).

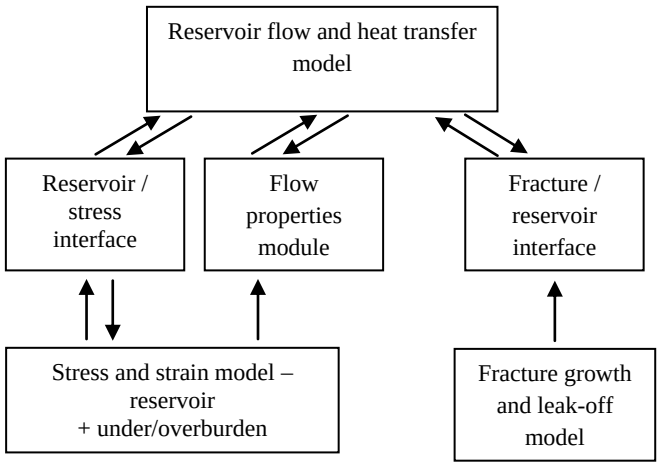

Figure 2.6 Schematic of coupling algorithm (after Settari and Mourits, 1998)

Their model is iterative and they express in spite of iterative algorithm “it satisfies the simultaneous system of stress and flow equations upon convergence”. They develop their work as six step algorithm of iteration but limited their development just to linear elasticity and nonlinear elasticity. Finally they provided three different examples in order to show the difference between coupled and uncoupled modelling.

Settari and Walters (2001) extended the previous work of Settari and Mourits (1998). At first they described the coupling process based on finite-element setting between reservoir and geomechanical equations. Then they expressed for compaction analysis elasto-plastic model necessary and used Drucker-Prager with cap hardening plasticity model (Figure 2.7) and nonlinear elastic constitutive equation but they believed elasto-plastic constitutive equation is preferable since nonlinear elastic model cannot capture post yield phenomena of rock. However, they believe by using elastic nonlinear model hardening of the material can be captured. They also discussed the effect of temperature on compaction and thermoporoelasticity.

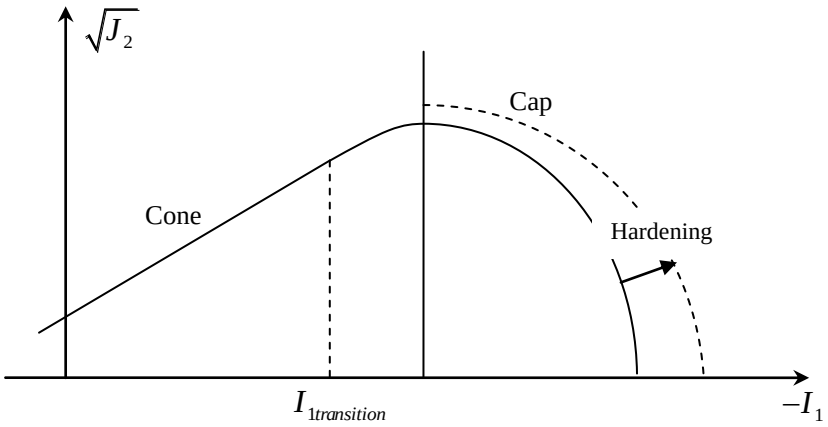

Figure 2.7 Drucker-Prager with cap hardening plasticity model (after Settari and Walters, 2001)

In one of their case studies which they investigated, a reservoir and surrounding structure were modelled in geomechanical simulation. They concluded because of soft overburden there is no remarkable difference in compaction. Their model grid was shown in Figure 2.8.

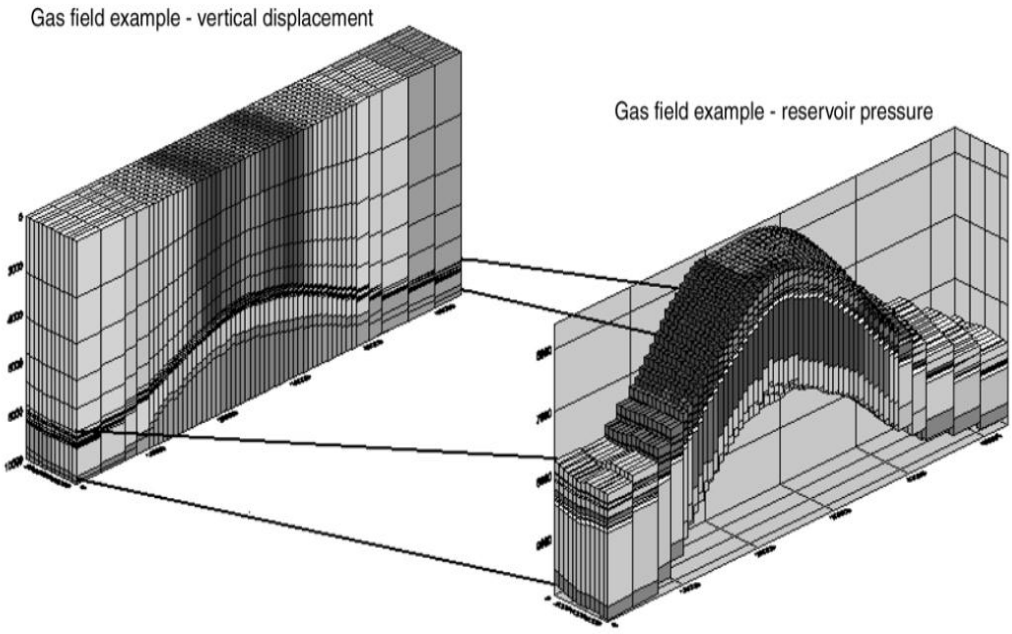

Figure 2.8 Reservoir and geomechanical FEM grid for case study (after Settari and Walters, 2001)

Fredrich et al. (2000) did an investigation on surface subsidence and well casing damage and failure in Belridge diatomite reservoir, Bakersfield, California where in around 20 years of production about 1000 wells experienced casing damage. Despite high thickness (about 1000 ft) and porosity (45-70%) and high estimated original oil in place (about 2 billion bbl) the three-quarter of the produced oil had come from the overlying Tulare sand. The production from the diatomite layer was restricted since the permeability was too low (about 0.1 mD) but enhanced later using hydraulic fracturing technique. The geomechanical modelling was carried out using nonlinear large deformation finite element code of JAS3D. They modelled two sections of the field: sections 33 and 29. The pore pressure determined from reservoir simulator was sent to the geomechanical simulator as an external load. The reservoir including diatomite and porcelanit layers was discritized into nine layers in section 33 and ten layers for section 29. Underburden is Lower porcelanite and discritized into six elements vertically but since reported casing damage located mostly in overburden, the refinement was done within the overburden layer and was discritized into 10 elements vertically. The depth of underburden and overburden are about 2200 ft and 650 ft, respectively. There are also three contact surfaces in the numerical model. The models contained eight-noded Lagrangian elements. Two classes of plasticity models were used for the entire model: Drucker-Prager and generalized cap plasticity

model. The first constitutive model was used for the overburden and the lowermost reservoir layer and underburden. The second constitutive model was used for eight layers of reservoir. Three aspects of the modelling results are of particular importance: surface subsidence, deformation along vertical profiles (well damage) and changes of in-situ stress field. Surface subsidence was estimated as 7 ft and 5 ft for sections 33 and 29, respectively. The shear deformation predicted to be ±0.5 ft/year.

2.7 Summary

A review of production induced stresses in relation with the flow of fluid in porous reservoir formations were presented in the first part of this Chapter. This was followed by discussing different coupled algorithms which could be used to link the geomechanical behavior of formations with fluid flow responses. It was explained why the partially coupled algorithm is advantageous over one-way and fully coupled algorithms for such applications. The remaining part of this Chapter discussed the need for using numerical simulations for solving the rock engineering problems where inhomogeniety and non-linearity are the inherent properties of the materials. Comparing different numerical methods it was discussed why FEM is a more robust technique and that this is the numerical method which will be used in this research study. In the next two Chapters detail review of the finite element program developed for the purpose of geomechanical simulations in this study will be given.

3 Isotropic linear elastic finite element simulations

Finite element method (FEM), as the most effective and powerful numerical technique in continuum solid mechanics has been widely applied to simulate solid material behaviour under loading especially in linear static structural analysis. The applications of FEM in the field of petroleum geomechanics have been reported since 1990s where several researchers modelled the behaviour of reservoir formation and its surrounding structures under different loadings. Pioneered work in this area was focused on linear elastic behaviour of geomaterial. Isotropic linear elastic analysis has two advantages: it is rather simpler than nonlinear models and gives an initial understanding of the response of the structure subjected to loading.

In this Chapter the details of a developed 3D finite element algorithm using FORTRAN language programming in this research will be introduced. The developed code is specifically designed for direct applications in reservoir geomechanics simulations. The analysis is limited to isotropic linear elastic models at this stage. A robust meshing and post processing algorithm have also been developed in conjunction with the main code. The validity of the program results was checked for three simple cases where close formed solutions are available. The developed code was then applied to three case studies. The first simulation considers injection into a finite rectangular porous zone. The results include the injection-induced stress and displacement fields and the practical implications of such engineering operation will be discussed. In the second example gas injection into a curved structure, i.e. an anticline is compared to that of a horizontal layer. The simulation results indicated high shear stress concentration at the flank of the anticline. The third case study simulates depletion of a coal layer in a coal bed methane (CBM) with an emphasize on the subsequent surface subsidence.

3.1 Introduction

Finite element (FE) procedure nowadays is used in wide range of problems in engineering design. The usage of finite element method for solving engineering problems dates back to the advent of digital computer where excessive amount of calculations could be rendered. It is difficult to assign a "date of invention" but roots of finite element method go back to three separate research groups: mathematicians, physicians, and engineers. Since the early 1960s a large amount of research has been devoted to the development of this numerical and computational technique. In engineering ground the original development was in the field of solid and structure analysis but soon after it was found that it is applicable in the solution of field problems including heat transfer and fluid flow (Bathe, 1996).

The linear elastic constitutive model has been used widely in rock mechanics and in particular in petroleum geomechanics. This is due to the fact that this model needs small number of variables as input, mainly Young's modulus and Poisson's ratio but provides a very good insight of loading and unloading consequences. In petroleum geomechanics applications the poroelastic behaviour of porous material needs to be understood. Settari and Mourits (1998) assumed linear elastic models for the study of pore volume coupling between stress and reservoir simulations. As a result they proposed algorithms for pore volume coupling corresponding to both linear and nonlinear elasticity. In another attempt in using linear elastic behaviour for geomaterial, Minkoff et al. (2003) investigated 25 years of production (injection/depletion) history and compared the results of their loosely coupled algorithm (which used IPARS/JAS3D loosely coupled algorithm) with those of fully coupled module of ARCO simulator, ACRES. ACRES uses finite difference method for multiphase flow simulation part and finite element method (linear poroelastic equation) for the structural part of the model. Their study showed that the loosely coupling algorithm could give the same results as fully coupled algorithm with less computation and run time.

Another FE numerical simulation reported by Yin et al., (2007) where they used coupling between the Displacement Discontinuity Method (DDM) as a boundary method to finite element model. They used finite element method for reservoir section and the DDM for surrounding media. In their work a poroelastic based finite element method was used for reservoir interval which provides stress and strain

estimations for the outer DDM model. The DDM model provides the outer boundary load vector for the next step of finite element model. Settari and Sen (2008) reported two case studies where they used linear elastic behaviour for reservoir formation and surrounding media; one from North Sea chalks and other from deep water terbidites. They considered a Young's modulus of 3GPa in their first case study. In their second case study they investigated the case of offshore turbidite deposit which alternating of shale and sand layers. They simply considered that the overburden, sideburden and underburden rocks have the same value of stiffness to that of shale. The stiffness (Young's modulus) ranges from 0.413 to 0.515 GPa for shale. From this study they concluded that the soft overburden deforms easily with respect to the reservoir deformation but stiff overburden resists against reservoir compaction.

Several numerical codes based on FEM has been developed and introduced. Some of these codes are commercial but others are developed for more research applications. JAS3D is a FE code which has been used for various reservoir geomechanics simulations by several researchers (Fredrich et al. 2000; Fredrich and Fossum, 2002; Minkoff et al., 2003; Minkoff et al., 2004). JAS3D is a multiprocessor code which uses a parallel iterative solver useful for large-scale reservoir geomechanics simulations. This code was developed under the US Department of Energy Defence Program for analysing large nuclear weapons problems (Fredrich and Fossum, 2002). VISAGE is another FEM based numerical simulator which has been used for reservoir geomechanics related problems (Longuemare et al., 2002; Yale, 2002; Pettersen, 2008).

This study introduces a new finite element code which has been developed in FORTRAN programming language for stress and displacement simulations, with particular applications in reservoir geomechanics. In this study the isotropic linear elastic analysis of the developed code is presented but nonlinear elasto-plastic analysis is the continuation of this study which is discussed in detail in next Chapter. Having access to the program source enhances the ability of any further modification for different application purposes to a great extent.

3.2 Isotropic linear elastic continuum mechanics

Due to loading the continuum body deforms and the internal field of stress is induced inside the continuum solid. For a general deformable continuum solid there are three classes of unknowns. These are six stress components

$\left(\sigma_{xx} \quad \sigma_{yy} \quad \sigma_{zz} \quad \sigma_{xy} \quad \sigma_{yz} \quad \sigma_{zx}\right)^T$, six strain components $\left(e_{xx} \quad e_{yy} \quad e_{zz} \quad e_{xy} \quad e_{yz} \quad e_{zx}\right)^T$ and three components of displacement $\left(u \quad v \quad w\right)^T$ (Sadd, 2005).

Also, three classes of independent equations are to be solved. The *Equilibrium equations* ensure that stress components inside the body would satisfy the equilibrium state of the continuum statically. These set of equations contain three independent partial differential equations as (Sadd, 2005):

$$\sigma_{ij,j} + F_i = 0 \tag{3.1}$$

Where F_i are the body force components and notation comma implies differentiation operation.

The *Strain-displacement equations* describe the relationship between displacement field components and strain field inside and at the boundary of the continuum. According to small deformation theory these equations contain six independent differential equations in the form of:

$$e_{ij} = \frac{1}{2}\left(u_{i,j} + u_{j,i}\right) \tag{3.2}$$

The *Stress-strain* or *constitutive* relationships explains the behaviour of material under loading. Based on the elasticity theory, for linear isotropic materials, the relationship between stress and strain is expressed as:

$$\sigma_{ij} = \lambda e_{kk}\delta_{ij} + 2\mu e_{ij} \tag{3.3}$$

where δ_{ij} is the Kronecker delta, λ is the Lame's constant and μ is the shear modulus of the material. These set of equations contain six independent equations and is called generalized Hooke's equations for isotropic linear solids (Sadd, 2005). Generally constitutive equation for elastic materials is written as the following equation in tensorial form which is more convenient for numerical discussion

$$\sigma_{ij} = C_{ijkl}e_{kl} \tag{3.4}$$

where C_{ijkl} is the elasticity tensor.

For any loaded continuum there are three different classes of boundary conditions to be considered. These are the boundary with prescribed displacement, boundary with prescribed traction, and mixed boundary.

3.3 Finite element formulation

In this section a brief introduction to the FE formulation is given. The material presented here is taken from Weaver and Johnston (1984).

Fifteen independent equations should be solved simultaneously in order to find the fifteen unknowns of stress, strain and displacement components all over the structure. The solution should satisfy the boundary conditions of the structure.

Finding exact solutions for a generic case of a structure with given boundary conditions is impossible unless we consider simplified structures with simple boundary conditions. However, finite element method could provide an approximate solution for a specific structure under specific boundary conditions. In this numerical approach the structure domain is firstly discritised into finite number of subdomains named *elements*. Each element is characterized by its imaginary nodes, lines and surfaces which determine the element geometry. The displacement field is approximated inside each element as:

$$\mathbf{u} \approx \hat{\mathbf{u}} = \mathbf{N}\mathbf{u}^e \tag{3.5}$$

In this equation $\mathbf{N}$ is the matrix containing shape functions, and $\mathbf{u}^e$ is the nodal displacement vector of element. (Bold-face letters indicate vector or matrix).

Shape functions have two important characteristics:

$$\mathbf{N}_i\left(\mathbf{x}_i\right) = \mathbf{I} \text{ at node } i \tag{3.6}$$

$$\mathbf{N}_i\left(\mathbf{x}_j\right) = \mathbf{0};\ i \neq j \text{ at other nodes} \tag{3.7}$$

Shape function value depends upon the position of the point inside the element. Based on displacement value the strain value can be determined by differentiation of displacement as

$$\boldsymbol{\varepsilon} = \mathbf{d}\mathbf{u} = \mathbf{d}\mathbf{N}\mathbf{u}^e = \mathbf{B}\mathbf{u}^e \tag{3.8}$$

Where $\mathbf{d}$ is the differentiation operator matrix and $\mathbf{B}$ is a matrix which relates strain tensor components to nodal displacement vector and contains the differentiate of shape functions.

Based on the strain tensor we can determine the stress tensor as

$$\boldsymbol{\sigma} = \mathbf{D}\boldsymbol{\varepsilon} \tag{3.9}$$

where $\mathbf{D}$ is the elasticity matrix.

According to principle of virtual work for any permissible small virtual deformation the virtual work done by external loads is equal to the virtual energy of internal stresses inside the element. Considering a finite element under the nodal actions $\mathbf{p}$ and body forces $\mathbf{F}$, the virtual energy due to the internal stresses is:

$$\delta W_{\text{internal stresses}} = \int_{V^e} \delta\boldsymbol{\varepsilon}^T \boldsymbol{\sigma} dv = \int_{V^e} \delta\mathbf{u}^{eT} \mathbf{B}^T \boldsymbol{\sigma} dv = \int_{V^e} \delta\mathbf{u}^{eT} \mathbf{B}^T \mathbf{D}\mathbf{B}\mathbf{u}^e dv \quad (3.10)$$

The virtual work due to external loads of nodal actions and body forces is

$$\delta W_{\text{external loads}} = \delta\mathbf{u}^{eT} \mathbf{p} + \int_{V^e} \delta\mathbf{u}^T \mathbf{F} dv = \delta\mathbf{u}^{eT} \mathbf{p} + \int_{V^e} \delta\mathbf{u}^{eT} \mathbf{N}^T \mathbf{F} dv \quad (3.11)$$

According to the principle of virtual work:

$$\int_{V^e} \delta\mathbf{u}^{eT} \mathbf{B}^T \mathbf{D}\mathbf{B}\mathbf{u}^e dv = \delta\mathbf{u}^{eT} \mathbf{p} + \int_{V^e} \delta\mathbf{u}^{eT} \mathbf{N}^T \mathbf{F} dv \quad (3.12)$$

which leads to:

$$\left(\int_{V^e} \mathbf{B}^T \mathbf{D}\mathbf{B} dv \right) \mathbf{u}^e = \mathbf{p} + \int_{V^e} \mathbf{N}^T \mathbf{F} dv \quad (3.13)$$

The coefficient matrix $\left(\int_{V^e} \mathbf{B}^T \mathbf{D}\mathbf{B} dv \right)$ is called the element stiffness matrix $\mathbf{K}^e$ and the integral of $\int_{V^e} \mathbf{N}^T \mathbf{F} dv$ is called equivalent nodal force due to body forces, $\mathbf{p}_b^{equ}$. In summary, the main equation for finite element simulation of structural analysis can be expressed in the form of:

$$\mathbf{K}^e \mathbf{u}^e = \mathbf{p} + \mathbf{p}_b^{equ} \quad (3.14)$$

If a similar approximation function (shape function) is used for geometry and displacement then the formulation is called isoparametric finite element formulation. We have used also this isoparametric formulation in the finite element code developed for this study.

3.4 Developed 3D finite element program

A finite element program was developed based on three-dimensional hexahedron 8-noded element using isoparametric formulation. This program mainly supports the loading due to body forces (e.g. gravity force) throughout the structure domain and prescribed traction on outer boundary of elements (e.g. constant pressure due to overburden on top of the buried model). However, loading due to nodal point force and/or prescribed nodal displacement (by means of penalty method) are also supported for some validation purposes. Assemblage strategy is based upon variable

profile storage method and the solver is based on Gauss elimination method regarding the variable profile storage feature of the global stiffness matrix. In addition, for the sake of better computational speedup all equations related to the fixed degree of freedom (DOF) are removed. These especial features together helped us to reduce remarkably the required storage memory, computational cost and subsequently run-time duration in order to overcome the limitations of available computing platform for this research to a great extent. Concept of effective stress and Biot's theory are regarded in the formulation and developed numerical procedures in order to account for the effects of pore pressure changes. The program is developed in incremental form because of two main reasons: capability of simulating the successive loading and unloading which is very essential for geomechanical applications and our upcoming aims toward accounting for nonlinear behaviours such as elasto-plastic constitutive models. However, in this Chapter we only focus on the isotropic linear elasticity. In addition to the main finite element program, we developed two other programs: one for mesh generation (pre-processing) and other for extraction of the results along different profiles (post-processing). All of these programs were written in FORTRAN programming language.

3.5 Program validation

In order to check the accuracy of the developed code and for validation purposes, here, the results of the code applied to some simple cases are presented and compared against closed form solutions available.

3.5.1 A unit cube under nodal point forces

A simple case of a unit cube under four unit nodal point forces, as shown in Figure 3.1, is considered in this example. The cube is fixed from underneath.

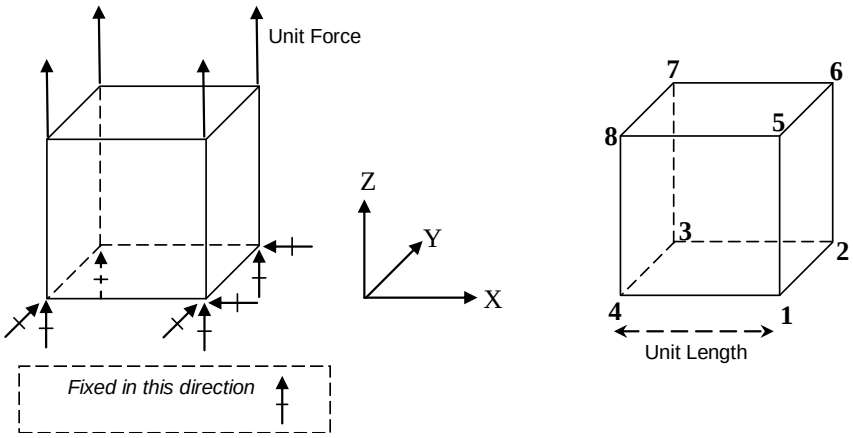

Figure 3.1 Geometry of a cube subjected to nodal point forces

For simplicity let's assume a density of 1.0 gr/cm^3, a Poisson's ratio of 0.3 and a Young's modulus of 10 Pa for the hypothetical material.

Table 3.1 shows the nodal displacement of the cube as obtained from the program. Table 3.1 provides reasonable values with respect to what is expected from elastic models. For example, the elastic displacement at each upper node (i.e. nodes 5 to 8) based on elastic approach is calculated as $\delta L = L \times \varepsilon = L \times \left(\frac{\sigma}{E}\right) = L \times \left(\frac{P}{AE}\right) = 1.0 \times \left(\frac{4.0}{1.0 \times 10.0}\right) = 0.4$ which is identical to the results shown in Table 3.1. The vertical stress of this simple example simply estimated as 4.0 Pa. The stress of this simple example at Gaussian sampling points (GP) was shown in Table 3.2. End force for nodal points was shown in Table 3.3 which indicates the accuracy of the results.

Table 3.1 Nodal displacements in nodal point force example

NODE#	U_X	U_Y	U_Z
1	0.00E+00	0.00E+00	0.00E+00
2	0.00E+00	-1.20E-01	0.00E+00
3	1.20E-01	-1.20E-01	0.00E+00
4	1.20E-01	0.00E+00	0.00E+00
5	-5.68E-08	-4.14E-08	**4.00E-01**
6	-6.37E-08	-1.20E-01	**4.00E-01**
7	1.20E-01	-1.20E-01	**4.00E-01**
8	1.20E-01	-6.54E-08	**4.00E-01**

Table 3.2 Stresses at Gaussian sampling points in nodal point force example

GP#	σ_{xx}	σ_{yy}	σ_{zz}	σ_{xy}	σ_{yz}	σ_{zx}
1	9.88E-07	5.11E-07	**4.00E+00**	0.00E+00	-1.59E-07	-2.18E-07
2	1.01E-07	1.01E-07	**4.00E+00**	-1.68E-07	-4.62E-07	-2.45E-07
3	8.55E-07	1.09E-06	**4.00E+00**	4.53E-08	-4.12E-07	-1.37E-07
4	2.29E-08	-2.15E-07	**4.00E+00**	1.94E-07	-2.52E-07	-1.00E-07
5	2.53E-07	-7.25E-07	**4.00E+00**	6.59E-08	-2.82E-07	6.13E-07
6	-5.87E-07	-1.16E-06	**4.00E+00**	-2.44E-07	-6.40E-07	-5.38E-07
7	2.79E-07	5.44E-07	**4.00E+00**	-7.85E-08	6.13E-07	-5.38E-07
8	-4.54E-07	-6.92E-07	**4.00E+00**	2.63E-07	8.51E-07	7.32E-07

Table 3.3 End-forces vector components in nodal point example

NODE#	F_X	F_Y	F_Z
1	5.22E-08	3.64E-08	**-1.00E+00**
2	1.01E-07	6.19E-08	**-1.00E+00**
3	-6.35E-08	5.22E-08	**-1.00E+00**
4	-1.97E-08	-8.82E-08	**-1.00E+00**
5	-2.68E-09	5.74E-08	1.00E+00
6	-6.24E-08	-1.41E-07	1.00E+00
7	-6.19E-08	3.46E-08	1.00E+00
8	-5.82E-08	3.13E-08	1.00E+00

3.5.2 A unit cube under facet traction

In this example we consider the same cubic element in section 3.5.1 under similar restrictions but apply unit compressive traction at the upper face of the cube equal 1.0 Pa. Using analytical elastic solutions the vertical stress and displacements in both vertical and lateral directions are calculated as:

$$\sigma_z = \frac{P_z}{A_{xy}} = \frac{-1.0}{1.0 \times 1.0} = -1.0 \tag{3.15}$$

$$U_z = L_z \frac{\sigma_z}{E} = 1.0 \times \frac{-1.0}{10.0} = -0.1 \tag{3.16}$$

$$\left|U_{lateral}\right| = \nu \left|U_z\right| = 0.3 \times 1.0 = 0.03\,. \tag{3.17}$$

The program results for this validation example were shown in Tables 3.4 to 3.6. Again these results indicate the accuracy of the program calculation. The $\left|\ \right|$ symbol indicates the absolute value.

Table 3.4 Nodal displacements in unit compression traction example

NODE#	U_X	U_Y	U_Z
1	0.00E+00	0.00E+00	0.00E+00
2	0.00E+00	**3.00E-02**	0.00E+00
3	**-3.00E-02**	**3.00E-02**	0.00E+00
4	**-3.00E-02**	0.00E+00	0.00E+00
5	1.41E-08	1.27E-08	**-1.00E-01**
6	2.04E-08	**3.00E-02**	**-1.00E-01**
7	**-3.00E-02**	**3.00E-02**	**-1.00E-01**
8	**-3.00E-02**	2.10E-08	**-1.00E-01**

Table 3.5 Stresses at Gaussian sampling points in unit compression traction example

GP#	σ_{xx}	σ_{yy}	σ_{zz}	σ_{xy}	σ_{yz}	σ_{zx}
1	-2.73E-07	-1.54E-07	**-1.00E+00**	0.00E+00	4.87E-08	5.41E-08
2	-5.16E-08	-5.16E-08	**-1.00E+00**	5.72E-08	1.08E-07	7.85E-08
3	-3.43E-07	-4.02E-07	**-1.00E+00**	1.07E-08	1.31E-07	3.45E-08
4	-5.73E-09	5.39E-08	**-1.00E+00**	-4.89E-08	8.09E-08	2.54E-08
5	-1.28E-07	1.18E-07	**-1.00E+00**	-7.91E-09	7.29E-08	-2.13E-07
6	1.72E-07	2.57E-07	**-1.00E+00**	6.23E-08	1.33E-07	1.91E-07
7	-1.06E-07	-1.49E-07	**-1.00E+00**	-1.05E-08	-2.13E-07	1.31E-07
8	1.73E-07	2.33E-07	**-1.00E+00**	-7.65E-08	-2.43E-07	-2.43E-07

Table 3.6 End-force vector components in unit compression traction example

NODE#	F_X	F_Y	F_Z
1	-5.60E-09	-1.10E-08	**2.50E-01**
2	-4.75E-08	-4.29E-09	**2.50E-01**
3	2.80E-08	-5.60E-09	**2.50E-01**
4	1.24E-08	2.76E-08	**2.50E-01**
5	-6.78E-09	-1.43E-08	-2.50E-01
6	8.16E-09	2.40E-08	-2.50E-01
7	1.55E-08	-1.80E-08	-2.50E-01
8	1.45E-08	-7.81E-09	-2.50E-01

3.5.3 A unit cube under body force

In this example the same cube of previous examples is subjected to a unit body force in downward *Z* direction. Using elastic analytical solutions the amount of displacement inside the element for the upper face is calculated as:

$$\delta U_z = \varepsilon_z \delta L = \varepsilon_z \delta z = \frac{\sigma_z}{E} \delta z = \frac{-(1 - z B_z)}{E} \delta z \qquad (3.18)$$

$$U_z = \frac{1}{E}\int_0^{1.0} -(1 - zB_z)dz = -0.05 \qquad (3.19)$$

The program result was shown in Table 3.7 which indicates the accuracy of calculation. It should be noted that the minus sign in equations 3.15 and 3.18 stems from the fact that in standard solid mechanics, elasticity theory and finite element procedure the tensile stress is regarded as positive value.

Table 3.7 Nodal displacements for a cube subjected to body force

NODE#	U_X	U_Y	U_Z
1	0.00E+00	0.00E+00	0.00E+00
2	0.00E+00	1.50E-02	0.00E+00
3	-1.50E-02	1.50E-02	0.00E+00
4	-1.50E-02	0.00E+00	0.00E+00
5	-8.80E-09	3.77E-09	**-5.00E-02**
6	-3.73E-09	1.50E-02	**-5.00E-02**
7	-1.50E-02	1.50E-02	**-5.00E-02**
8	-1.50E-02	5.84E-09	**-5.00E-02**

3.6 Example case studies

In this section three simulation examples are presented to demonstrate the applications of the developed 3D finite element code. The analyses are based on the isotropic linear elastic behaviour of geomaterials.

3.6.1 Simulation of injection into a horizontal porous zone

In this example study, the effects of gas injection into a hypothetical depleted reservoir are simulated. The porous reservoir formation is assumed to have a very large extension in *Y*-direction with limited dimensions in the other two directions. Therefore, the plane strain analysis can be used. To use the developed 3D program for this purpose, all degrees of freedom parallel to *Y*-direction are fixed; however the element is three-dimensional 8-noded hexahedron based isoparametric finite element formulation.

Model Geometry

Figure 3.2 shows the geometry of the problem. The porous formation has a rectangular cross-section in *XZ*-plane with a length of 80 m in *X*-direction, and a height of 40 m in *Z*-direction and strike of several hundreds of meter aligned in *Y*-direction. The midpoint depth of the porous formation in *Z*-direction is 500 m and the

height of the porous formation is from 80.0 to 120.0 m from the bottom of the model. In *Z*-direction the model extends to the surface: this allows investigation of the surface induced incidences such as probable uplift or subsidence due to reservoir injection/depletion. The width of the porous formation in *X*-direction is from 160.0 m to 240.0 m from the left side of the model. The model extends 200 m in both sides (overaly 400 m) in *X*-direction to ensure that it reaches to the out of the influenced zone. The three-dimensional model is restricted in deformations normal to the plane in all lateral planes and bottom side while vertical sliding of the lateral planes are permitted. This model consists of 5936 nodes and 2860 three-dimensional 8-noded hexahedron finite elements.

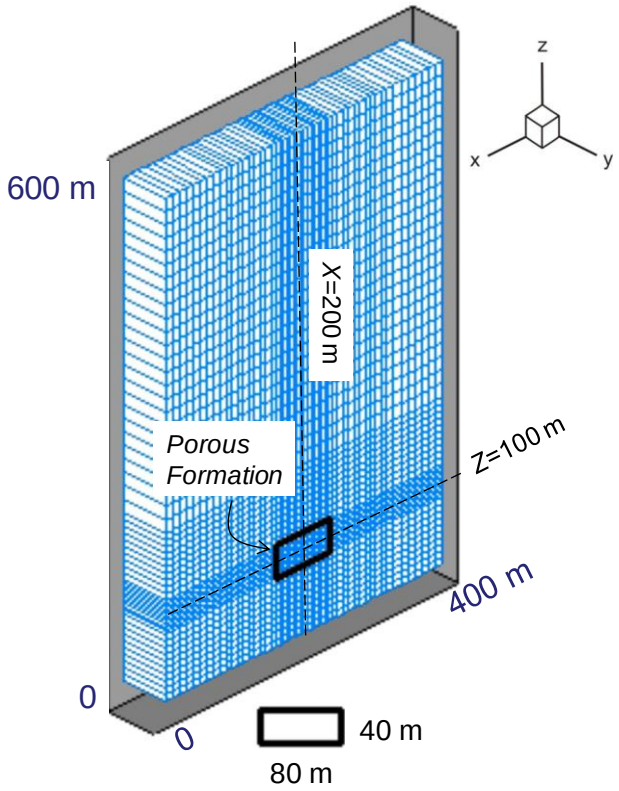

Figure 3.2 Model Geometry: simulation of injection into a porous zone

A formation Young's modulus of 10GPa was assumed for the porous zone in this study. This value was used in the entire model within the reservoir section and also across the overburden and underburden. This represents a moderate stiffness for the rock. The simulation started by allowing the model to consolidate under gravitational force and then injecting into the porous formation up to 5.6 MPa (~800 psi).

Stress contours

The vertical, horizontal and shear stress contours after gravitational consolidations were calculated. These plots are shown in Figures 3.3 to 3.5 together with corresponding pure injection-induced stresses (i.e. the gravitation stresses were discarded).

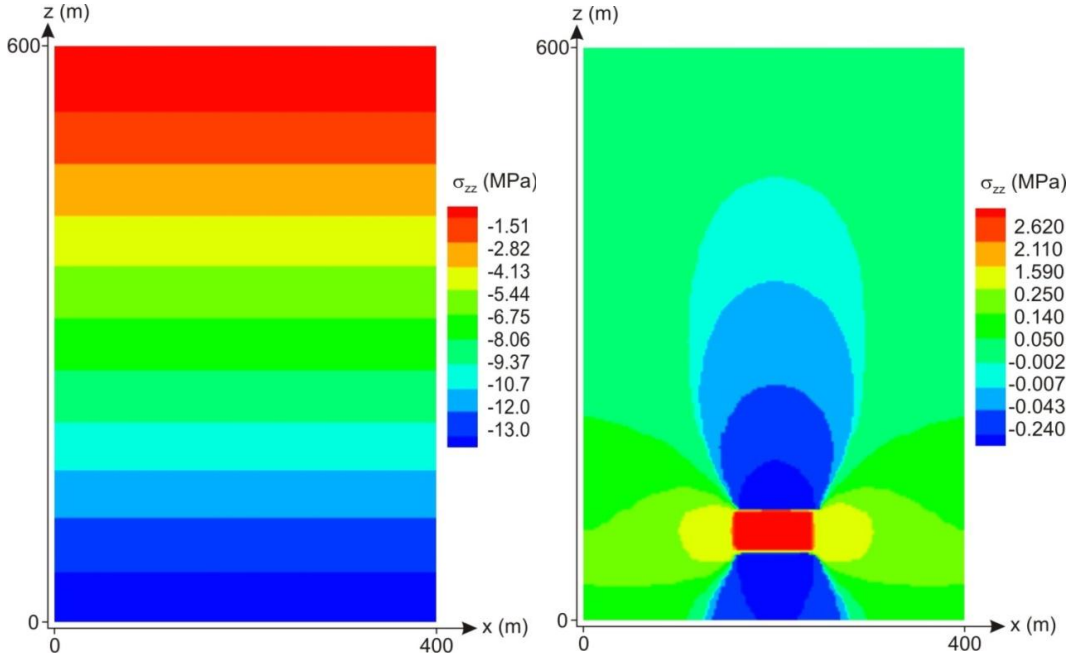

Figure 3.3 Vertical stress σ_{zz} after gravitational consolidation (left); and Induced vertical stress σ_{zz} due to injection (right)

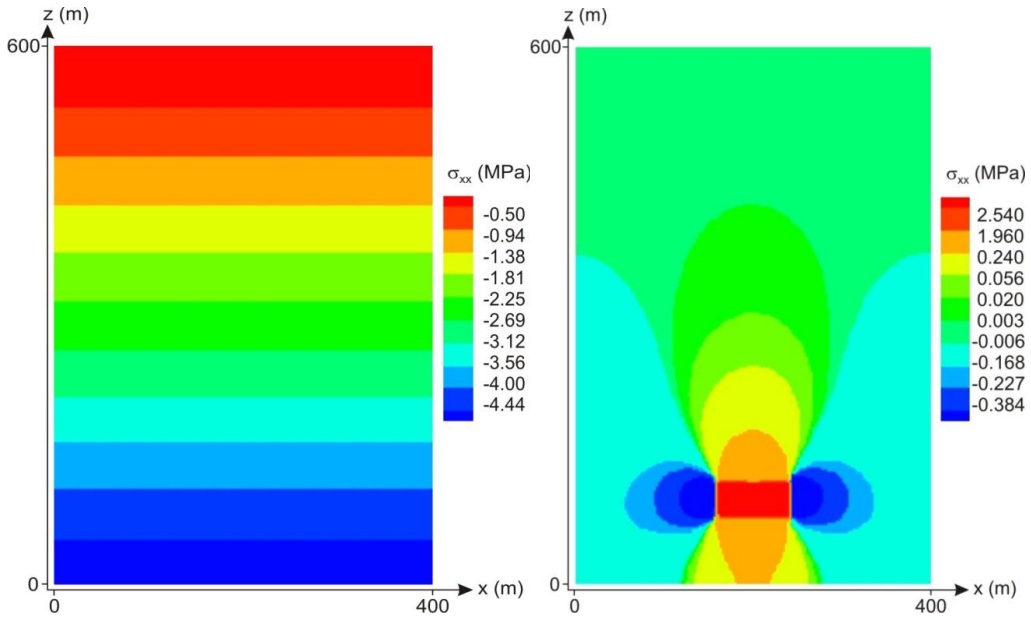

Figure 3.4 Horizontal stress σ_{xx} after gravitational consolidation (left); and Induced horizontal stress σ_{xx} due to injection (right)

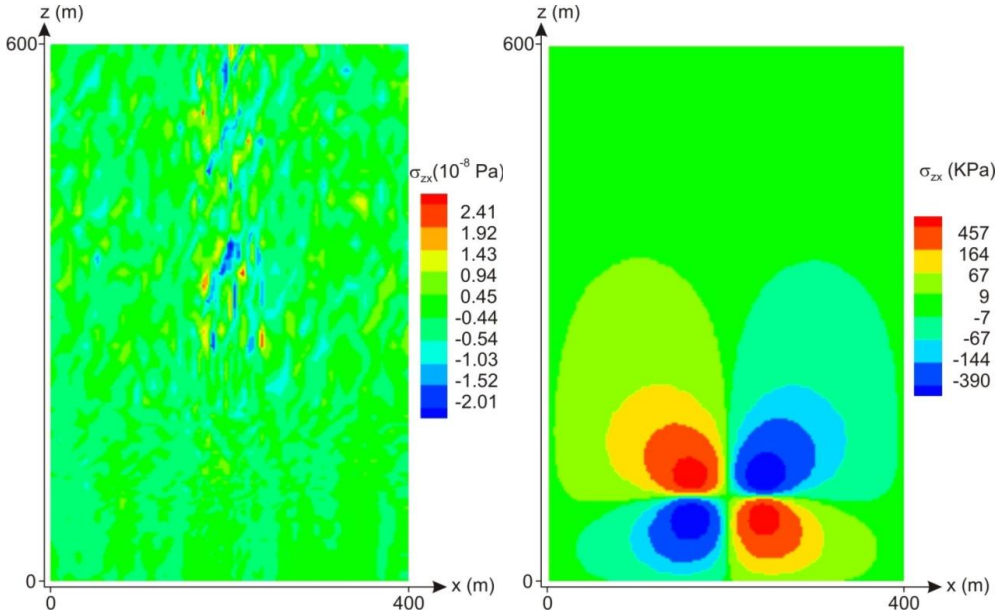

Figure 3.5 Shear stress σ_{xz} after gravitational consolidation (left); and Induced shear stress σ_{xz} due to injection (right)

From plots of Figures 3.3 to 3.5 following conclusions can be outlined:

- The vertical and horizontal stresses resulted from gravitational consolidation are two principle stresses since the shear stress in this plane is negligible (in order of 10^{-8} Pa).

- Injection results in increasing the effective *vertical* stress inside the porous reservoir as well as decreasing the vertical stress in immediate overburden and underburden considering tensile stresses as positive stresses.

- Injection results in increasing the effective *horizontal* stress inside the porous reservoir as well as decreasing the horizontal stress in immediate sideburden.

- A remarkable shear stress zone near to injected zone shows that the vertical and horizontal stresses near this zone are no longer principle stresses after injection or in another word, injection makes the principle stress direction to rotate around the injected zone.

- Injection induces a tensile stresses inside the porous formation as well as its sideburden from vertical stress point of view. It also induces compressive vertical stresses in immediate overburden and underburden.

- The injection induces a tensile horizontal stresses inside the porous formation as well as in immediate overburden and underburden and induces compressive horizontal stresses within the sideburden.

From above conclusions following practical applications can be addressed:

- Increasing the vertical compressive stresses in overburden could create a compaction zone above the injected horizon which has vital importance in collapse of casing.

- Decreasing the horizontal compressive stresses in overburden will decrease the shear strength and even activate the near to vertical sliding surfaces since for this type of discontinuity the horizontal stress acts as normal stress.

- Shear stress zone development and rotation of principle directions near to injected zone can decrease the shear stability and even activate the inclined sliding surfaces.

Stress and displacement profiles

In order to investigate the extension of the stress perturbation zone above the injected porous formation the vertical and horizontal stress profiles corresponding to five parallel profiles at Z= 160, 184, 200, 232, and 264m are shown in Figure 3.6. Also, injection induced vertical displacement U_z along these five profiles are shown in Figure 3.7. According to the results of these figures it can be concluded that for the case of injection of equivalent to 5.6 MPa pore pressure the effect of injection induced stresses decreases remarkably for horizons above 140 m. It is important to note that this conclusion is correct for this specific case with its given geometry and elasticity parameters.

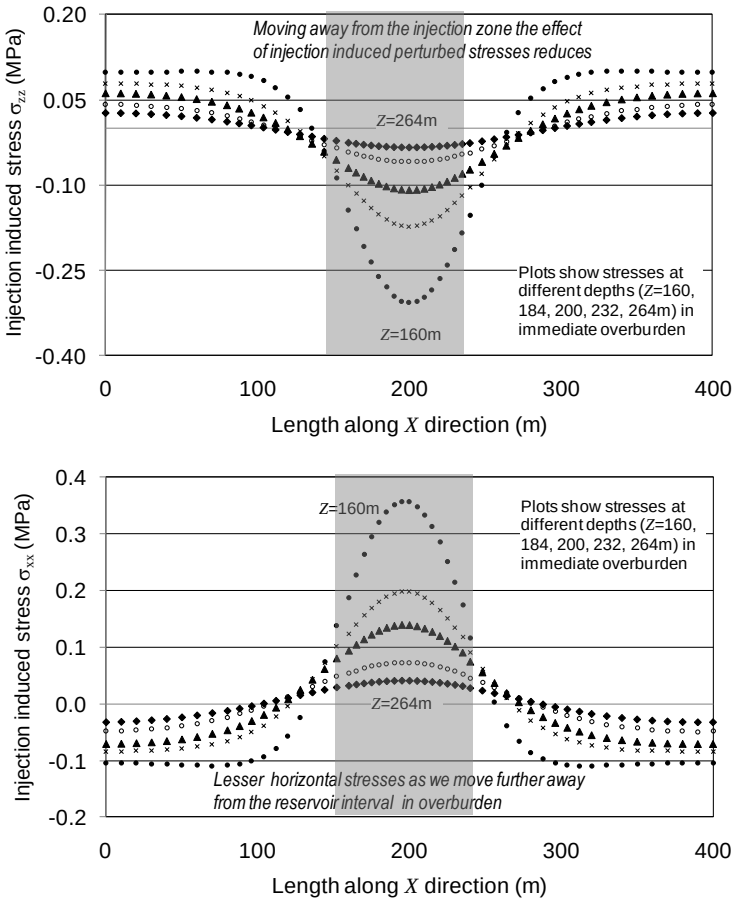

Figure 3.6 Injection induced stress σ_{zz} (Top) and σ_{xx} (bottom) along five profiles located in immediate overburden

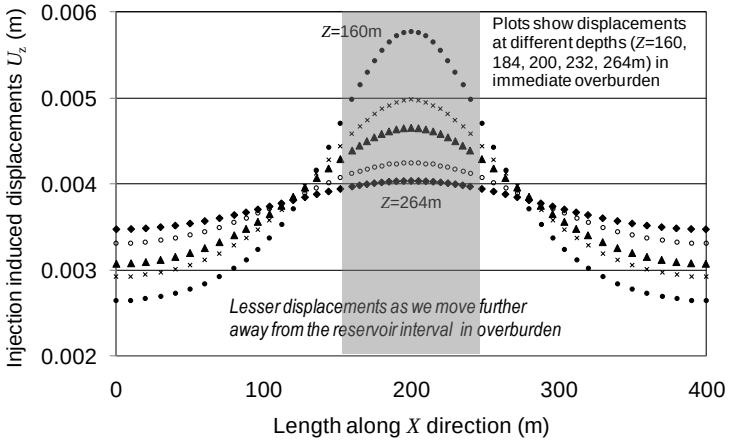

Figure 3.7 Injection induced vertical displacement U_z along five profiles located in immediate overburden

3.6.2 Simulation of injection into a non-horizontal porous zone

In this Section the simulation results are presented for three structures subjected to gas injection. One horizontal layer with two anticline shape formations with different slopes is modelled to study the stress redistribution due to gas injection.

Model Geometry

The geometries of the studied structures are shown in Figure 3.8. All geometries have similar thickness (of 40 m) and horizontal extensions. The distance of the highest point of the layer to the surface is 500 m, and the horizontal extension of the injected zone is 200 m (i.e. from x= 400m to x=600 m). The material used for the analyses has a density of 2500 kg/m^3, a Young's modulus of 10 GPa and a Poisson's ratio of 0.25. The Biot's coefficient was assumed to be 1.0. We used refining of elements closer to the injected zone in order to enhance the finite element modeling results as can be seen in Figure 3.8. The strike of these structures assumed to be parallel to y-axis. The three-dimensional models are restricted in their deformations normal to the plane in all lateral planes and bottom side while vertical sliding of the lateral planes are permitted. Similar to the previous example, the effect of gravitational loading was discarded from the results to only record the injection-induced effects. The reservoir zone was injected up to 3.0 MPa and the induced stresses estimated. In Figure 3.8, profiles are shown along which the stress redistribution after gas injection was compared. As is seen from this figure these profiles are curved geometry in case of anticline structures. The result of injection-induced vertical, horizontal and shear stresses in XZ plane are shown in Figure 3.9 for anticline structure S3.

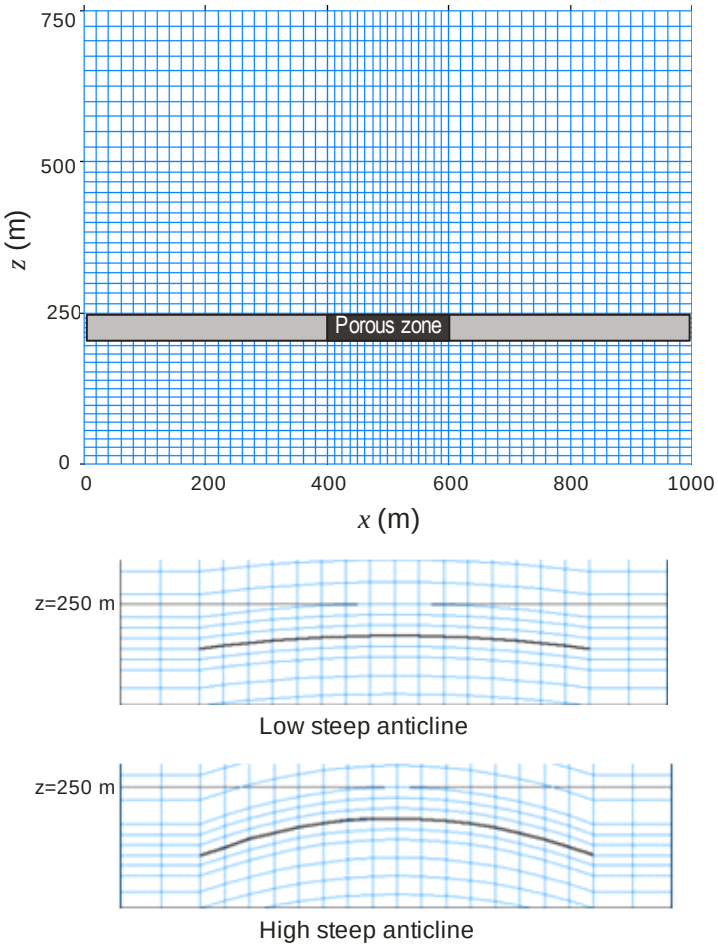

Figure 3.8 A 2D section of mesh generated for horizontal structures S1 (top) and anticlines S2 (middle) and S3. The stress redistribution was modeled along the shown profiles.

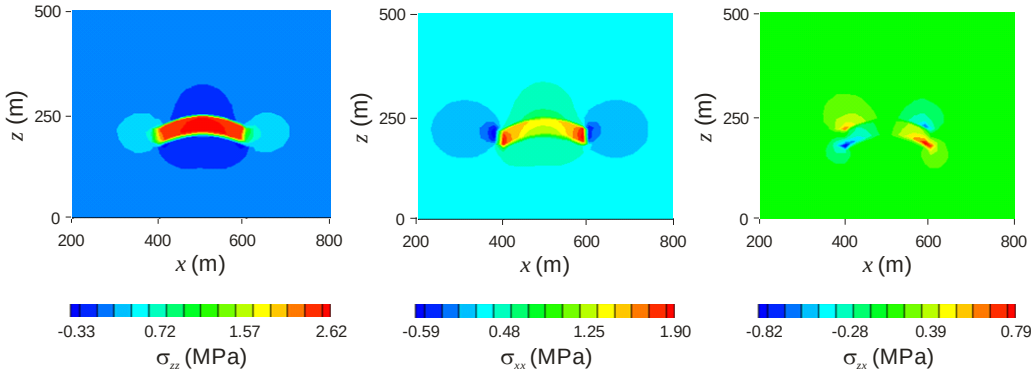

Figure 3.9 Injection-induced vertical (left), horizontal (middle) and shear stress contours for an anticline structure S3

Stress contours

The injection-induced shear stress (σ_{zx}) is the most likely component which will be affected by the geometry of the structure. From practical point of view the magnitude of this stress is used to evaluate the potential for pre-existing fault or fracture reactivation and sliding of the interbeds with low cohesion along each other: this may result in loss of uncase wellbore in short term period after drilling or collapse of casing in long term production from the reservoir. From the plots of injection-induced stresses shown in Figures 3.9 for the case of the anticline with larger slope (S3) it is seen that the magnitude of the shear stress component (σ_{zx}) increases at the corners when the structure deviates from being horizontal (7.86×10^5pa). This result is expected due to stress concentration at sharp corners. However, the more important conclusion is the development of the shear stress zone at the flank area of the anticline structures as can be seen in this figure. The latter result may be attributed to the curvature of the structure but not to stress concentration due to sharp corners. This conclusion suggests that extra precautionary measures should be taken when drilling wellbores at the flank areas in curved structures such as anticlines as the possibility of interbeds movement and reactivation of any pre-existing fracture plane is high due to large shear stresses applied in these zones.

Stress profiles

The injection induced shear stresses were estimated along curve profiles and shown in Figure 3.10 and compared against the stresses along the horizontal profile at the centre of the porous zone. From this figure, again, it is seen that for the horizontal structure the shear stress only appears at corners of the porous zone, yet it is very minor and negligible. For anticline structures shear stresses not only appears at the corners but also exist within the porous zone too and its magnitude is a direct function of the slope of the anticline. The results indicate clearly the potential impact of the induced shear stresses on a wellbore drilled at the flank of the anticline and the subsequent problems including fault or fracture reactivation or casing collapse during the life of the reservoir subjected to gas injection.

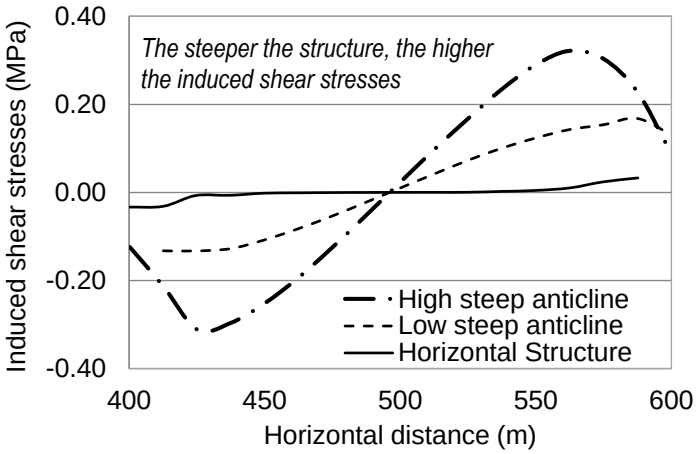

Figure 3.10 Injection-induced shear stresses for three studied structures.

It should be noted that the stresses in this part of the current study were estimated along curved profiles. This is important as in general, linear profiles, comparing to curved profiles within the given formation, may pass through different layers with different mechanical properties. This means that the stress changes in this case could be due to change in formation properties as well as geometry effects. However, by choosing curved profiles passing within the studied layer it is ensured that we only consider the changes in stress distribution due to the geometry effect.

3.6.3 Simulation of depletion induced stresses in a coal layer

As the final example, in this section we simulate gas depletion from a coal layer in a Coalbed Methane (CBM) case to investigate the subsequent changes in stress and deformations.

Model Geometry

The model geometry for this example is shown in Figure 3.11. The finite element model was extended vertically upward to the surface and 280 m under the coal seam layer whereas laterally it covers 200 m on each side of the centre line of the model. In terms of boundary conditions, all the sidewalls of the model are restrained in normal direction to its corresponding sidewall and the bottom of model is restrained in vertical direction.

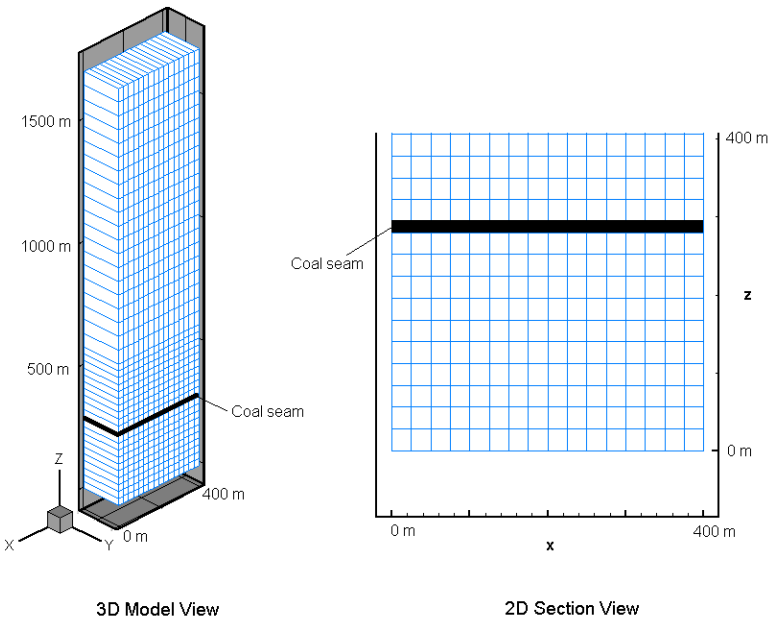

Figure 3.11 Model Geometry for CBM simulations

The model data which was used for this study is tabulated in Table 3.8. This is what previously used by Connell & Detournay (2009) for studying a typical CBM.

Table 3.8 Model data used for simulations of CBM (Connell &Detournay, 2009)

Property	Value
Initial reservoir pressure	4789 KPa
Depth to coal seam	1400 m
Coal seam thickness	14 m
Other layers Young's modulus, Poisson's ration, bulk density	12 GPa, 0.21, 2450 kg/m3
Coal seam Young's modulus, Poisson's ration, bulk density	2 Gpa, 0.35, 1470 kg/m3

Stress contours

Figure 3.12 indicates the contours of vertical and horizontal stresses due to gravitational loading; respectively. The important feature of these results after gravitational consolidation is the increasing ratio of horizontal to vertical stresses inside the coal seam due to a higher Poisson's ratio of the coal comparing to surrounding rocks.

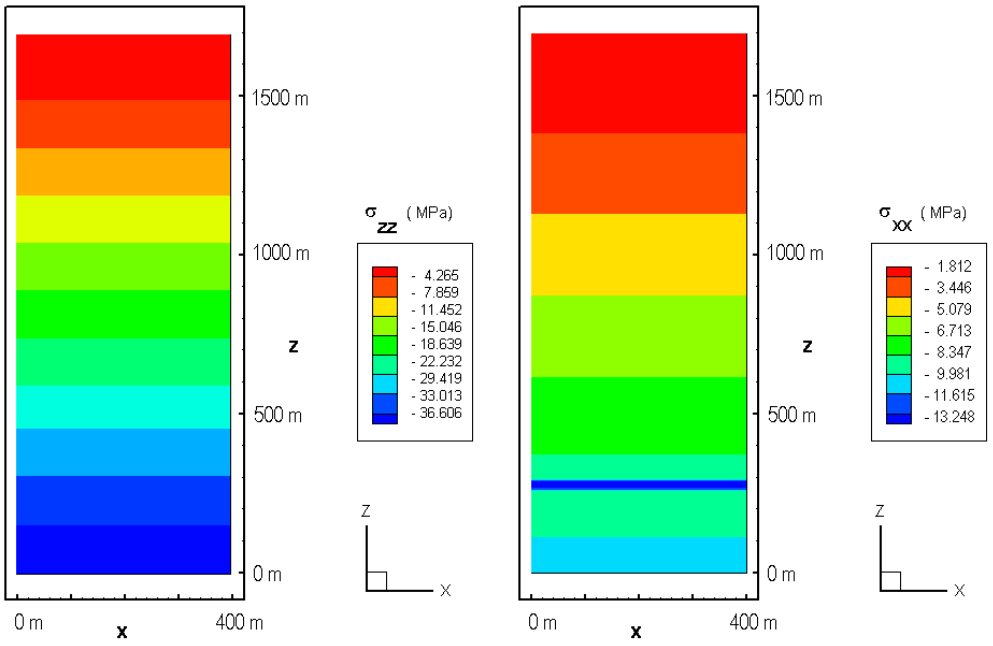

Figure 3.12 Vertical, σ_{zz} ,(left) and horizontal, σ_{xx} , (right) stress contours due to gravitational consolidation.

In entire the model this ratio is 0.2658 except inside the coal layer where this ratio is 0.5384. These ratios equal to the elastic stress ratio coefficient, i.e. $\frac{\nu}{1-\nu}$ in both coal and other formations. For coal seam this ratio is:

$$\frac{\nu}{1-\nu}=\frac{0.35}{1-0.35}=0.5384 \tag{3.20}$$

whereas for other layers it is equal to:

$$\frac{\nu}{1-\nu}=\frac{0.21}{1-0.21}=0.2658 \tag{3.21}$$

For coal layer where the amount of Poisson's ratio is different from other part of the model, the increase of horizontal stresses is clearly observed in Figure 3.12.

Subsidence due to depletion

In order to see the importance of subsidence due to depleting the coal layer, the reservoir pressure increased up to the initial reservoir pressure and then it was reduced in three unloading steps of 75, 50, and 25 % of the initial value. Due to the depletion of the reservoir, the subsidence occurs in overburden and especially at the ground surface. In order to highlight the effect of coal seam depletion the effect of gravitational consolidation was discarded and the result of subsidence of the ground

surface is shown in Figure 3.13.The negative values in this figure indicate ground *downward* movement, subsidence, due to production of coal layer. The linear nature of subsidence, as is seen from this figure, is due to the linear elastic analysis used for this case study.

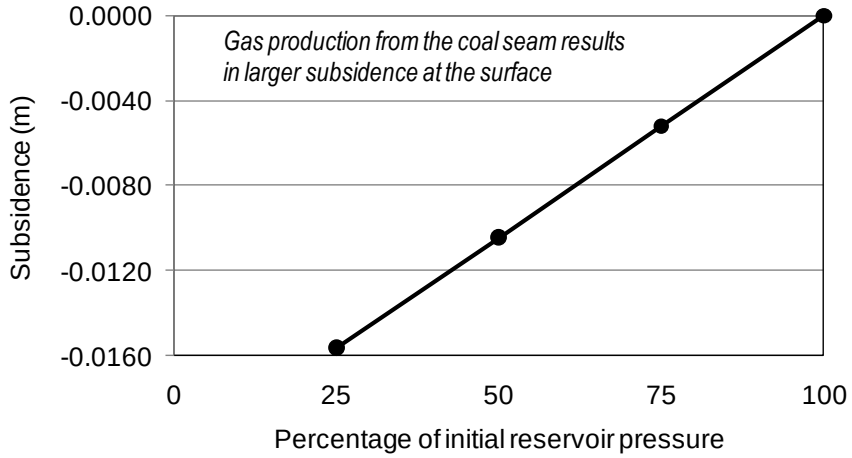

Figure 3.13 Subsidence at the ground surface due to depletion of coal seam pressure

The other interesting point which is to be highlighted is the fact that the amount of depletion-induced downward movement is the same in entire overburden zone from above the coal seam to top of the model. The main reason for such a result is that in the model presented here the coal seam was assumed to have an infinite lateral extension: this would result in no arching and sideburden effects and therefore the model behaves unidirectional in vertical direction, similar to the behaviour of a rigid column of rock in overburden. In addition, due to the assumption of free movements in this model at the top, all the overburden moves similarly as a rigid translation due to production occurs inside the coal seam without any straining and stressing happening. This is again due to discarding the effect of sideburden and assuming a large lateral extension for the coal seam.

The above discussion indicates that in the particular model presented here the characteristics of the overburden rocks have no direct consequences on the production-induced subsidence. However, the properties of the coal seam, in particular the thickness and Young's modulus of the coal, have substantial effects on the amount of subsidence.

3.7 Summary

In this part of the current study a new 3D finite element program coded in FORTRAN was introduced. The program mainly supports the loading due to body force throughout the structure domain and prescribed traction on outer boundary of elements. Different meshes can be generated and post processing functions allow extraction of stress and displacements along different profiles. The model results were validated for three simple cases where close formed solutions are available. The simulator was then applied to simulate stress and displacements induced due to depletion of or gas injection into a formation.

The results of injection into a horizontal formation showed how increasing the vertical compressive stresses in overburden could create a compaction zone above the injected horizon which has vital importance in collapse of casing. Also, it was observed that shear stress zone development and rotation of principle directions near to injected zone can decrease the shear stability and even activate the inclined sliding surfaces.

The results of simulating curved structures indicated the concentration of shear zones along the flank of the structure. This conclusion suggests taking extra precautionary measures when drilling wellbores at the flank areas in curved structures such as anticlines as the possibility of interbeds movement and reactivation of any existing fracture plane is high due to large shear stresses applied in these zones.

In final example, the simulations results of gas depletion from a coal layer showed potential of subsidence in overburden and especially at the ground surface.

4 Elasto-plastic finite element simulations

The development of yield or plastic zone due to an engineering construction is a subject of study in different disciplines. In Petroleum engineering depletion from and injection of gas into a porous rock can cause development of a yield zone around the reservoir. The study requires elasto-plastic analysis of geomaterial, in this case the porous rocks. In this Chapter, which is a continuation of previous Chapter where isotropic linear elastic behaviour of geomaterial was presented, the elasto-plastic responses of geomaterial are studied. A 3D finite element (FE) code was developed which can consider different constitutive models. The code features are explained and some case studies are presented to validate the output results of the code. The numerical model then was applied to study the development of the plastic zone around a horizontal porous formation which was subjected to the injection of gas. The details of the model will be explained and the results presented. It was seen how by reducing the cohesion of rocks the extension of the plastic zone increases. Comparing to the elastic model the ability to estimate the extension of the yield and plastic zone is the main advantage of an elasto-plastic model.

4.1 Introduction

Development of plastic zones in porous materials such as soils and rocks due to an engineering activity is a topic of study by many researchers (Lewis and Shrefler, 1998). An example of this is production from a porous reservoir formation or injection into a depleted reservoir for underground storage purposes. The permanent deformation as a result of plastic deformation is irrecoverable contrary to elastic behaviour if the material is unloaded. The plastic zone represents the extent of the yield of the geomaterial and can be mathematically determined using appropriate constitutive models of plasticity theory (Lewis and Shrefler, 1998). The plastic shear failure could be characterised using Mohr-Coulomb type plasticity constitutive

models (Owen and Hinton, 1980). Drucker-Prager constitutive model is also used to determine the plastic zone, for example, due to gas injection into a reservoir formation, which is considered in this study. While both constitutive models are pressure-sensitive, Drucker-Prager model has no singularities and therefore is a better model in this regard. This statement is supported by different researchers, some of which are discussed here.

Fredrich and Fossum (2002) carried out several case studies using elsato-plastic and viscoplastic constitutive models. They discussed the advantages of continuous surface yielding criterion against traditional cap plasticity models. They declared that the traditional cap plasticity models have indeterminacy at the point of intersection between shear failure surface and hardening cap surface. Also, the horizontal tangency of cap hardening surface at the intersection point makes it impossible that the model dilatants before final failure. The continuous surface yielding criteria does not have these two disadvantages. For the implementation of the continuous yield surfaces criterion they referred to the work of Fossum and Fredrich (2000) where they implemented this type of plasticity model in JAS3D nonlinear finite element code. Fredrich and Fossum (2002) discussed the effects of production and reservoir depletion on the surrounding rocks, surface subsidence and casing damages. They also did several case studies using the new continuous surface elasto-plastic models for geomaterial. They estimated the pore pressure using the black-oil model reservoir simulator which was used as the input into the geomechanical model in the form of external loads. Fredrich and Fossum (2002), in their first case study considered a highly porous diatomaceous formation (a porosity of 45%) located in San Joaquin Basin, named Belridge diatomite and Lost Hill fields where numerous casing damage had been reported. They studied two sections in Belridge Diatomite and one at the Lost Hill field using three-dimensional nonlinear finite element code JAS3D. The results of their modelling revealed that the sliding surface and bedding surface between reservoir and upper formations are the main sources for large horizontal deformation of casing. They also reported that the horizontal displacement was negligible in the first 10 years while production switches to waterflood processes and injection which shows high shear displacement in the sample well. The modelling results also indicated the tendency of rotation of principle stresses in the field during the course of production as the minimum principle stress rotated from horizontal to vertical direction.

Minkoff et al. (2003) described comprehensively the advantages and disadvantages of fully coupled, loosely coupled and one-way coupled methods between fluid flow and geomechanics set of equations. Despite the perfectness of fully coupled models, they stated that it is extremely hard to set up the set of simultaneous equations for multiphase flow and nonlinear geomechanical behaviour. On the other hand the one-way coupled method does not possess this perfectness of simultaneous solution of fluid flow and geomechanical set of equations but it makes easier to use advanced and sophisticated fluid flow and geomechanics code to handle the problem. This allows capturing features in advanced problems such as multiphase fluid flow or nonlinear elasto-plastic behaviour of geomaterial. They explained that the loosely coupled method, in between the other two way of coupling, enhances the capability of one-way coupling method since it allows the updated data transfer between two simulators in order to increase the degree of coupling of the solution. On the other side, the loosely coupled method permits the use of highly progressed and advanced simulators since they run independently. Using the loosely coupled method they coupled two advanced simulators of IPARS as a reservoir simulator, which is capable of handling multiphase flow and faults and JAS3D, an advanced geomechanics simulator, which handles nonlinear complicated constitutive models for geomaterial. In these coupled programs pore pressure is determined using a reservoir simulator and it is applied as an external load to geomechanical simulator. After some iterations in time reservoir properties (i.e. porosity and permeability) are updated using newly determined stress, strain and displacement fields. Using this approach Minkoff et al. (2003) simulated a single layer of Belridge field, California, where the initial oil in place is estimated at 500 Mm^3.

Settari and Walters (2001) discussed the effect of coupling on the analysis of producing reservoirs. They compared three types of coupling: uncoupled, partially coupling and fully coupling. They explained how partially coupling is beneficial when using the advanced reservoir and geomechanics simulators in the sense that they run separately but information is transferred between the two simulators at any certain time step. They also discussed the importance of elasto-plastic constitutive models for compaction analysis. They referred to Drucker-Prager cap plasticity model and hyper-elastic nonlinear model and expressed that the first model is useful for post-failure analysis whereas the second model is good for pre-failure analysis. This is while both models are capable of modelling nonlinear stress-strain behaviour.

Comparing the two constitutive models, they concluded that the run time of the elasto-plastic model is nearly as twice as the nonlinear hyperbolic elastic model.

In this work we developed a 3D finite element code which is capable of elastic analysis of porous material for elasto-plastic analysis. The main goal is to investigate the effect of injection on plastic zone development around a porous formation. Having access to the source code of is an advantage which allows adding any other constitutive models which is suitable for any type of geomaterials. The developed code is validated against some simple case studies and then is used for analysis of stress and displacements due to injection into a porous reservoir.

4.2 Mathematical treatment of plasticity theory

There are many textbooks which explain the mathematical aspects of plasticity theory in detail. Here, a brief introduction to the plasticity theory is given. It is to be noted that most of the material presented in this section is taken from Owen and Hinton (1980).

Elaso-plastic solids behave in such a way that when stress exceeds a limited threshold named yield stress an irreversible straining will happen. Three basic fields of mathematical subjects are needed in order to completely cover the elasto-plastic behaviour (Owen and Hinton, 1980):

- explicit relationship between stress and strain for elastic condition i.e. before yielding starts;
- a yield criterion showing the stress level at which plastic flow starts; and
- stress-strain relationship for post yield behaviour.

These concepts and related aspects of plastic behaviour are explained in brief in the following sub-sections.

4.2.1 Elastic condition

Before plastic yielding starts the stress-strain relationship is generalized Hook's law i.e.

$$\sigma_{ij} = C_{ijkl}\varepsilon_{kl} \tag{4.1}$$

For isotropic material:

$$C_{ijkl} = \lambda\delta_{ij}\delta_{kl} + \mu\delta_{ik}\delta_{jl} + \mu\delta_{il}\delta_{jk} \tag{4.2}$$

where λ and μ are Lame's Constants and δ_{ij} is Kronecker delta.

4.2.2 Yield Criteria

Yield criterion describes the relationship of stresses level at which the plastic deformation starts. Generally it is written as:

$$f\left(\sigma_{ij}\right) = k\left(\kappa\right) \tag{4.3}$$

where f is a function and k is a material parameter determined experimentally and κ is a hardening parameter. Physically the yield criterion should be "independent of the orientation of coordinate system and therefore it should be a function of stresses invariant" (Owen and Hinton, 1980). J_1, J_2 and J_3 are invariant of stress field. Some yield criteria are independent of the hydrostatic pressure and therefore they are functions of deviatoric stress invariant J_2' and J_3'. The mostly used yield criteria are explained below.

The von Mises yield criterion

This yield criterion is based on the fact that when the value of the second invariant of deviatoric stress field reaches the threshold the yielding starts:

$$\sqrt{J_2'} = k\left(\kappa\right) \tag{4.4}$$

The Mohr-Coulomb yield criterion

This yield criterion was first defined by Coulomb (1773) as the straight line in (σ_n, τ) space as:

$$\tau = c - \sigma_n \tan\varphi \tag{4.5}$$

where τ is the shear stress, σ_n is the normal stress, c and ϕ are cohesion and internal friction angle, respectively. It is notable that tensile stress is positive. By some mathematical manipulation the form of yield criterion suitable for computational plasticity is driven as:

$$\frac{1}{3}J_1\sin\varphi + \sqrt{J_2'}\left(\cos\theta - \frac{1}{\sqrt{3}}\sin\theta\sin\varphi\right) = c.\cos\varphi \tag{4.6}$$

The Drucker-Prager yield criterion

This criterion is a modification of von Mises yield criterion which is also an approximation to Mohr-Coulomb criterion. In mathematical form this criterion is expressed as:

$$\alpha J_1 + \sqrt{J_2'} = \kappa' \tag{4.7}$$

in which α and k' reflect the fact that the Drucker-Prager yield criterion coincide with the outer apices of the Mohr-Coulomb hexagon and therefore are represented as:

$$\alpha = \frac{2\sin\varphi}{\sqrt{3}(3-\sin\varphi)} \qquad \kappa' = \frac{6c\cos\varphi}{\sqrt{3}(3-\sin\varphi)} \tag{4.8}$$

or coincide with the inner apices of the Mohr-Coulomb hexagon, in which case are calculated as:

$$\alpha = \frac{2\sin\varphi}{\sqrt{3}(3+\sin\varphi)} \qquad \kappa' = \frac{6c\cos\varphi}{\sqrt{3}(3+\sin\varphi)} \tag{4.9}$$

4.2.3 Work hardening

After initial yielding the yield surface may be a function of degree of plastic strain that the material has experienced. If the yield surface does not depend on the plastic straining occurs in the material the material is known as an elastic perfectly plastic material. If the yield surface keeps its original shape but continues in expanding the material is known as an isotropic hardening material. Finally if the yield surface keeps its original shape and orientation but translates in the principal stress space it is known as a kinematic hardening material. In this study we only consider elastic perfectly plastic and isotropic hardening behaviours.

The hardening parameter can be a function of the work which is done during the plastic deformation and therefore is said to be a work hardening phenomenon. Mathematically:

$$\kappa = W_p \tag{4.10}$$

where

$$W_p = \int \sigma_{ij} \left(d\varepsilon_{ij}\right)_p \tag{4.11}$$

In this equation "$\left(d\varepsilon_{ij}\right)_p$ is the plastic components of strain occurring during a strain increment" (Owen & Hinton, 1980).

If $f < k$ then the material is in the elastic domain but for $f = k$ plastic deformation initiates. After initiation of plastic behaviour the increment change in the yield surface is dependent to the stress change:

$$df = \frac{\partial f}{\partial \sigma_{ij}} d\sigma_{ij} \tag{4.12}$$

where three cases may be considered:

- if $df < 0$ it is elastic unloading and the stress state returns back inside the yield surface;
- if $df = 0$ it is neutral loading and the stress point remains on the yield surface; and
- if $df > 0$ it is plastic loading and the yield surface expands and the stress point remains on expanded yield surface.

4.2.4 Elasto-plastic stress-strain relationship

Outside the yield surface the material behaviour is elasto-plastic and the strain is partly elastic and partly plastic. In mathematical term the total strain can be represented as:

$$d\varepsilon_{ij} = \left(d\varepsilon_{ij}\right)_e + \left(d\varepsilon_{ij}\right)_p \tag{4.13}$$

For the elastic part the stress- strain relationship is:

$$\left(d\varepsilon_{ij}\right)_e = \frac{d\sigma'_{ij}}{2\mu} + \frac{(1-2\nu)}{E}\delta_{ij} d\sigma_{kk} \tag{4.14}$$

where $d\sigma'_{ij}$ is the deviatoric stress field.

The plastic strain increment it is a function of the *plastic potential*, Q , gradient, i.e.:

$$\left(d\varepsilon_{ij}\right)_p = d\lambda \frac{\partial Q}{\partial \sigma_{ij}} \tag{4.15}$$

where $d\lambda$ is the *plastic multiplier*. The above equation is named the *flow rule*. Q, like f is a function of the deviatoric stress invariants but its determination is a very complicated experimental task. Therefore for many cases in the field of mathematical theory of plasticity it is assumed that $f \equiv Q$ and it is named the *associated* flow rule and *normality condition* since the $\frac{\partial f}{\partial \sigma_{ij}}$ is normal to the yield surface.

4.3 Developed 3D finite element program

We previously developed a 3D finite element program for isotropic linear elastic analysis in the preceding stages of this research. Here, we have expanded our program for elasto-plastic analysis including the von Mises, Drucker-Prager and Mohr-Coulomb models. For von Mises model which has hardening effect stress controlled mode was considered in the analysis. However, for the other two models displacement control mode was considered. Both stress and displacement control modes are integrated in the written code.

The developed 3D finite element program supports three-dimensional isoparametric hexahedron element with variable nodes from 8 to 20 nodes, however in this study we use 8-noded isoparametric hexahedron.

Having access to the source of the code allows coupling it with other reservoir simulators, which is the future objective of this study. Also, it enables us to integrate any other constitutive models in the analysis where is needed.

4.4 Program validation

To validate the results of the developed FE code, in this section we present the results of some simple case studies for which the analytical solutions are available.

The first three examples consider the 8-noded unit cubic element shown in Figure 4.1 subjected to three sequential steps of displacements as following:

- load step 1: +0.2 unit of tensile displacement;
- load step 2: -0.4 unit of compression displacement; and
- load step 3: +0.1 unit of tensile displacement.

Each step is divided into 40 sub-steps and large displacement effect is neglected. The behaviour of this cube is studied using three different constitutive models introduced in the previous sections.

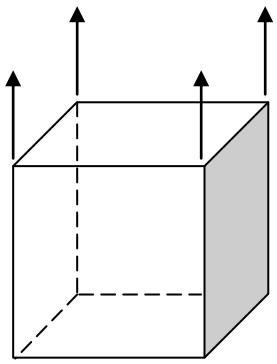

Figure 4.1 A unit cubic element under displacement loading

4.4.1 von Mises constitutive model

In this example the material of the cubic element shown in Figure 4.1 is assumed to be elastic-perfectly plastic with hardening parameter of zero and a yield stress of equal to 0.1 MPa. It is also assumed to have a Young's modulus of 1.0 MPa and a Poisson's ratio of 0.3 for demonstration purposes. The material behaviour under above three loading and unloading steps is shown in Figure 4.2. The loading path corresponding to each step is indicated in this figure. From this figure it is seen that the material yields in a similar manner in both tension and compression. This is an expected result as there is no Buschinger effect for von Mises behaviour.

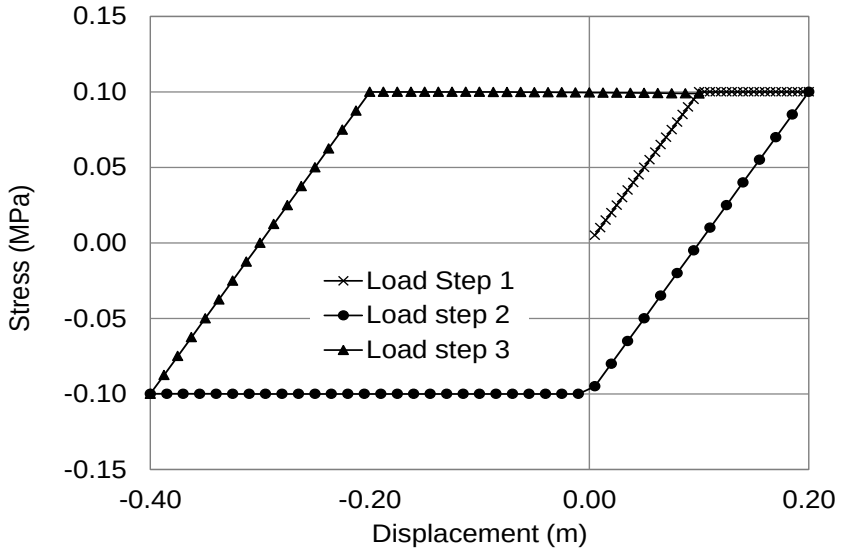

Figure 4.2 Material behaviour under three loading steps considering von Mises constitutive model without hardening (perfectly plastic)

4.4.2 Mohr-Coulomb constitutive model

In this example, the behaviour of the cubic material in Figure 4.1 is studied when its behaviour is assumed to be according to Mohr-Coulomb constitutive model. As it is seen in equations 4.5 and 4.6 the two shear strength parameters for this constitutive model are cohesion and internal friction angle. There are a mathematical relationships between these two shear strength parameters and corresponding uni-axial tensile strength (*UTS* or f_t') and uni-axial compressive strength (*UCS* or f_c') of the material based on this constitutive model which are described in detail in Section 5.3.2. For computation purposes of this validating example *UTS* and *UCS* are assumed equal to 0.1 MPa and 0.3 MPa, respectively. The corresponding cohesion and internal friction angle are 0.0866 MPa and 30 degree, respectively (see Section 5.3.2).

Figure 4.3 presents the material behaviour under three loading and unloading steps, similar to previous example. Contrary to the previous example, the material behaves differently under tension and compression. This is a valid result as the material yielded in a tensile stress of equivalent to 0.1 MPa and in a compressive stress of equivalent to 0.3 MPa. Since there is no hardening effect in perfectly plastic behaviour the material yielded again at 0.1 MPa under the third loading step.

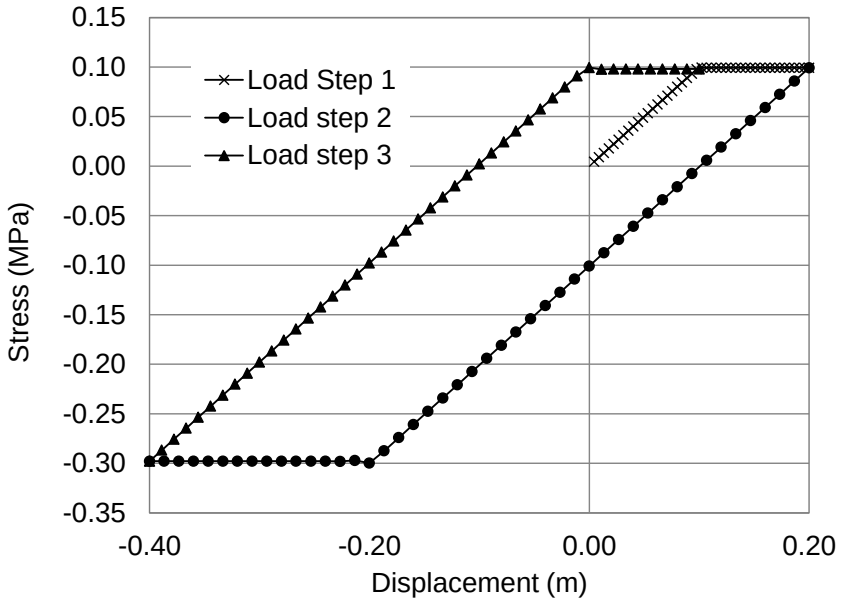

Figure 4.3 Material behaviour under three loading steps considering Mohr-Coulomb constitutive model

4.4.3 Drucker-Prager constitutive Model

In this validating example, the behaviour of the cubic material in Figure 4.1 is studied assuming Drucker-Prager constitutive model. The input parameters to this model are (α, k') but the program uses cohesion and friction angle parameters similar to Mohr-Coulomb criteria. As explained in Section 4.2 there are two types of similarity between these two models: one is in tensile meridian and another in compression meridian. Figure 4.4 shows the material behaviour under three loading and unloading steps. The material behaviour is in such a manner that the Drucker-Prager envelope meets the Mohr-Coulomb envelope at the tensile meridian. Therefore it is seen that the material yielded at a tensile stress of 0.1 MPa which is identical to that of Figure 4.3 under tensile loading. The resemblance of Figure 4.3 and Figure 4.4 under tensile behaviour is notable.

In Figure 4.5, the material behaviour was set in such a way that the Drucker-Prager envelope meets the Mohr-Coulomb envelope at the compressive meridian. Therefore it is seen that the material yielded at a compressive stress of -0.3 MPa which is equivalent to that stress of Figure 4.3 under compressive loading. Again the resemblance of Figure 4.3 and Figure 4.5 under compressive behaviour is notable.

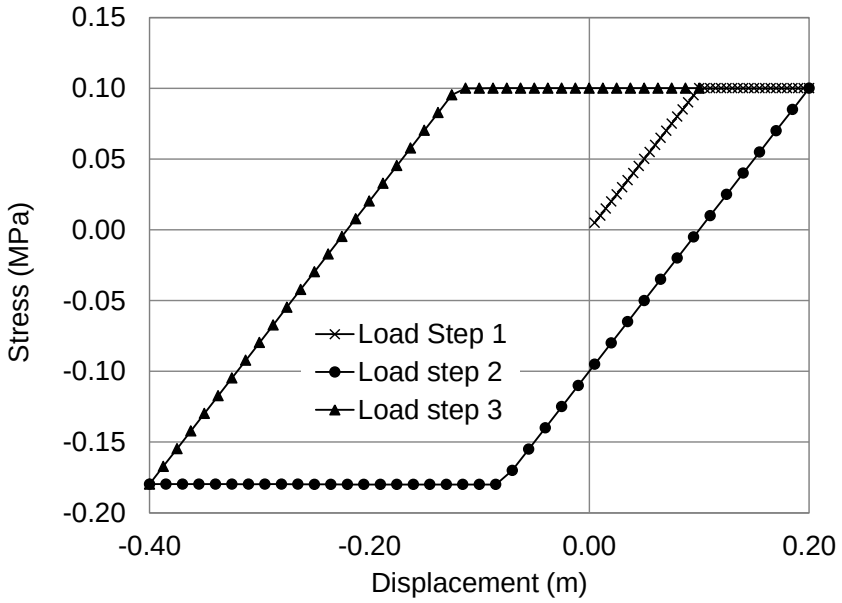

Figure 4.4 Material behaviour under three loading steps considering Drucker-Prager yield surface meets Mohr-Coulomb yield surface at tensile meridian

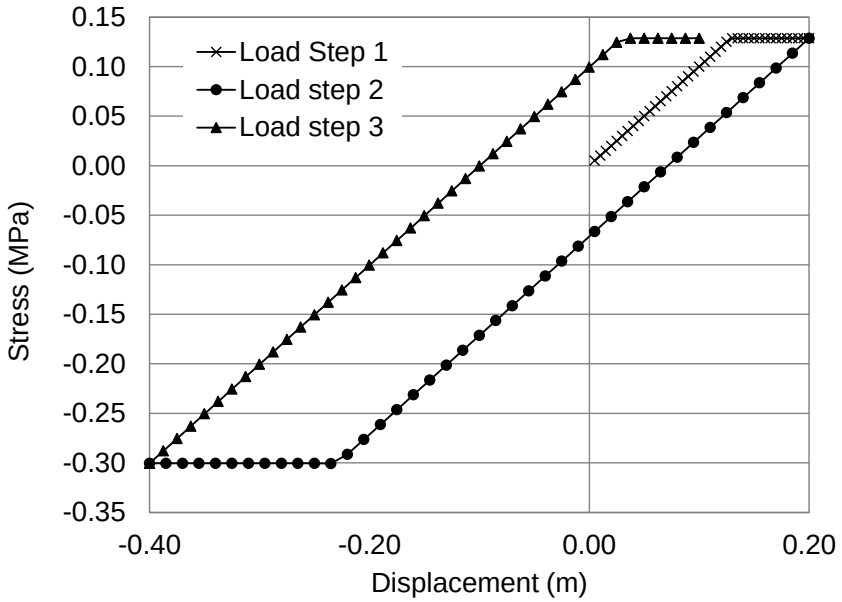

Figure 4.5 Material behaviour under three loading steps considering Drucker-Prager yield surface meets Mohr-Coulomb yield surface at compression meridian

4.4.4 A cylindrical hole in Mohr-Coulomb media

In this final validating example we consider a cylindrical hole in a Mohr-Coulomb media. Figure 4.6 shows the geometry of the problem: this is a quarter of the whole model due to its symmetry. Figure 4.7 presents a 2D section of the model mesh, which in fact is a 3D model.

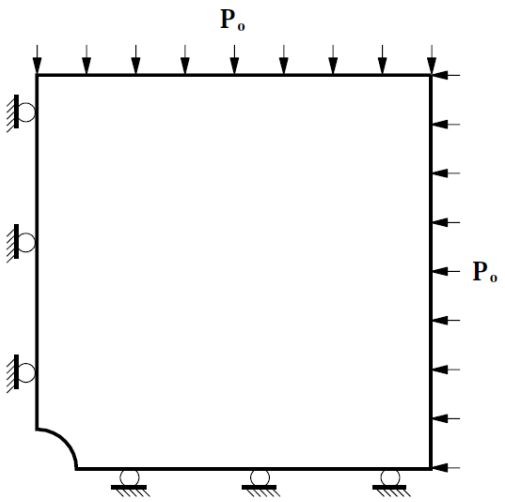

Figure 4.6 Model geometry of a cylinder in a Mohr-Coulomb media (after FLAC user's manual, Version 4.0, 2000)

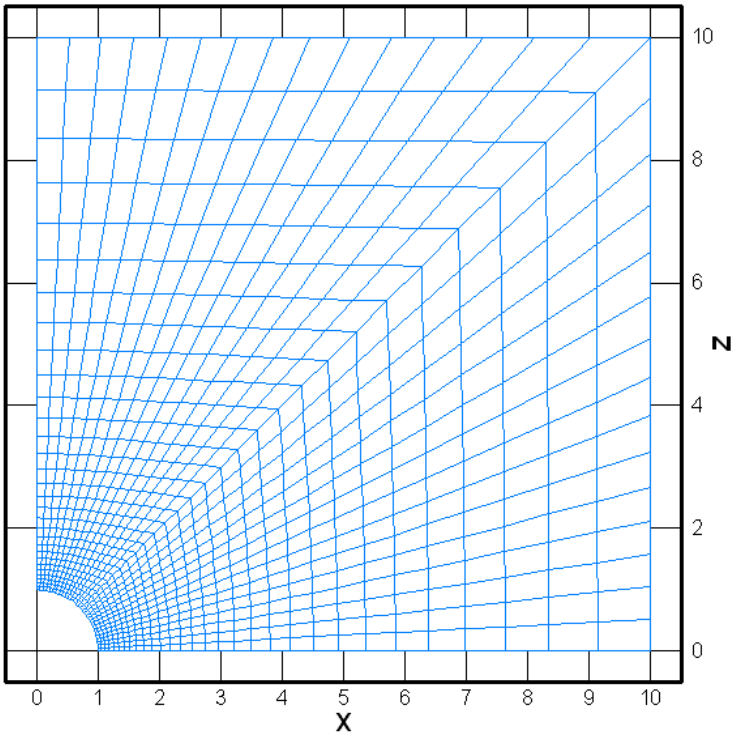

Figure 4.7 Mesh generated for geometry of Figure 4.6

The closed form solution for this problem has been proposed by Salencon (1969) under plane strain condition (FLAC user's manual, Version 4.0, 2000). The plastic zone radius, R_0, is given analytically as:

$$R_0 = a\left[\frac{2}{K_p+1}\frac{P_0+\dfrac{q}{K_p-1}}{P_i+\dfrac{q}{K_p-1}}\right]^{\frac{1}{K_p-1}} \tag{4.16}$$

where a is the radius of the hole, P_o is the magnitude of the initial in-situ stress and P_i is the internal pressure inside the hole. Also,

$$K_p = \frac{1+\sin\phi}{1-\sin\phi}; \tag{4.17}$$

$$q = 2c\tan\left(\frac{\pi}{4}+\frac{\phi}{2}\right). \tag{4.18}$$

The radial stress at the elastic-plastic interface is:

$$\sigma_{re} = -\frac{1}{K_p+1}\left(2P_0 - q\right) \tag{4.19}$$

and the radial and tangential stresses at a distance r from the center of hole within the plastic zone are:

$$\sigma_r = \frac{q}{K_p-1} - \left(P_i + \frac{q}{K_p-1}\right)\times\left(\frac{r}{a}\right)^{K_p-1} \tag{4.20}$$

$$\sigma_\theta = \frac{q}{K_p-1} - K_p\left(P_i + \frac{q}{K_p-1}\right)\times\left(\frac{r}{a}\right)^{K_p-1} \tag{4.21}$$

The stresses outside the plastic zone, i.e. within the elastic zone are:

$$\sigma_r = -P_0 + \left(P_0 - \sigma_{re}\right)\times\left(\frac{R_0}{r}\right)^2 \tag{4.22}$$

$$\sigma_\theta = -P_0 - \left(P_0 - \sigma_{re}\right)\times\left(\frac{R_0}{r}\right)^2 \tag{4.23}$$

The radial and tangential stresses were calculated using the above closed form solutions and also obtained from the FE code numerically. The results are compared in Figures 4.8. The results show a very good agreement between the results of the two models. It should be noted here that according to the linearization happened along each load increment which is modified by iteration process to capture the material behaviour nonlinearity, the magnitude of each load increment needs to be

reasonably low as much as possible to satisfy more appropriately the equilibrium state and decrease the residual force vector norm.

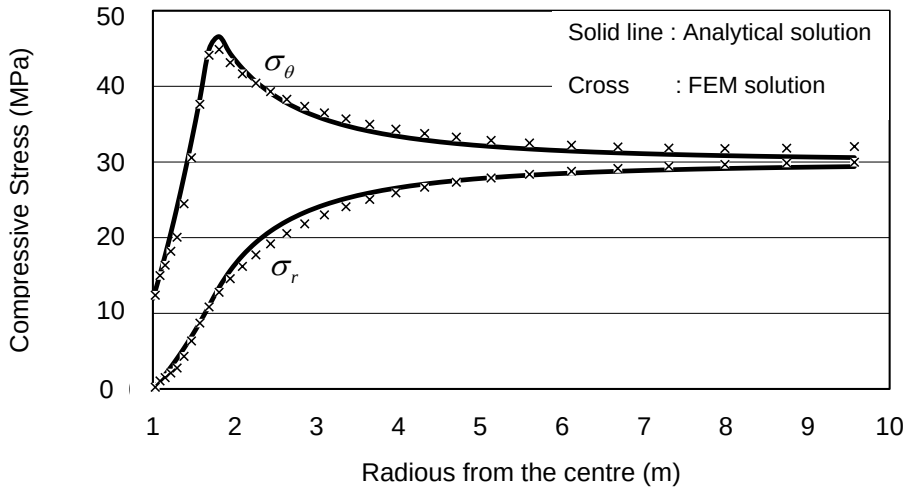

Figure 4.8 Comparison between FE program results and closed form solution for tangential and radial stresses and plastic zone extension

The above examples demonstrate the applicability of the developed FE code for plastic analysis. In the following section the program is used to analyse the plastic zone development due to injection into a porous zone.

4.5 Injection into elasto-plastic media

In the previous Chapter the results of injection into a porous formation assuming isotropic linear elastic behaviour for material have been presented. A 2D section of the model in *XZ* plane is shown in Figure 4.9. The porous formation has a rectangular cross-section in *XZ*-plane with a length of 80 m in *X*-direction, and a height of 40 m in *Z*-direction and strike of several hundreds of meter aligned in *Y*-direction. The midpoint depth of the porous formation in *Z*-direction is 500 m and the height of the porous formation is from 80.0 to 120.0 m from the bottom of the model. In *Z*-direction the model extends to the surface: this allows investigation of the surface induced incidences such as probable uplift or subsidence due to reservoir injection/depletion. The width of the porous formation in *X*-direction is from 160.0 to 240.0 m from the left side of the model. The model extends 200 m in both sides (overaly 400 m) in *X*-direction to ensure that it reaches to the out of the influenced zone. This model consists of 5936 nodes and 2860 isoparametric 8-noded finite elements.

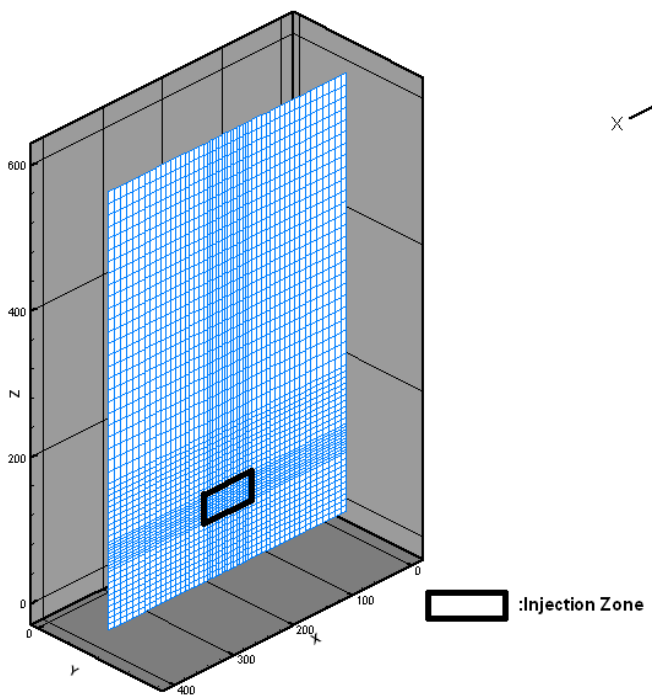

Figure 4.9 A 2D section in *XZ* plane and the location of the injected zone

A formation Young's modulus of 10GPa was assumed for the porous zone in this study. This value was used in the entire model within the reservoir section and also across the overburden and underburden. This represents a moderate stiffness for the rock. The simulation started by allowing the model to consolidate under gravitational force and then injecting into the porous formation up to 5.6 MPa (approximately 800 psi).

In particular, we are interested to determine the extension of the plastic zone due to injection into the porous zone. This is important from practical point of view in various applications of reservoir geomechanics such as casing collapse and fracture reactivation. We performed sensitivity analysis on cohesion value assuming a constant value of 30° for the internal friction angle. The injected pressure was assumed to be 5.6 MPa which was applied at five successive sub-steps. The iteration number to converge the model is tabulated in Table 4.1.

The results of this figure show how the extension of the plastic zone reduces as material cohesion increase. At cohesion of approximately above 1.6 MPa no plastic zone develops. Also, from this figure it is seen that two spots at the corners of the injection zone are the nucleation zone for the plastic zone. As the cohesion reduces the plastic zone increases and at low values of cohesion the two plastic zones developed at the two sides of the porous zone intersect and generate a large plastic

zone which further extends into the overburden and underburden formations. For cohesion values of smaller than 300 KPa the model does not converge, which means that the degree of plastification is too high.

Table 4.1 Iterations number to convergence for each model at five different sub-steps

Cohesion (MPa)	1	2	3	4	5	Total Iteration
0.3	5	12	16	16	22	71
0.4	2	10	12	17	17	58
0.5	2	8	12	12	15	49
0.6	2	6	10	12	14	44
0.7	2	2	9	12	11	36
0.8	2	2	7	10	12	33
0.9	2	2	6	9	11	30
1	2	2	2	8	10	24
1.1	2	2	2	7	9	22
1.2	2	2	2	6	9	21
1.3	2	2	2	2	8	16
1.4	2	2	2	2	7	15
1.5	2	2	2	2	6	14
1.6	2	2	2	2	2	10

The extension of plastic zone for different values of cohesions is shown in Figure 4.10.

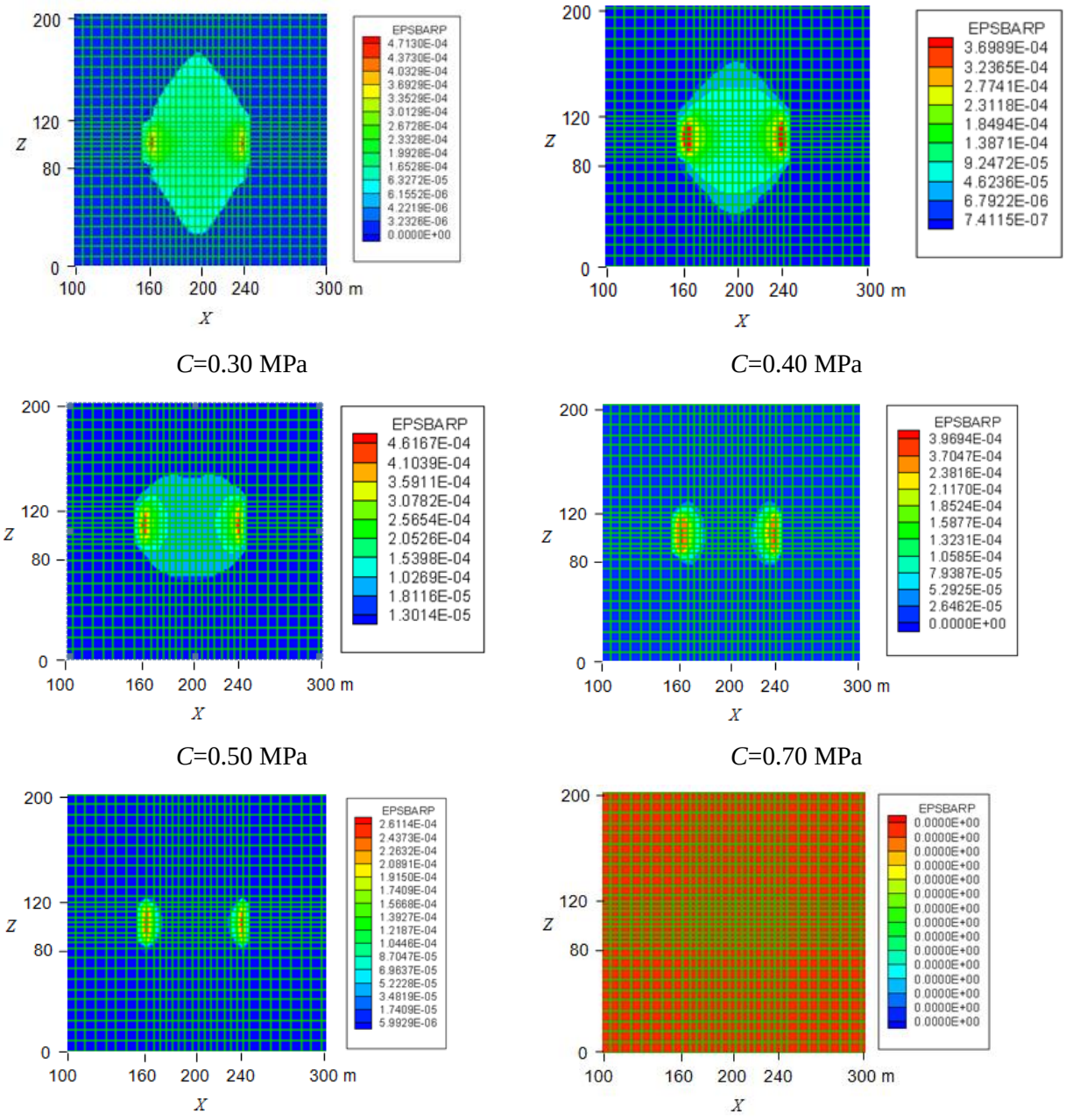

C=0.30 MPa

C=0.40 MPa

C=0.50 MPa

C=0.70 MPa

C=1.00 MPa

C=1.60 MPa

Figure 4.10 Reduction in plastic zone around the injected zone due to an increase in cohesion.

4.6 Summary

In this Chapter the elaso-plastic behaviour of geomaterials was studied. A 3D finite element code developed for elasto-plastic analysis which can use different constitutive models. The features of the code were explained and its validity was checked by analysing some simple case studies. Comparing to elasto-plastic analysis, the elastic analysis was used to calculate the stress, displacement and strain fields which are useful in predicting the high stress concentration zones and the direction of minor and major stresses and displacement pattern. This information is used for wellbore stability design and to identify the propagation direction of a hydraulic fracture. However, the elastic analysis does not provide any information about the failure or yielded zones. In this study, as one example, the elasto-plastic analysis was applied to study the yield zone development due to gas injection into a porous zone. The results indicated that for geomaterials with cohesion of less than 1.6 MPa the yield zones developed according to Drucker-Prager yield criterion. The lower the cohesion of the geomaterial, the larger the volume of the failure zones will be. For cohesion values of less than 300 kPa the entire model showed to be unstable numerically due to high degree of plastification.

5 Case Study: Analysis of injection into a porous sandstone reservoir

In this Chapter a case study is presented where injection induced stresses and displacements are analysed in a sandstone formation. Formation mechanical properties including elasticity and strength properties were extracted through a log-based analysis, which were made available to us. This data are used to investigate the stress and displacement changes due to CO_2 injection into this depleted sandstone reservoir. For comparison purposes the results of a simplified analytical model will be presented and its shortcomings are discussed. Then the results of finite element (FE) analysis assuming isotropic linear elastic and elasto-plastic behaviour for the geomaterials will be presented and discussed in detail.

5.1 Formations properties

The target formation is referred to as Formation X in this Chapter. The name of the well and the information of the field cannot be released due to confidentiality purposes. The input data which will be used in the analytical and finite element models in the following sections are summarized in Table 5.1. These parameters were estimated from a log based analysis through correlations with physical properties through petrophysical logs. These are the mechanical parameters corresponding to the intact rock. The mechanical properties present the average values across the target sandstone formation interval. In this Table the cohesion value was calculated indirectly based on the values of *UCS* and internal friction angle according to the procedure described comprehensively in Section 5.4.2. As is seen in this Table, the formation top of this sandstone is at about 840m and ends at 1500m. The injection zone is assumed 660m in this study to consider the worst scenario in terms of the surface uplift. This is while a narrower interval may be considered for the injection during different phases.

Table 5.1 Average mechanical properties in target sandstone formation X

Property	Formation X
Top of the formation (m) - MDRT	840
Thickness (m)	660
Density (g/cm^3)	2.25
Young's Modulus (GPa)	10
Poisson's Ratio	0.3
Internal friction angle (deg.)	25
UCS (MPa)	25
Cohesion (MPa)	7.96

5.2 Analytical model

In this section, analytical formula developed based on rock's poro-elastic behaviour is used to estimate the amount of ground surface uplift which maybe expected due to injection into Formation X.

Fjaer et al. (2008) developed the following equation to estimate the uniaxial subsidence due to depletion from a porous reservoir

$$\frac{\Delta h}{h} = \frac{1}{E_{sta}} \cdot \frac{(1+\nu_{sta}) \cdot (1-2\nu_{sta})}{(1-\nu_{sta})} \cdot \alpha \cdot \Delta P \qquad (5.1)$$

In this equation E_{sta}, ν_{sta}, α, ΔP and h are static Young's modulus, static Poisson's ratio, Biot coefficient, change of pore pressure and reservoir thickness, respectively. Δh is the amount of reservoir compaction due to depletion of the reservoir.

This analytical model and related equations were developed based on some initial assumptions. At first it is assumed that the deformation due to change in effective stresses takes place in three orthogonal directions (one vertical and two perpendicular horizontal directions) according to the Hook's law. It is assumed that the porous formation and produced zone extend infinitely or remarkably greater than the formation thickness in two horizontal directions, therefore it is restrained in these two horizontal directions. Finally, this model assumes that the total vertical stress

does not change during the period of pore pressure changing, i.e. depletion. It should be noted here that Fjaer et al. (2008) developed this analytical model for depletion of a porous reservoir. However, according to the mentioned assumptions used for developing this model it appears correct to apply it to estimate the amount of uplift due to injection into a porous formation. Therefore, as part of the studies in this work we apply equation 5.1 to estimate the amount of ground uplift due to CO_2 injection into Formation X. It is assumed that this sandstone layer is a depleted reservoir and CO_2 injection increases the amount of pore pressure up to 75% in four successive steps corresponding to 10, 25, 50 and 75 percentage of initial reservoir pressure at the centre of Formation X (i.e. approximately 12.0 MPa). For instance, in the third step, i.e. 50%, the injected pore pressure will increase up to 6.0 MPa.

Using data in Table 5.1, and applying equation 5.1 the maximum expected ground surface uplift for these four successive steps of pore pressure build up inside the injected interval, i.e. Formation X, were estimated and the results are shown in Table 5.2.

Table 5.2 Estimated uplift applying equation 5.1

Injection step	**Reservoir Thickness (m)**	**Initial reservoir pressure, P_i (MPa)**	**Injection pressure**		**Uplift Δh (cm)**
			ΔP (%)	**ΔP (MPa)**	
I	660	12.0	10	1.2	5.9
II	660	12.0	25	3.0	14.7
III	660	12.0	**50**	**6.0**	**29.4**
IV	660	12.0	75	9.0	49.1

As it will be discussed in the next section this ground displacement overestimates the amount of uplift due to the intrinsic assumptions considered in equation 5.1. The results of numerical simulations in the next section will demonstrate how this amount of displacement may reduce significantly if the model specifications are changed.

Based on the aforementioned assumptions of the analytical equation 5.1, the change in effective horizontal stress and vertical stress inside the injected zone due to change of pore pressure can be obtained as:

$$\Delta\sigma'_H = \Delta\sigma'_h = \left(\frac{\nu}{1-\nu}\right)\cdot\alpha\cdot\Delta P \tag{5.2}$$

$$\Delta\sigma'_V = \alpha\cdot\Delta P \tag{5.3}$$

Using these equations the magnitude of induced effective stresses corresponding to the four mentioned successive injection steps were calculated and the results are shown in Table 5.3.

Table 5.3 Changes of stresses due to injection applying equations 5.2 and 5.3

Injection step	**Initial reservoir pressure, P_i (MPa)**	**Injection pressure**		$\Delta\sigma'_H$ **or** $\Delta\sigma'_h$ **(MPa)**	$\Delta\sigma'_V$ **(MPa)**
		ΔP **(%)**	ΔP **(MPa)**		
I	12.0	10	1.2	0.51	1.2
II	12.0	25	3.0	1.29	3.0
III	12.0	**50**	**6.0**	**2.57**	**6.0**
IV	12.0	75	9.0	3.86	9.0

It should be noted that this analytical model suffers from some shortcomings. It is basically a unidirectional model of induced vertical displacement and it neglects some influential factors such as depth of the depleted/injected zone, mechanical properties of surrounding media especially overburden and arching effects which happens due to limited lateral extension of the depleted/injected zone. In addition, it gives no information regarding the influence of depletion/injection on immediate overburden and upper strata. As it will be discussed later the source of this shortcoming is the assumption of having infinite lateral extension for the injection zone in this analytical model. This assumption causes upward movement of the overburden strata without any induced stresses.

The bolded figures in Tables 5.2 and 5.3, corresponding to 50% injection pressure, are the values that we use in the following sections of this Chapter for comparison against numerical analysis which will be performed to estimate the induced displacements and stresses fields both inside the injected intervals and within surrounding formations. Similar analysis can be carried out for any other injection pressures.

5.3 Finite element simulations

In this section we investigate the effects of CO_2 injection up to 6.0 MPa (increasing pore pressure) into Formation X.

The finite element model was built and geomechanical properties of the Formation X according to Table 5.1 were attributed to the entire elements in the model. It was assumed that the injected zone extends vertically across the whole

section of the Formation X (i.e. from depth 840 m to 1500 m) and horizontally 100 m symmetrically around the vertical centerline of the model. The model extends 200 m in each side, i.e. 400 m in total in *X*-direction and 300 m within the underburden interval to ensure that it passes the influenced zone as shown in Figure 5.1. In *Z*-direction the model extends to the surface: this allows investigation of the surface induced incidences such as possible ground uplift due to injection into the porous formation. The porous reservoir formation is assumed to have a very large extension in *Y*-direction (formation strike assumed parallel to this direction) with limited dimensions in the other two directions (*X* and *Z* directions). Therefore, the plane strain condition is expected in two-dimensional sections perpendicular to *Y*-direction. To use the developed 3D program based on three-dimensional elements in this condition, the extension of the model in *Y*-direction was limited and all degrees of freedom parallel to *Y*-direction are fixed on sides perpendicular to the *Y*-axis.

At first, a mesh generator program was developed to produce the mesh for this three-dimensional model (elements and nodes) based on three-dimensional 8-noded isoparametric finite elements. As shown in Figure 5.1, the mesh generator program was developed in a way that it can create finer meshes near and inside the injected zone in order to analyse the rock behaviour within the and stress induced zone. It is rational to have larger elements at a distance beyond the zone of influence. This model consists of 2880 three-dimensional 8-noded isoparametric finite elements and a total of 6014 nodes. This number of elements and nodes is nearly the largest volume that could be handled with the available computing platform for this research including hardware (computer architecture, CPU and memory) and software (programming language software and compiler) capabilities and limitations. Models with finer meshes or with larger extension in three directions would have much larger number of elements and nodes. The mesh generator program can produce the mesh required in this situation but the developed finite element program encounters "stack overflow" run-time error due to the mentioned limitation of the available computing platform. However, remarkable effort was made to produce the acceptable rational element geometry (e.g. element size and aspect ratio) as much as possible considering model extension and the limitations of computing platform.

It should be noted that as it is seen in Figure 5.1 the mesh generator produced elements in a way that all nod's coordinates (*x*, *y*, *z*) are positive as working with positive values is easier for human being (not for computer). Therefore the *z* value is

not the depth of the certain point but it is (1800 m – depth). In another word, the horizon of z=0 is at a depth of 1800 m and the horizon of z=1800m is the ground level or free surface.

In terms of boundary condition all lateral sides of the model were restrained from movement in perpendicular direction to the side and only vertical sliding was permitted. The bottom of the model was fixed in vertical direction. The upper surface of the model is free since it is the ground level.

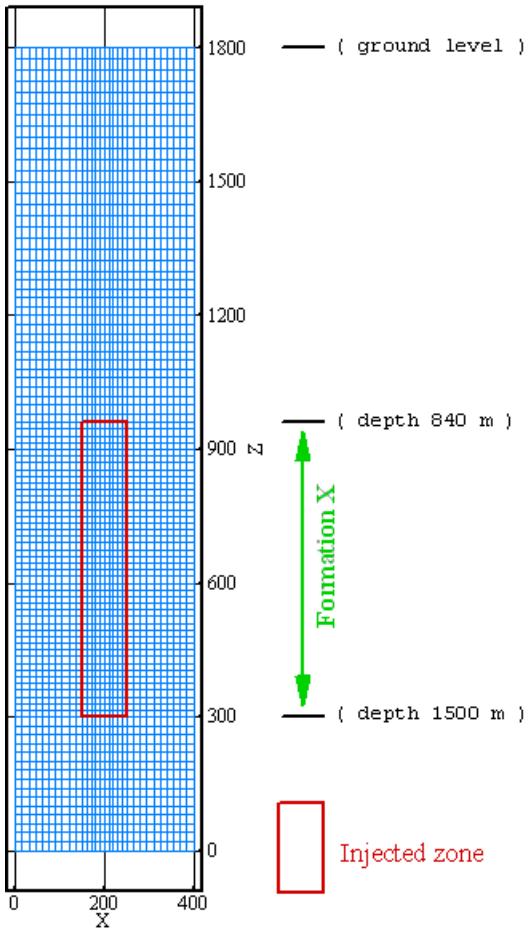

Figure 5.1 Finite element model geometry and the location of the CO_2 injected zone

5.3.1 Linear elastic finite element analysis

In this subsection the results of numerical simulations based on the assumption of linear elastic behaviour for Formation X are presented. The results corresponding to elasto-plastic formation behaviour due to CO_2 injection into this formation will be discussed in the next subsection.

Qualitative results

In this subsection we present qualitative discussions of the results obtained within an extracted section perpendicular to the *Y*-axis. In the next subsection some quantitative measures are presented. It should be noted that all stresses are expressed in Pascal unit.

The finite element simulation of CO_2 injection into Formation X consists of two successive steps. Firstly, the model was allowed to consolidate gravitationally based on the density and elastic properties of the material and it reached the preexisting or in-situ stresses. Then the pore pressure inside the injected zone was built up to 6.0 MPa.

Plots of vertical (σ_{zz}), horizontal (σ_{xx}) and shear (σ_{zx}) stresses after first step, i.e. gravitational consolidation step, are depicted in Figures 5.2 to 5.4, respectively. These results will be referred to as "Results **FEM-A**" in the following sections of this Chapter.

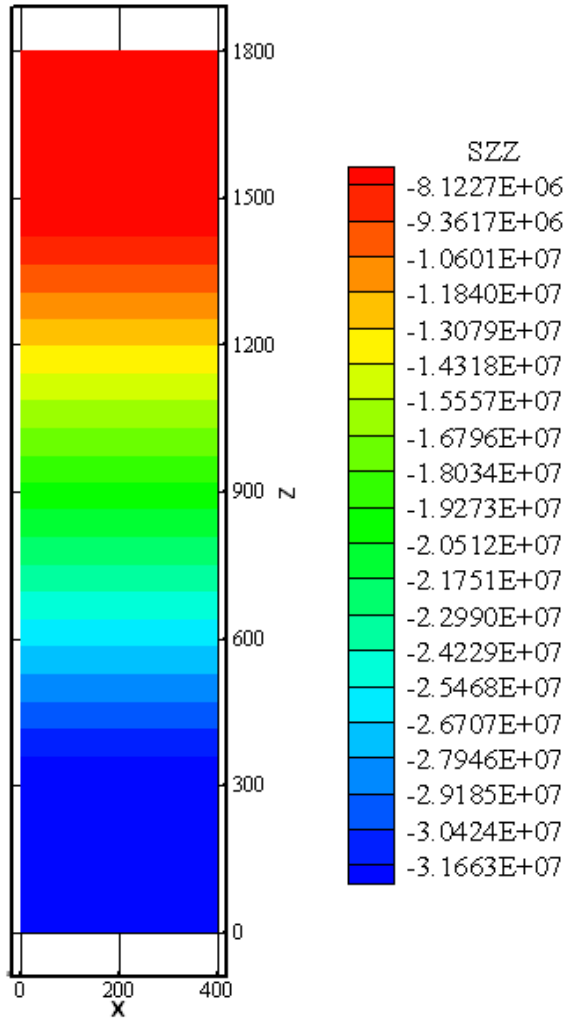

Figure 5.2 Vertical stress (σ_{zz}) after gravitational consolidation

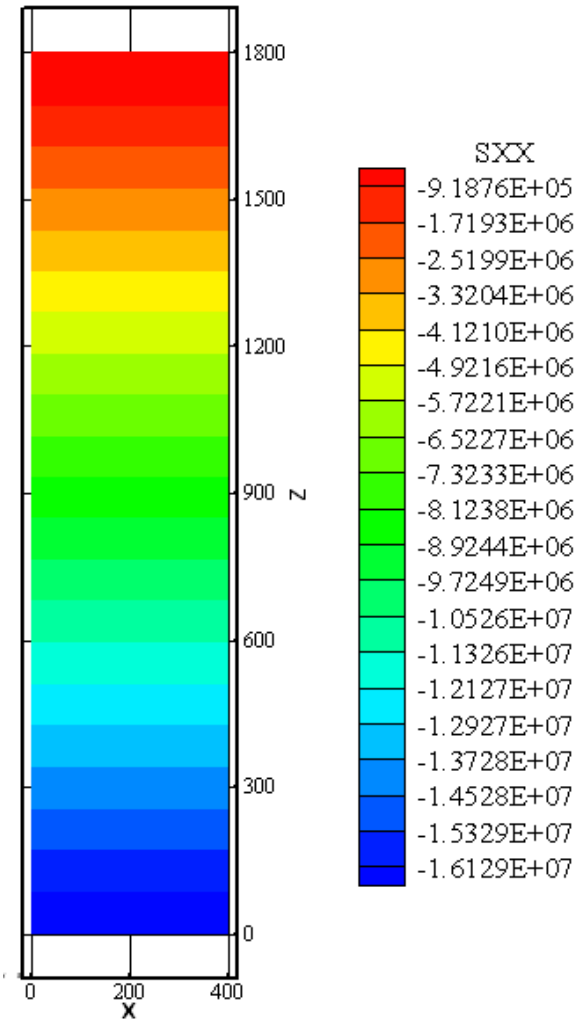

Figure 5.3 Horizontal stress (σ_{xx}) after gravitational consolidation

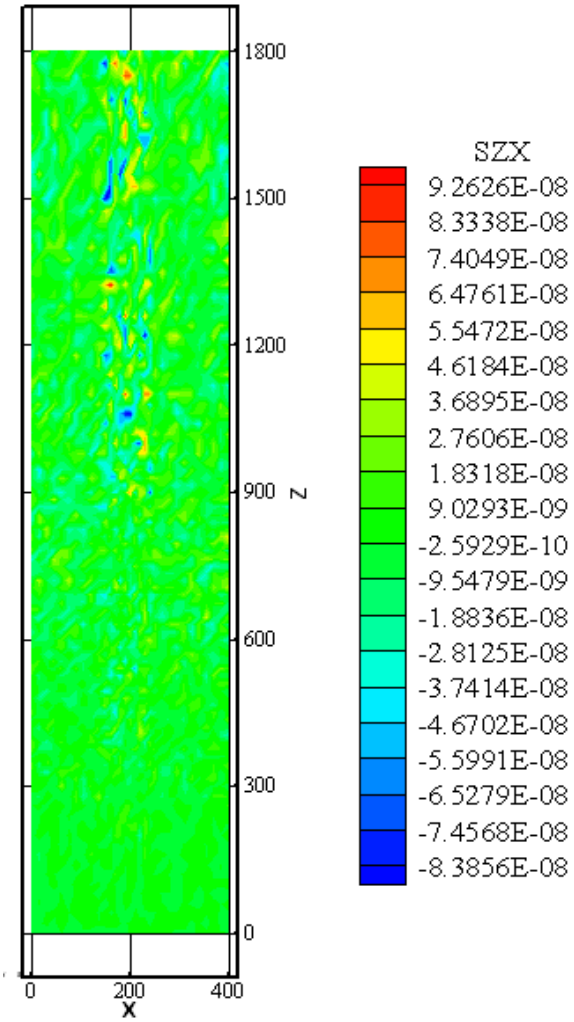

Figure 5.4 Shear stress (σ_{zx}) after gravitational consolidation

From the results presented in Figures 5.2 to 5.4 (Results **FEM-A**) it can be understood that the vertical and horizontal stresses resulted from gravitational consolidation are principle stresses since the shear stress in this plane is negligible (in the order of 10^{-8} Pa in Figure 5.4).

Plots of vertical (σ_{zz}), horizontal (σ_{xx}) and shear (σ_{zx}) stresses after gravitational consolidation plus injection into the injected zone are depicted in Figures 5.5 to 5.7, respectively. These results will be referred to as "Results **FEM-B**" in the following sections of this Chapter.

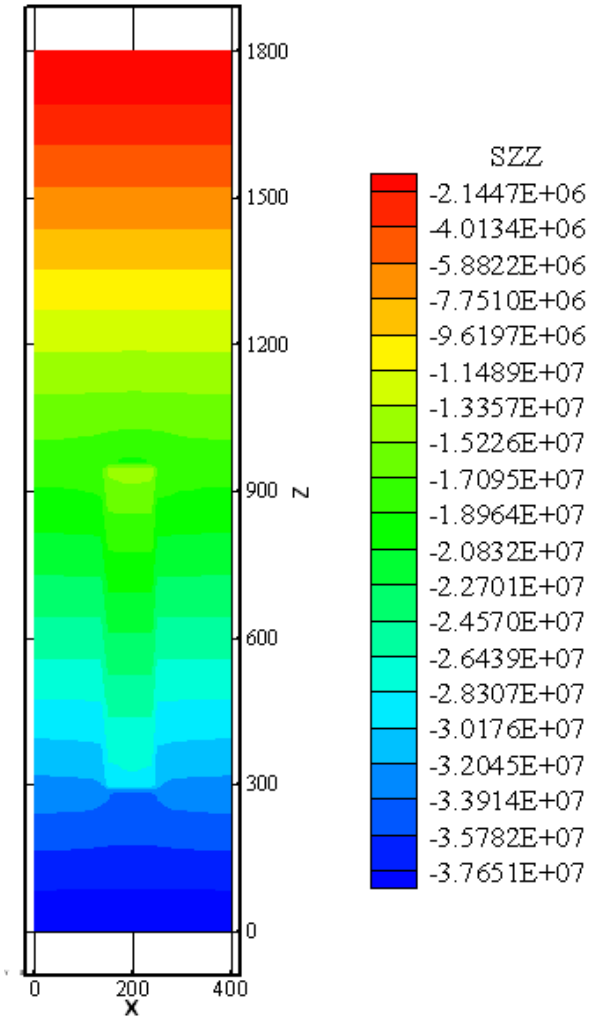

Figure 5.5 Vertical stress (σ_{zz}) after gravitational consolidation plus CO_2 injection

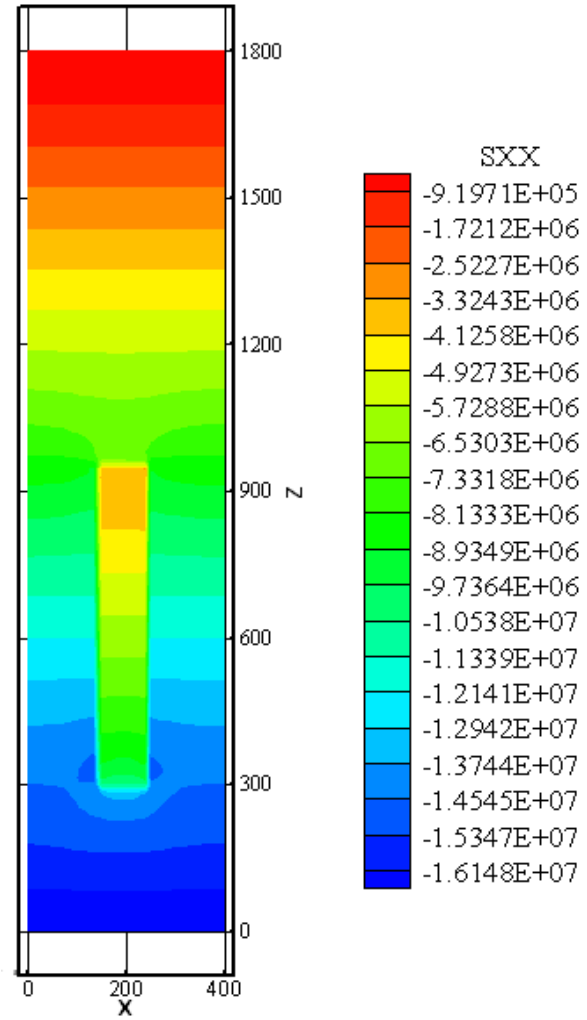

Figure 5.6 Horizontal stress (σ_{xx}) after gravitational consolidation plus CO_2 injection

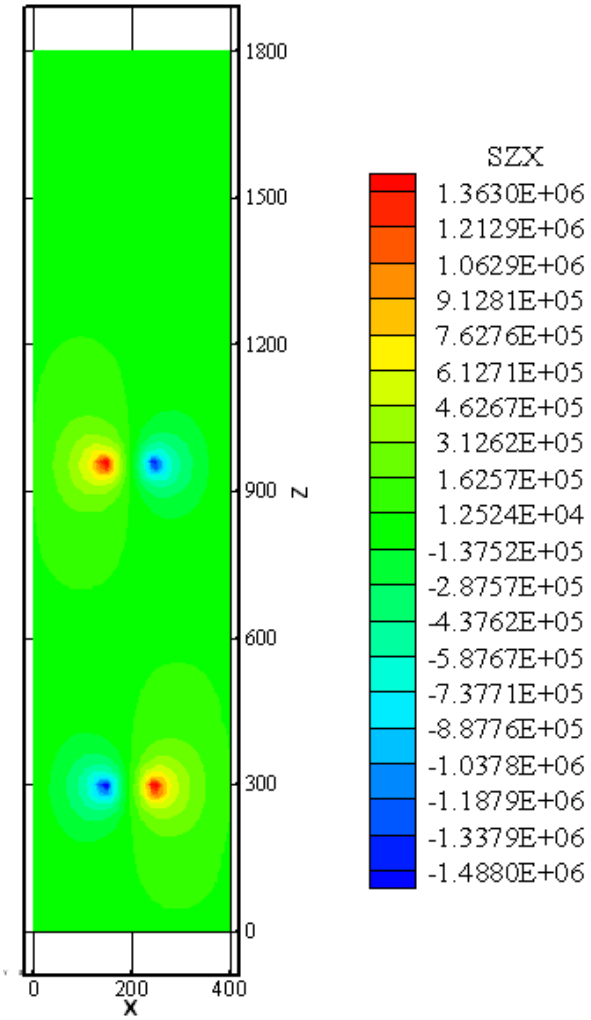

Figure 5.7 Shear stress (σ_{zx}) after gravitational consolidation plus CO_2 injection

From the results presented in Figures 5.5 to 5.7 (Results **FEM-B**) the following conclusions can be drawn:

- Injection results in increasing the effective vertical stress inside the injected zone as well as decreasing the vertical stress in immediate overburden and underburden (Figure 5.5). The observation from Figure 5.5 indicates that the injection induces a tensile vertical stresses inside the porous formation as well as its sideburden (note that tensile stress is considered positive). It also induces compressive vertical stresses in immediate overburden and underburden intervals.
- Injection results in increasing the effective horizontal stress inside the injected zone as well as decreasing the horizontal stress in the immediate sideburden (Figure 5.6). From practical point of view this means that the injection induces a tensile horizontal stresses inside the porous formation as well as in immediate

overburden and underburden and induces compressive stresses within the sideburden.

- Nucleation of remarkable shear stress near to injected zone shows that the vertical and horizontal stresses near this zone are no longer principle stresses (Figure 5.7), i.e. injection makes the principle stress direction to rotate around the injected zone.

In order to highlight the effect of CO_2 injection itself on the model, the gravitational stress components was discarded and the corresponding results are shown in Figures 5.8 to 5.10, respectively. These results will be referred to as "Results **FEM-C**" in the following sections of this Chapter. Discarding the gravitational effect is an acceptable practice for elastic linear analysis as superposition principle is valid in linear elastic constitutive behavior of material in such models.

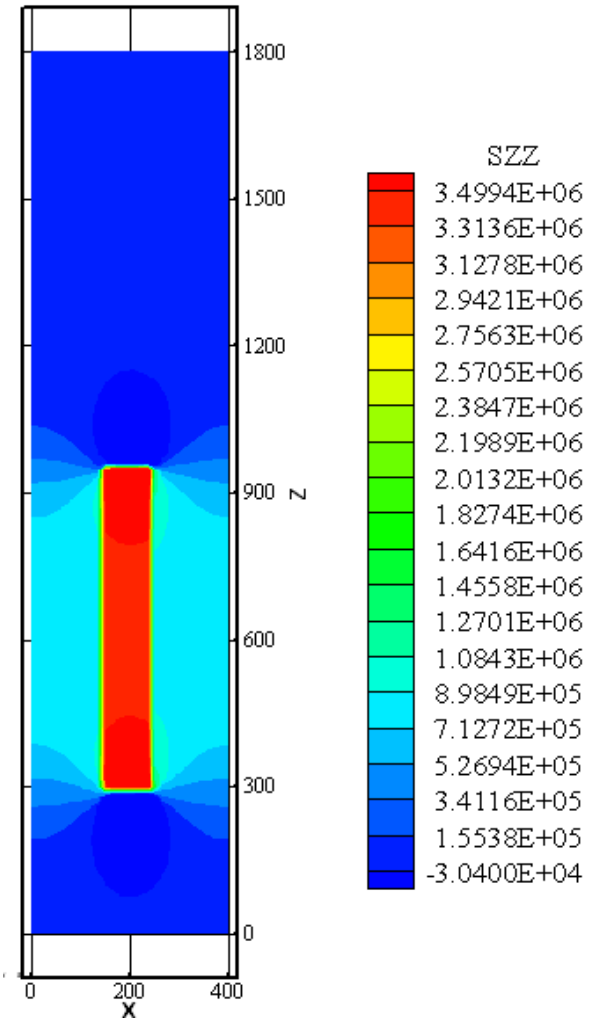

Figure 5.8 Induced vertical stress (σ_{zz}) due to CO_2 injection

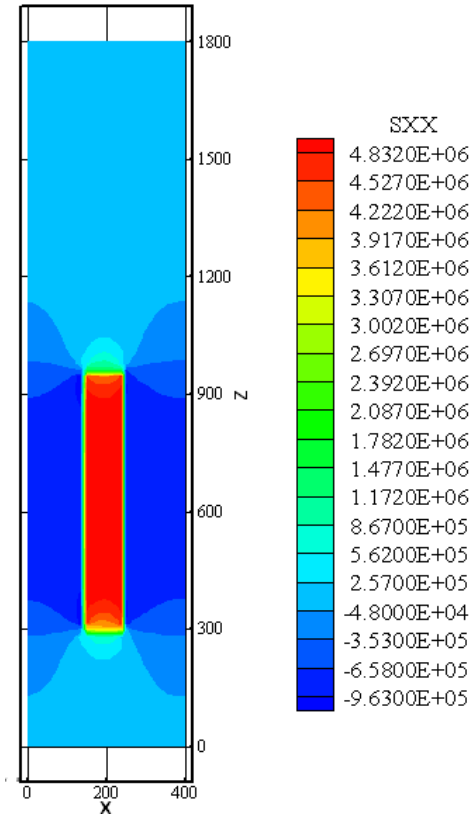

Figure 5.9 Induced horizontal stress (σ_{xx}) due to CO_2 injection

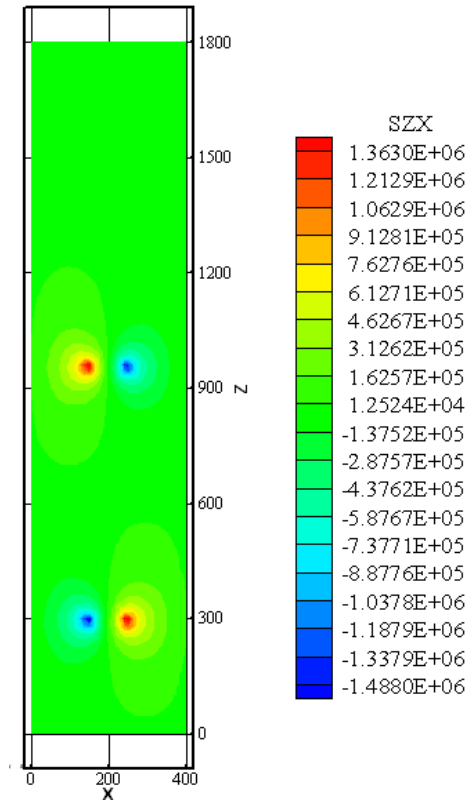

Figure 5.10 Induced shear stress (σ_{zx}) due to CO_2 injection

The net effects of CO_2 injection and induced stresses field which are shown in Figures 5.8 to 5.10 (Results **FEM-C**) after discarding the stresses due to gravitational consolidation confirm the conclusions which were made based on the results presented in Figures 5.5 to 5.7.

- Figure 5.8 shows that the CO_2 injection from vertical stress point of view develops a remarkable tensile stress zone inside the injected zone and induces tensile stress relaxation in sideburdens but it compresses the immediate overburden and underburden.
- Figure 5.9 shows that the CO_2 injection from horizontal stress point of view develops a remarkable tensile stress zone inside the injected zone and induced tensile stress relaxation in overburden and underburden but it has compressive influences on the immediate sideburdens.
- Figure 5.10 shows that the principle reason of shear stress field development in the model is the CO_2 injection. The amount of this shear stress increases remarkably in comparison to the gravitational consolidation model (increases from the order of 10^{-8} Pa in Figure 5.4 to the order of 10^{+6} Pa in Figure 5.10).

Quantitative analysis along two profiles passing through the center of injected zone (Results FEM-C)

To see quantitatively the effects of CO_2 injection in the model two profiles I and II were extracted from the finite element model results, to analyze the changes in stress and displacements. These profiles pass through the center point of the injected zone: Profile I is a horizontal profile at Z=630 m (depth 1170 m) and Profile II is a vertical profile at X=200 m as shown in Figure 5.11. Again the gravitational consolidation effect has been discarded (Results **FEM-C**) to highlight the induced effects of CO_2 injection process. The results of various analyses conducted along these two profiles are given in Figures 5.12 to 5.14.

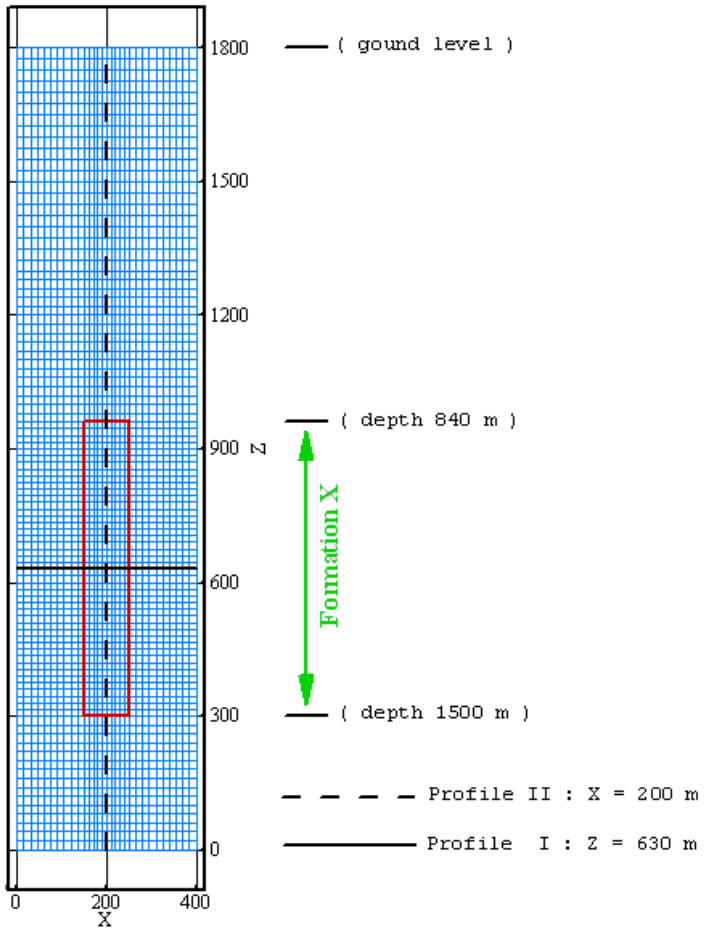

Figure 5.11 Position of Profiles I and II used for data analysis

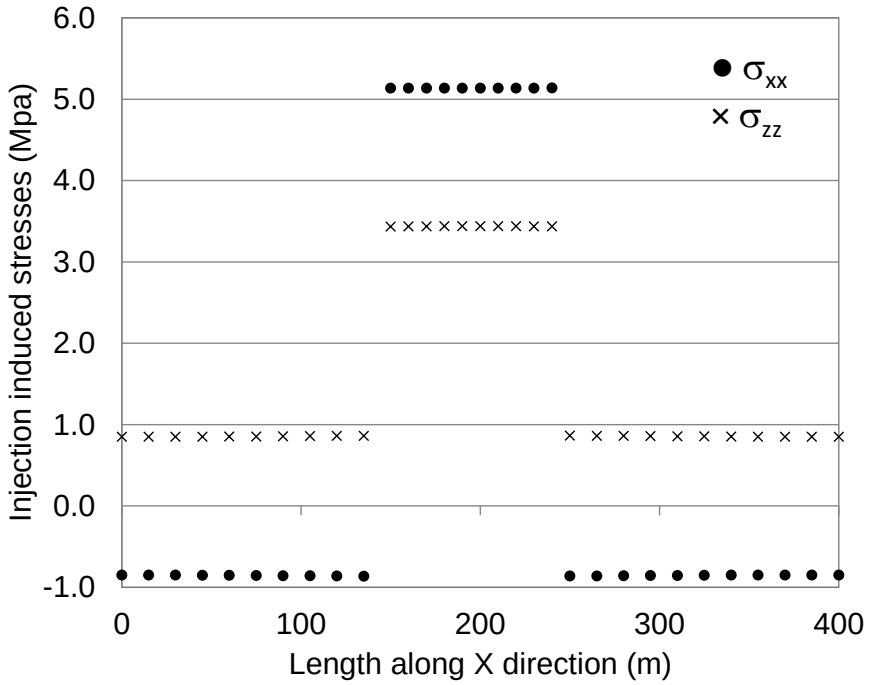

Figure 5.12 Injection induced stresses σ_{xx} and σ_{zz} along Profile I

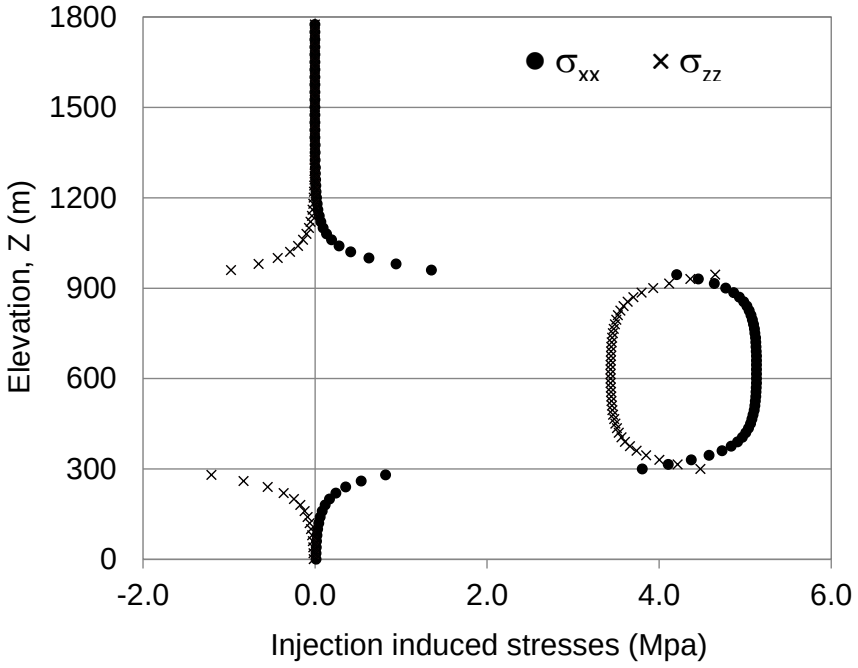

Figure 5.13 Injection induced stresses σ_{xx} and σ_{zz} along Profile II

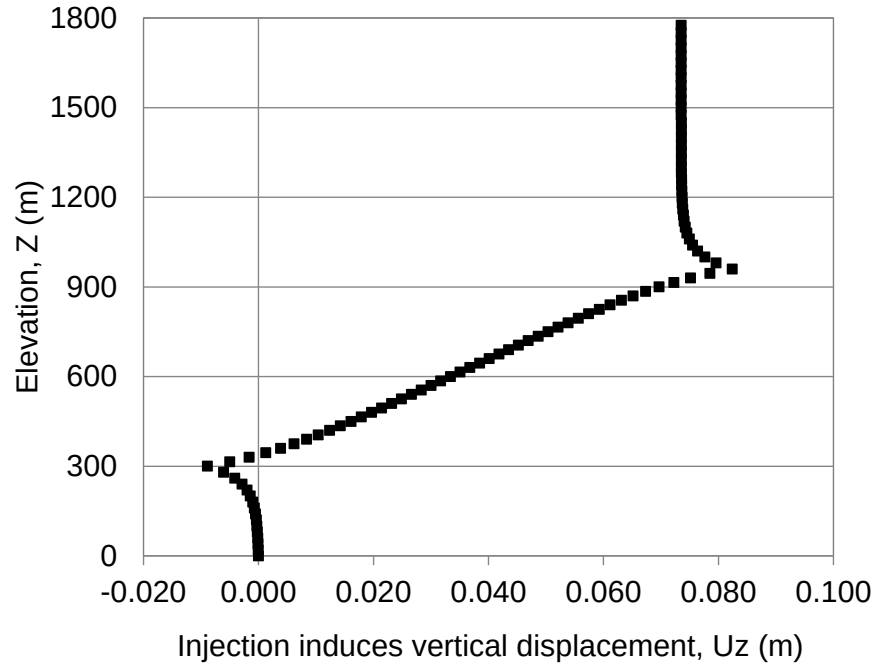

Figure 5.14 Injection induced vertical displacement U_z (m) along Profile II

The results of these figures, which are based on "Results **FEM-C**", confirm the qualitative conclusions made in the previous subsection:

- Figure 5.12 shows that the CO_2 injection induces horizontal compressive stresses in sideburdens (see changes in σ_{xx}) and results in stress relaxation with respect

to vertical stress (σ_{zz}). This figure also shows that CO_2 injection develops a tensile stress zone inside the injected zone (from *X*=150 m to *X*=250 m) in both vertical and horizontal directions.

- Figure 5.13 shows that CO_2 injection compresses the immediate overburden and underburden in vertical direction (induced compressive vertical stress σ_{zz}). It also induces tensile stress zones in immediate overburden and underburden and causes stress relaxation in these zones from horizontal stress point of view. The results of this Figure also show that CO_2 injection develops tensile stress zone inside the injected zone (from *Z*=300 m to *Z*=960 m) in both vertical and horizontal directions.
- Figure 5.14 shows that the injection displaces the immediate underburden downward but due to free surface boundary at the upper part of the model the injection results in uplift of most areas of the injected zone and overburden. The amount of uplift reaches a constant value at approximately *Z*=1200 m (equivalent to a depth of approximately 600 m). The uplift at ground level is 7.3 cm.
- The results shown in Figure 5.12 (Profile I) in comparison to those of Figure 5.13 (Profile II) reveal interesting findings. As it is seen in Figure 5.12, the values of induced stresses show no noticeable changes and follow a constant trend in both inside as well as sideburden zones which is in contrast to the results shown in Figure 5.13. For Profile II the impact due to injection becomes more pronounced as getting closer to the injected zone. This has resulted from a remarkable height of the injected zone (660 m along *Z* direction) versus a limited width (i.e. 100 m along *X* direction). In another word, the injected zone is a column with its height being about six times greater than its horizontal width. This structure geometry for the injected zone causes the behavior similar unidirectional behavior in horizontal direction at points near to the center of the injected zone: this would be more influencing on Profile I which passes through the center of the injected zone.

Practical remarks

Based on the analysis results obtained using finite element simulation which were discussed qualitatively and quantitatively in preceding subsections some important aspects about the effects of CO_2 injection into Formation X are listed below:

- The injection induces tensile stresses inside the injected zone in both horizontal and vertical directions (see Figures 5.12 and 5.13). In another word, it releases to some extent the magnitudes of preexisting, i.e. in-situ, horizontal and vertical compressive stresses inside the injected zone. Therefore the applied load on the wellbore and casing across this interval will be decreased especially in horizontal directions which are more beneficial in terms of the stability of vertical wells.
- The release of stresses due to injection inside the injected zone, which results in a decrease in effective vertical and horizontal compressive stresses magnitudes, exacerbates the stability of near to horizontal and near to vertical preexisting major frictional fractures or fault planes in this zone. This is because the normal stress to the fracture or fault plane will reduce, which in turn increases the instability risks. This reduction on the effective compressive stress in horizontal direction will ease the potential for initiation of near to vertical hydraulic fractures inside the injected zone.
- The injection induces compression stresses in vertical direction in immediate overburden (see Figure 5.13). In another word, it has a compressive effect in this area and enhances the magnitude of preexisting effective vertical stress regime. In terms of the stability condition of near to vertical preexisting frictional major fractures or fault planes, this effect will be beneficial. However, in terms of wellbore and casing stability, this effect enhances the applied compression load in vertical direction on near to vertical wells which should be studied for potential buckling of casing or compression failure of immediate surrounding rocks to the wellbore.
- The injection induces tensile stresses in horizontal directions in immediate overburden (see Figure 5.13). In another word, it decreases the magnitude of preexisting effective compressive stress regime in this area. In terms of the stability condition of near to vertical preexisting frictional major fractures or fault planes, this effect is detrimental since for this type of preexisting fracture planes the effective horizontal stress acts as normal stress to the fracture plane

and its reduction means more risk for sliding. However, in terms of wellbore and casing stability this induced reduction in effective horizontal stress in immediate overburden is beneficial since it mitigates the applied load in horizontal directions to the near to vertical wells. This reduction on the effective compressive stress in horizontal direction in immediate overburden interval results in less pressure required to open a hydraulic fracture.

Quantitative analysis along Profile II (Results FEM-A and Results FEM-B)

Through numerical simulations conducted in this study the effective stress regimes before and after injection along vertical Profile II was identified based on "Results **FEM-A**" and "Results **FEM-B**", respectively. The main difference of the results of this subsection with the results presented in the previous subsection is that the combined effects of gravitational consolidation and injection can be seen simultaneously. In the previous subsection the contribution of the pre-existing stress regime, which is due to gravitational consolidation step in this study, was discarded to highlight the effects of injection itself. Figures shown in this subsection have a subtle difference with other figures extracted along Profile II. This difference is that the elevation (Z) was displaced by the amount of depth (d=1800-Z) in order to make the observation of the trend of the stress regimes before and after injection easier.

The results of vertical and horizontal stresses regimes extracted along Profile II at the end of gravitational consolidation step (Results **FEM-A**) are shown in Figure 5.15.

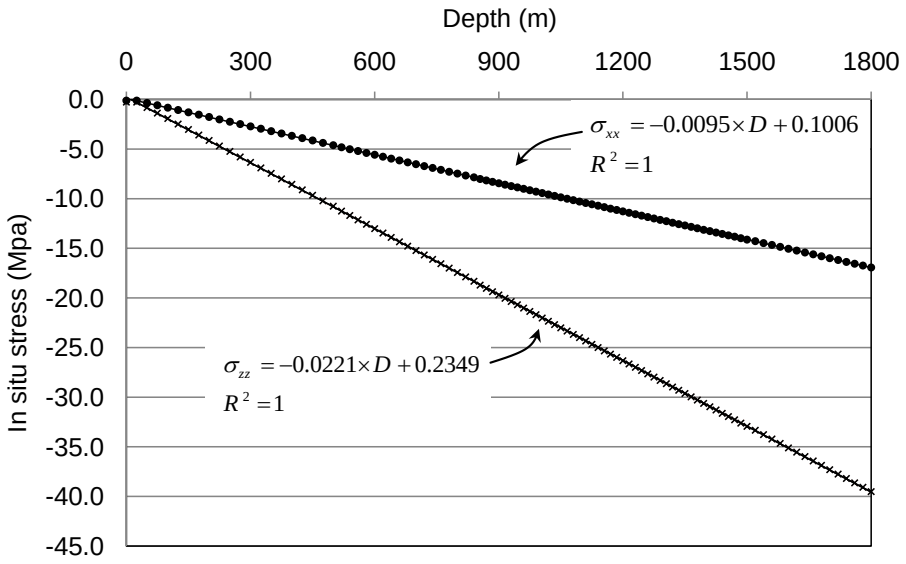

Figure 5.15 The trend of pre-existing stress regime due to gravitational consolidation for vertical and horizontal stresses

According to the results in Figure 5.15 it is observed that at the end of gravitational consolidation step the absolute gradient of vertical stress is 0.0221 MPa/m which is in exact agreement with the specified density and gravitational acceleration, i.e. $(2250 \times 9.81)/10^6 = 0.02207$ MPa/m. As it is seen in this figure, the absolute gradient of horizontal stress regime is 0.0095 MPa/m. Considering a Poisson's ratio of 0.3 and the gradient of vertical stress regime as 0.0221 MPa/m, the ratio of the horizontal to the vertical stress regime gradients under gravitational consolidation condition based on the FE results, i.e. $(0.0095/0.0221) = 0.429$, is comparable to its corresponding analytical value, i.e. $(\nu/(1-\nu)) = (0.3/0.7) = 0.429$. Both of these quantitative agreements show the validity of the FE simulation results again at a field-scale model. Based on the results of this figure it is seen that the pre-existing stress regime is compressive all over Profile II for either vertical or horizontal stresses which is rationally predictable.

Figure 5.16 and Figure 5.17 show the absolute magnitude of stress regimes before and after injection, respectively. Figure 5.18 shows these two figures for comparison purposes.

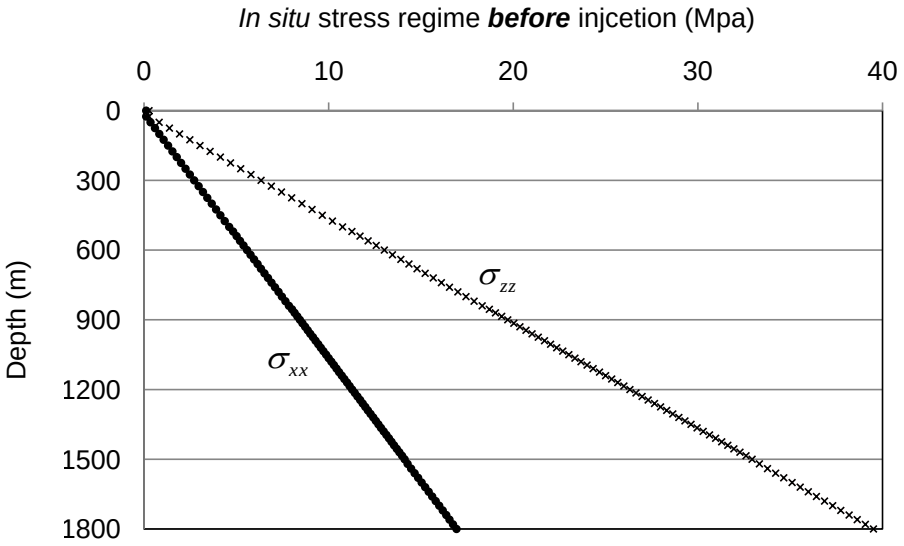

Figure 5.16 The stress regime before injection along Profile II

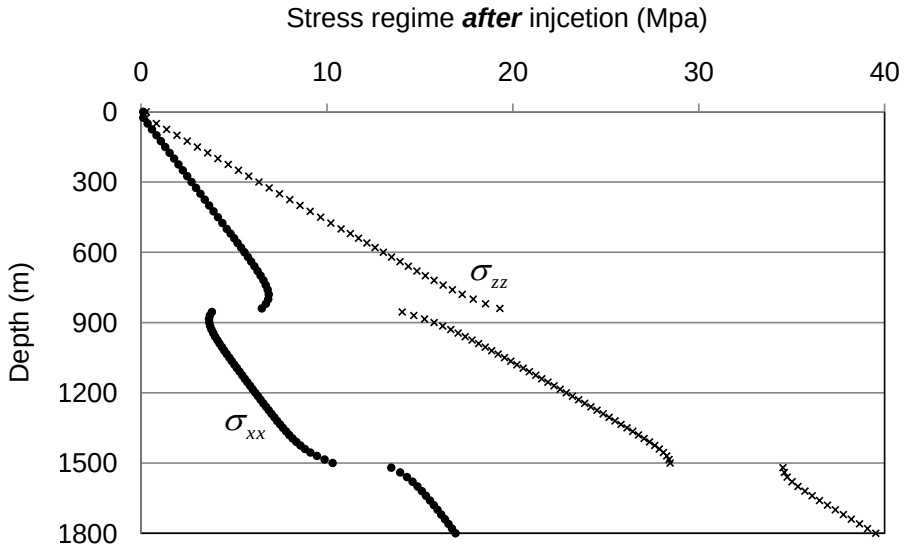

Figure 5.17 The stress regime after injection along Profile II

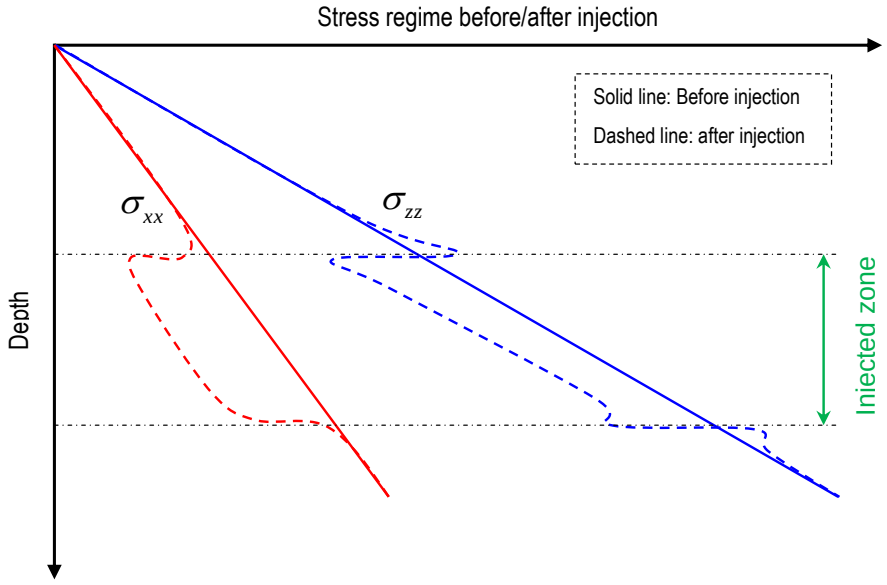

Figure 5.18 Stress regime change due to injection into a porous reservoir

Figure 5.18, which was obtained from the results of FE simulations, summarizes the trend of stress regime before and after injection in the presence of the effects of pre-existing gravitational consolidation stress regime along Profile II with respect to depth and location of the injected porous zone. It shows again the tensile nature of induced stress due to injection inside the injected zone which correspondingly means the reduction of pre-existing compressive stress in this interval. In addition the results of this figure also show that the effect of induced stresses on the immediate overburden along Profile II. These results are in agreement with detailed discussions presented before.

Quantitative analysis along three horizontal profiles located in immediate overburden

In order to study the effect of injection on stress and displacements of overburden layers the results of induced displacements as well as induced effective stresses along three horizontal profiles III, IV and V located in immediate overburden (see Figure 5.19), are shown in Figures 5.20 to Figure 5.22, respectively.

It should be mentioned that according to the results shown in Figures 5.13 and 5.14 it appears that the influenced zone extends vertically from elevation Z=960 m to approximately Z=1200 m in the model above the injected zone. It is noted again that the injected zone is limited vertically between Z=300 m and Z=960 m as well as horizontally from X=150 m to X=250 m. In order to have this horizontal profiles inside the influence zone at the immediate overburden their location was chosen at Z= 980 m, Z=1000 m and Z=1020 m for Profiles III to V, respectively.

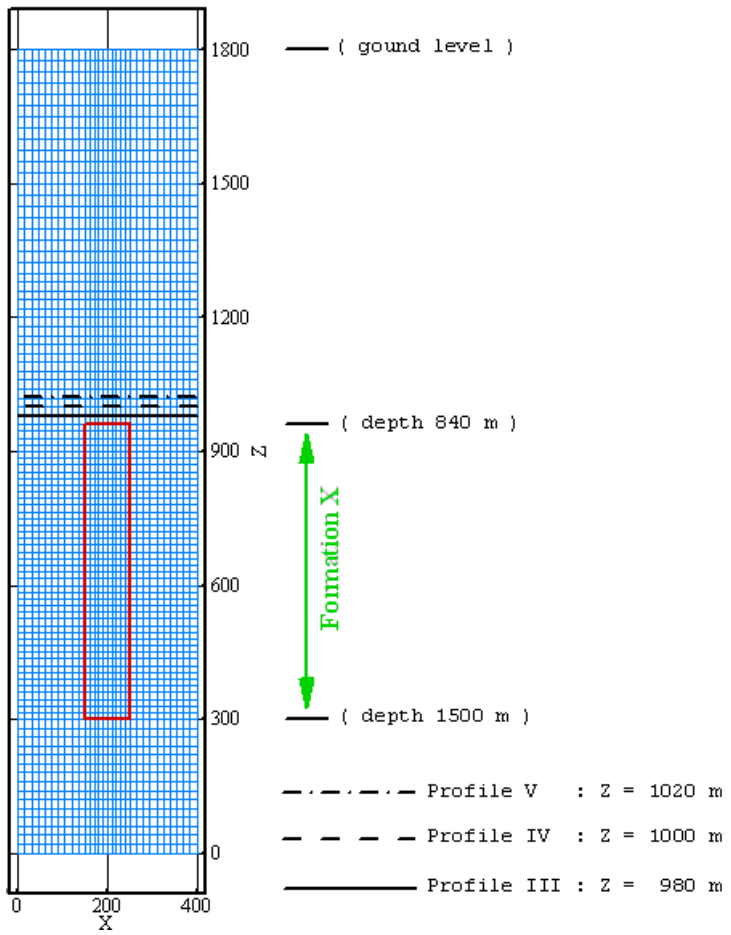

Figure 5.19 Location of Profiles III, IV and V in the immediate overburden

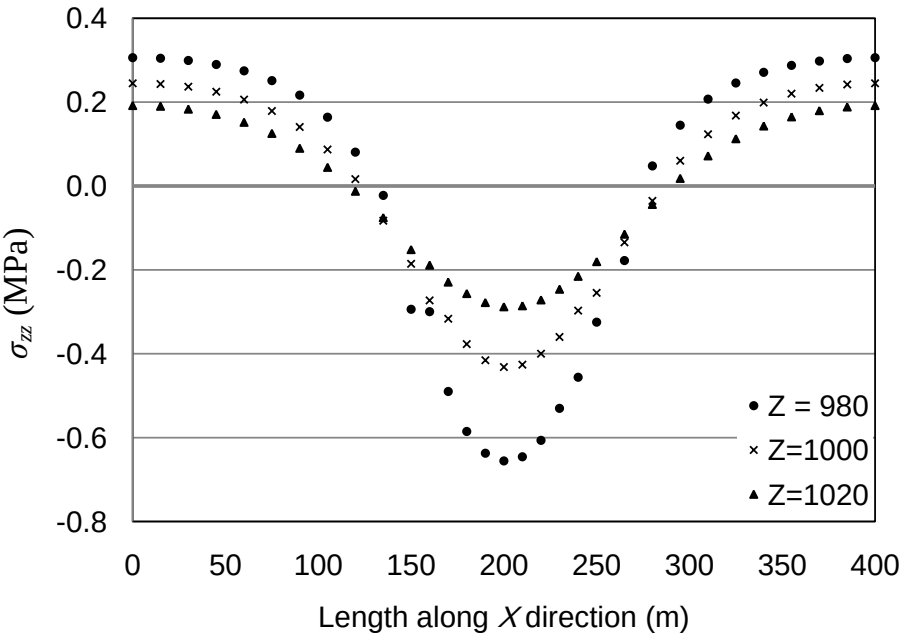

Figure 5.20 Induced vertical stress, σ_{zz} , along Profiles III, IV and V located in the immediate overburden

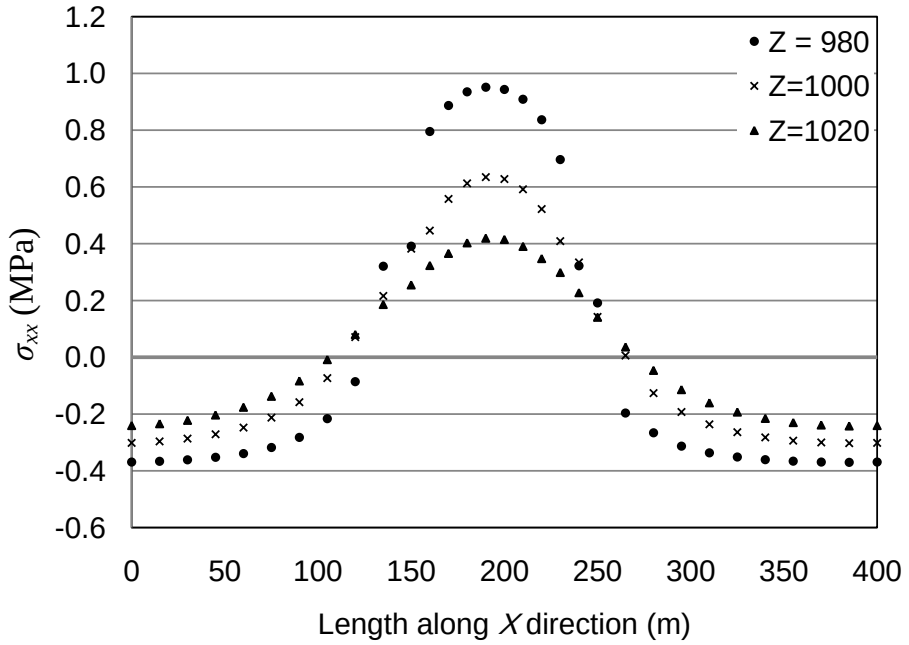

Figure 5.21 Induced horizontal stress, σ_{xx} , along Profiles III, IV and V located in the immediate overburden

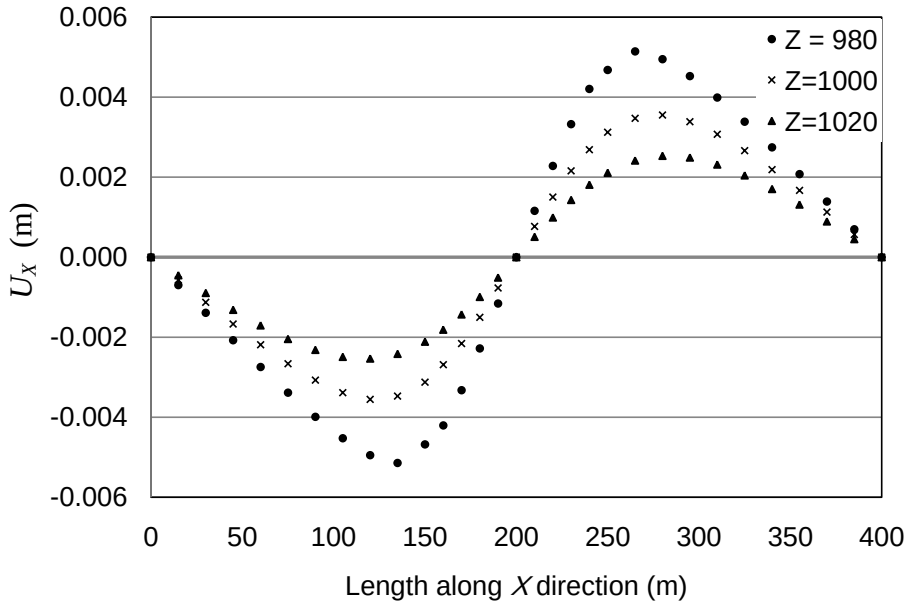

Figure 5.22 Induced horizontal displacement, U_x , along Profiles III, IV and V located in the immediate overburden

From the results presented in Figures 5.20 to 5.22 the following conclusions can be drawn about the influences of CO_2 injection on the immediate overburden:

- Figures 5.20 and 5.21 verify the conclusion presented in the previous subsection about the pattern of induced vertical and horizontal stresses due to injection. The

results show that the injection induces compressive vertical stress and tensile horizontal stress regimes at the centre part of the immediate overburden. These two figures reveal that these patterns of induced stress regimes are valid for the centre part of the immediate overburden but not the lateral parts. This is why this conclusion is not observed in the results corresponding to Profile II (see Figure 5.13) since it passes through the vertical centreline of the model and the injected zone and it does not provide any information about the lateral part of the immediate overburden. The horizontal extension of the centre part of the immediate overburden is approximately similar to the horizontal extension of the injected zone itself i.e. approximately from X= 150 m to X =250 m. In two lateral parts of the immediate overburden the induced stress regime is opposite to that of the centre part for both induced vertical and horizontal stresses. As an instance considering Figure 5.20, while the injection induces compressive vertical stress at the top of the injected zone in the centre part of the immediate overburden it induces tensile vertical stress at the two left and right lateral parts of the immediate overburden. It can be said that the induced vertical stress regime changes from compressive stress at the centre part to the tensile stress at the two lateral parts. A similar conclusion is seen in Figure 5.21 for induced horizontal stress regime in this area of the model. The change in the induced stress regime of the centre part and two lateral parts of the model stems from the effects of far field condition which the model is exposed to. While the upper side of the model is free to move in all three directions, since it is ground surface, the lateral sides of the model (X=0 and X=400 m) are restrained in horizontal direction and the bottom side of the model is restrained in all three directions as discussed earlier since they model the far field condition which is based on the assumption that they are out of the influenced zone due to injection. As an instance, when injection pushes the centre part of the immediate overburden upward vertically and causes compressive stress regime in vertical direction, the rocks at the lateral parts resist moving freely upward and therefore a tensile stress regime in vertical direction is developed at the lateral parts. This phenomenon is similar to the well-known arching effect. The same concept is applicable to the observed contrast for induced horizontal stress regime in the immediate overburden due to injection.

- Figure 5.22 reveals another interesting concept about the pattern of induced horizontal displacement field at the immediate overburden. According to the results shown in this figure, the absolute magnitude of horizontal displacement decreases towards the centre of the model as well as the outer lateral boundaries, the former stems from the symmetry of the model and the latter is caused by the far field condition which exhibits that these lateral parts are out of the injection influenced zone. However, the absolute magnitude of the induced horizontal displacement reaches the highest values at two regions which are located approximately at the top of the lateral borderlines between the injected zone and lateral sideburdens.
- The results corresponding to the displacements of immediate overburden show that the influences of the injection decreases gradually moving upward which is rationally predictable.

Simulation versus analytical results

The finite element simulation results showed a ground uplift of approximately 7.3 cm according to Figure 5.14 and discussions presented in the previous subsection. This is much less than the value of 29.4 cm obtained using analytical model (see Table 5.2 – Injection step III). In addition according to Figure 5.13 based on the finite element simulation results, the induced effective horizontal stress inside the injected zone is variable with the average and most frequently magnitudes of equal to 4.93 MPa and 5.10 Mpa, respectively. Both the range of the variability and the magnitude of these values are in contrast with the corresponding estimated stresses based on the analytical model (see Table 5.3 – Injection step III, 2.57 MPa in the fifth column). Similar discrepancy is observable related to the magnitude of induced effective vertical stress inside the injected zone. According to Figure 5.13 based on the finite element simulation results, the magnitude of this stress is variable over the depth of the injected zone with the average and most frequently magnitudes of equal to 3.63 MPa and 3.44 MPa, respectively. These are in contrast to the results obtained using the analytical model (see Table 5.3 – Injection step III, 6.0 MPa in the sixth column). The main reason for these discrepancies relies in one of the initial assumptions in the development of the analytical model by Fjaer et al. (2008). As mentioned in Section 5.3 it is assumed that the porous reservoir as well as injected zone extends infinitely in horizontal directions which is in contrast to the geometry of the injected zone

considered in the finite element model built in the previous subsection where it extended laterally just 100 m in the horizontal direction at the center of the model.

In order to clarify the above concept in further detail, a new finite element model was built. All the geometry, material properties and boundary conditions were kept unchanged but in the new model the injected zone was extended horizontally to the entire model (i.e. from X=0 to X=400 m) as shown in Figure 5.23.

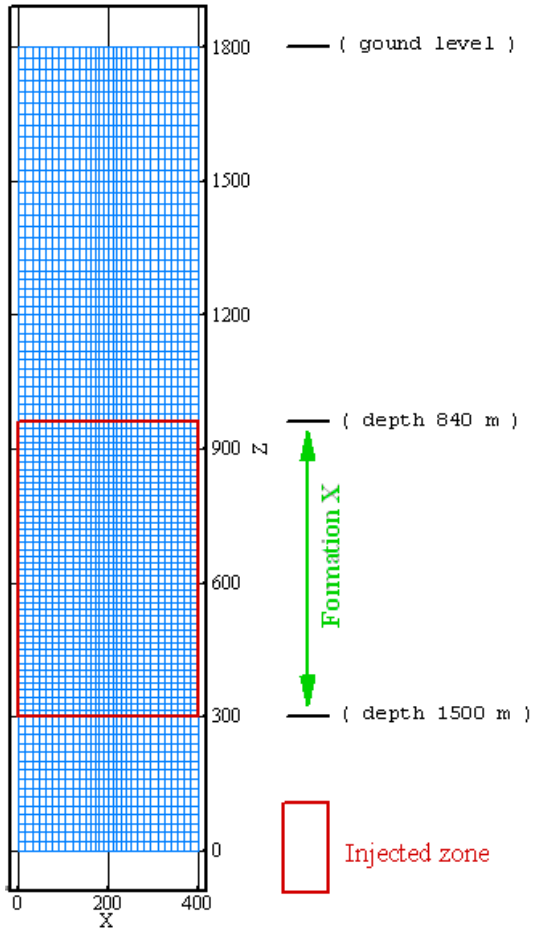

Figure 5.23 Finite element model with laterally extended injected zone (X=0 to X=400 m)

Again, the effect of gravitational consolidation was discarded and the results for induced vertical displacements and induced vertical and horizontal stresses due to injection into Formation X along Profile II are presented in Figure 5.24 and Figure 5.25. Based on the results shown in these two figures the following conclusion can be made:

- From Figure 5.24 it is seen that the model moves upward and the amount of uplift for entire overburden as well as ground surface is 29.4 cm, which is in complete agreement with the results of analytical model obtained from equation 5.1 (see Table 5.2 – Injection step III).

- From Figure 5.25 it is observed that the amounts of induced effective vertical and horizontal stresses are constant all over the injected intervals (from Z=300 m to Z=960 m) similar to the concept introduced by the analytical model which indicated that there is no variation in these amount across the injected interval. In addition, this figure shows that the amounts of induced effective horizontal and vertical stresses inside the injected zone are 2.57 MPa and 6.00 MPa, respectively, which are in exact agreement with the results obtained from analytical model using equations 5.2 and 5.3 (see Table 5.3 – Injection step III, fifth and sixth columns data).
- As it is seen in Figures 5.24, in this new FE model the amount of uplift is constant all over the overburden strata (in contrast to Figures 5.20 and 5.28). In addition, Figure 5.31 indicates that there are no induced stresses in both horizontal and vertical directions in the overburden strata in the results of this new FE model: this is in contrast to the results shown in Figures 5.13, 5.20 and 5.21, which is due to the assumption of having infinite lateral extension of the injected zone. In another word according to the results of Figures 5.24 and 5.25., this specific assumption causes upward movement of the overburden strata, like a rigid body, without any induced stresses and arching effect due to the absence of the effect of a non-injected lateral interval.

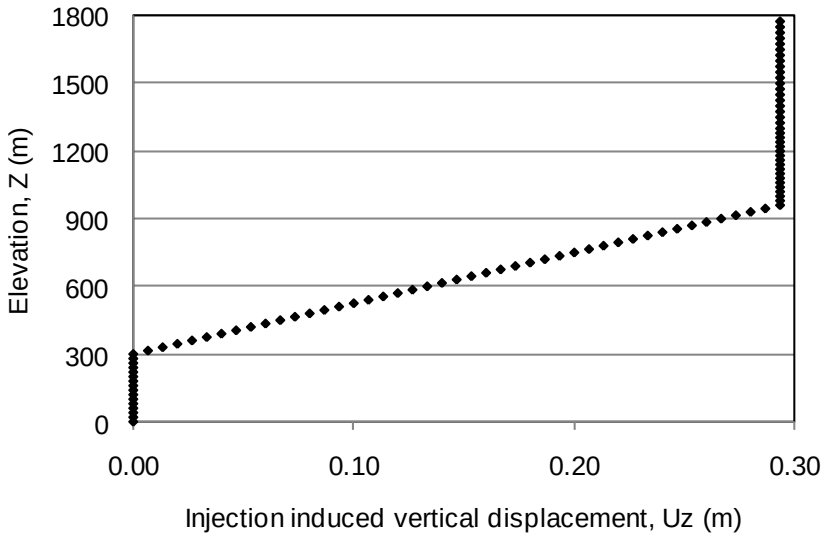

Figure 5.24 Injection induced vertical displacement U_z (m) along Profile II

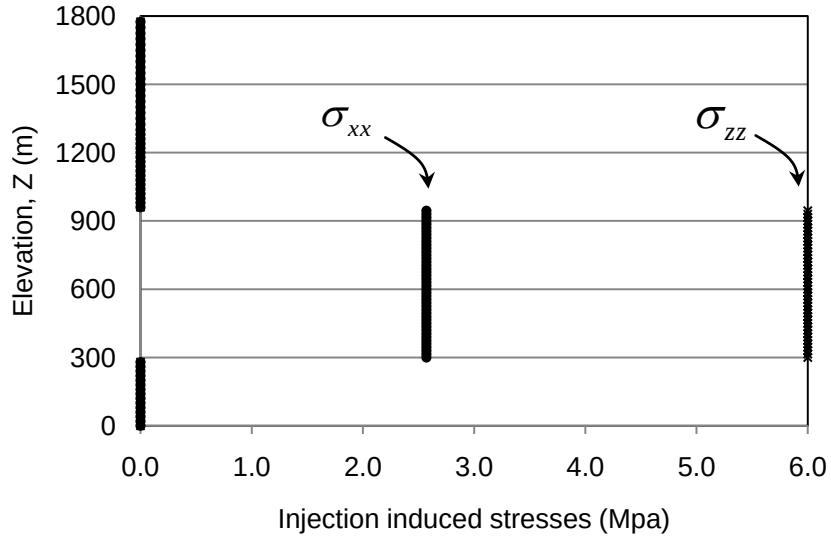

Figure 5.25 Injection induced vertical and horizontal stresses along Profile II

5.3.2 Elasto-plastic finite element analysis

In this section the finite element simulation of CO_2 injection into Formation X is carried out considering elasto-plastic behaviour for geomaterial. The benefits of this analysis is that it will indicate if a plastic zone will develop due to injection of CO_2 into the sandstone formation.

As described in Chapter 4, the input data for performing elasto-plastic analysis based on Mohr-Coulomb or Drucker-Prager yield criteria is elasticity properties (i.e. Young's modulus and Poisson's ratio) and strength properties (i.e. cohesion and internal friction angle). Table 5.1 presents the elasticity properties and strength properties of Formation X. The cohesion value should be determined too since it is one of the essential input data for these two yield criteria (see Section 4.2.2). However, the cohesion value is estimated from the *UCS* and internal friction angle parameters

As mentioned in Chapter 4 the Mohr-Coulomb criteria (in plasticity theory where tensile stress noted as positive) expresses that:

$$\tau = c - \sigma_n \tan\phi \tag{5.4}$$

With some mathematical manipulation the above equation can be expressed in principal maximum-minimum stress space ($\sigma_1 - \sigma_3$) as:

$$\left(\frac{\sigma_1}{\frac{2c\cos\phi}{1+\sin\phi}}\right)-\left(\frac{\sigma_3}{\frac{2c\cos\phi}{1-\sin\phi}}\right)=1 \tag{5.5}$$

or simply

$$\frac{\sigma_1}{\alpha}-\frac{\sigma_3}{\beta}=1 \tag{5.6}$$

This equation indicates that when $\sigma_3=0\rightarrow\sigma_1=\alpha=f_t'$ which is known as uni-axial tensile strength (or *UTS*) and when $\sigma_1=0\rightarrow\sigma_3=-\beta=-f_c'$ which is known as uni-axial compression strength (or *UCS*) of the material (see Figure 5.26).

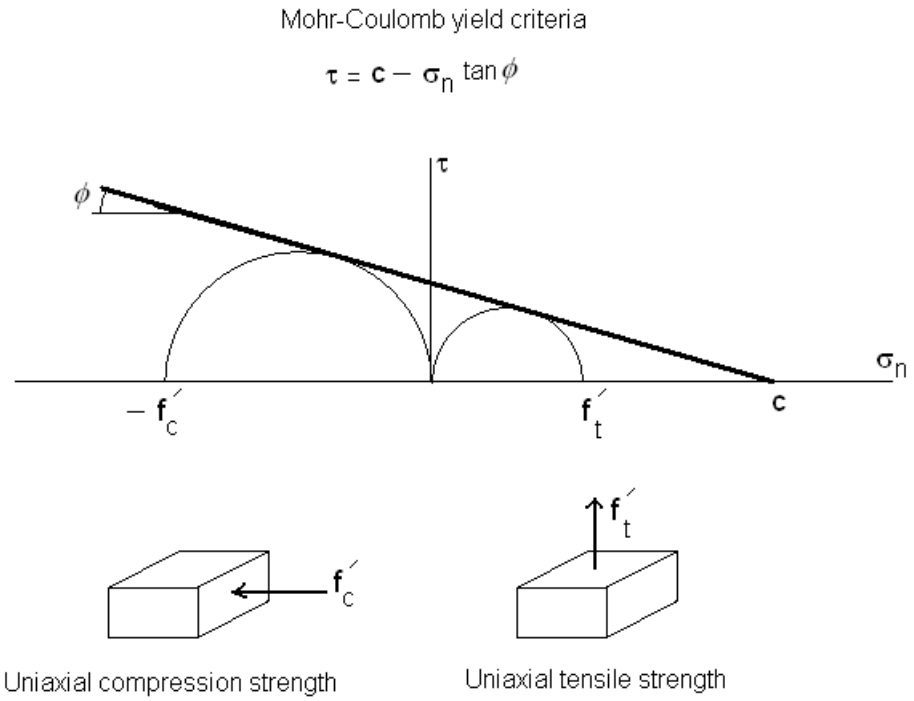

Figure 5.26 Mohr-Coulomb yield criteria in shear stress-normal stress ($\tau-\sigma_n$) space

Therefore based on equation 5.5 and the above discussion the relationship between cohesion, internal friction angle and *UCS* can be written as:

$$UCS=-\beta=-f_c'=\frac{2c\cos\phi}{1-\sin\phi} \tag{5.7}$$

or:

$$c=\left(\frac{1-\sin\phi}{2\cos\phi}\right)\times UCS \tag{5.8}$$

This equation was used to determine the cohesion value for the formation as shown in Table 5.1 based on the values of the internal friction angle and *UCS*.

The three-dimensional elasto-plastic finite element simulation of CO_2 injection into Formation X was performed using values in Table 5.1 corresponding to Formation X and attributed to entire model. The model geometry and the injected zone extension is similar to that of Figure 5.1 (i.e. from X=150 to X=250 m). The boundary conditions are also the same as before and the loading is due to the gravitational consolidation of the entire model and an injection of up to 6.0 MPa into the injected zone.

The result of elasto-plastic simulation demonstrates that no plastic or yielded zone is expected to develop due to an injection of up to 50% pore pressure (at initial pore pressure) into Formation X.

One of the major concerns in all engineering disciplines related to "Solid Mechanics" is the determination of the onset of yielding i.e. the condition that brings the structure to the edge of elastic and elasto-plastic deformation since any further progress in yielding causes permanent and irrecoverable deformation in part of the structure or finally overall functioning failure.

There are several factors contributing to the response of a specific structure in solid mechanics. They can be summarized to these factors: structure geometry contribution, structure materials contribution, boundary conditions and initial state contribution and loading contribution. In many cases, but not the majority of them, the contributions of the first three factors are fixed to some extent and loading is the major variable contributor in the response of the structure. As an instance, for injection problem into a potential porous formation the structure geometry (including depth and thickness of the formations especially the injection zone), material properties of the underground formations and boundary conditions as well as pre-existing stress regime, as initial state, are fixed and unchangeable to a great extent. However, the amount of injection pressure can be controlled and designed according to other characteristics of the site which is under study. This example shows that the magnitude of injection pressure corresponding to the onset of yielding inside the structure due to injection loading should be appropriately studied and determined. Therefore, in this part of the current research the amount of injection pressure were raised in successive 2.0 MPa steps in order to determine the corresponding injection pore pressure to the onset of yielding in this site. In a simple word, different models

having elasto-plastic behaviour with prescribed values of elasticity and strength properties, which determined previously in this Chapter, under different amount of injection pressures were built. The results of this sensitivity analysis demonstrated that CO_2 injection pressure up to approximately 18.0 MPa will not cause any yielding in the model and injection pressure of equal to 18.0 MPa corresponds to the onset of yielding phenomena in the model. The plastic zone corresponding to this onset of yielding is depicted in Figure 5.27.

The meaning of the "onset of yielding" needs to be discussed further here from computational point of view. The onset of yielding corresponds to the condition where the model shows the first signs of convergence issue during numerical analysis and it enters the iteration process in order to achieve the convergence seeking numerically for satisfaction of prescribed convergence criterion in the numerical procedures. It does not indicate the overall numerical instability of the model where convergence could not be achieved even after considerable number of iterations. The latter condition indicates the overall functioning issue of the model regarding the features of applied loads and other characteristics of numerical model which is under study. In terms of numerical treatment of the plasticity theory, the main source of initiation of iteration process in numerical procedures is the development of yielded or plastic zone in part of a model which causes the prevention of satisfaction of prescribed convergence criterion at the first iteration due to presence of remarkable unbalanced forces inside the structure. In the onset of yielding the model will converge numerically after some iteration because the plastic zone development has initiated locally in some part of the model but has not propagated in most part of the model. As described above, under this latter condition the model will not achieve the converged solution even after going through considerable number of iterations.

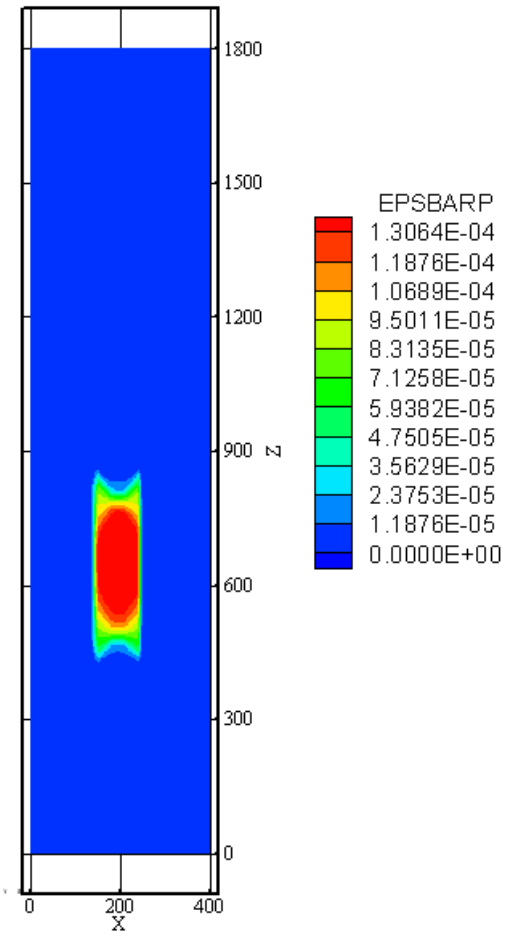

Figure 5.27 Equivalent plastic strain, $\overline{\varepsilon}_{plastic}$ indicating the developed plastic zone

The importance of cohesion

The amount of injection pressure of approximately equal to 18.0 MPa for the onset of yielding in this site seems to be very high and optimistic. The reason for this claim can become clearer considering the pre-existing amount of stress regime especially over the injected zone. Referring to Figure 5.16 the compressive horizontal stresses at the bottom and top of the injected interval are 14.12 MPa and 7.85 MPa, respectively. Let's focus on the upper parts of the injected interval near to the top of this formation where pre-existing horizontal stress is near to 8.0 MPa. Based on the results of the mentioned sensitivity analysis, the injection pressure of about 17.0 MPa as an instance will be considerably higher than the amount of pre-existing horizontal compressive stress at this level. This will develop a major tensile stress zone as we discussed comprehensively earlier that the injection reduces the amount of pre-existing compressive horizontal stress inside the injected zone.

The main reason of the absence of yielding phenomena even for such a remarkable high amount of injection pressure in comparison to the magnitude of pre-existing compressive stress regime especially for upper parts of the injected zone stems from the chosen procedure for the determination of cohesion value.

Let's consider again the corresponding equations of Mohr-Coulomb yield criterion in the maximum-minimum principal stress space (equations 5.5 and 5.6). Based on these equations, the contribution of cohesion as one of the two main strength parameters of the Mohr-Coulomb yield criterion is completely clear. But since there was no available data for this parameter, which governs the yield surface geometry in the three principal stresses space $(\sigma_1, \sigma_2, \sigma_3)$, an indirect procedure was chosen to determine its value based on two other estimated strength parameters *UCS* and internal friction angle which were determined according to log-based analysis results. For the mentioned potential injected formation, Formation X, the values of *UCS* and internal friction angle are 25.0 MPa and 25.0 degree, respectively. Based on the procedure described in the following part of equations 5.5 and 5.6, the value of cohesion estimated using equations 5.7 or 5.8 was equal to 7.96 MPa. According to equations 5.5 and 5.6, Mohr-Coulomb yield criterion governs intrinsically the ratio of *UCS* to *UTS* as follow:

$$\frac{UCS}{UTS} = \frac{1+\sin\phi}{1-\sin\phi} \tag{5.9}$$

In another word, based on this equation the amount of *UTS* is estimated to be 10.15 MPa, which corresponds to the ratio of equation 5.9 to be equal to 2.46: this is considering an internal friction angle of 25.0 degree. However, the most frequent reported value for this ratio for rocks and geomaterials is in the order of 10 (Harrison and Hudson, 2000) which gives the value of *UTS* of approximately equal to 2.5 Mpa in comparison to 10.15 MPa.

As per above discussion, here the cohesion was determined based on the value of *UTS* and internal friction angle according to the following equation obtained from equations 5.5 and 5.6 but this time with the contribution of *UTS* instead of *UCS*:

$$c = \left(\frac{1+\sin\phi}{2\cos\phi}\right) \times UTS \tag{5.10}$$

Based on this equation the value of cohesion is estimated to be equal to 1.96 MPa (in comparison to the earlier value of 7.96 MPa according to *UCS*-based calculations).

A similar sensitivity analysis was carried out this time with value of cohesion of equal to 1.96 MPa. The injection pressure corresponding to the onset of yield in the model determined approximately at 5.0 MPa (which is much less than the result of earlier sensitivity analysis, i.e. 18.0 MPa). The yielded zone corresponding to this onset of yielding in this new model according to the *UTS*-based calculated cohesion is depicted in Figure 5.28.

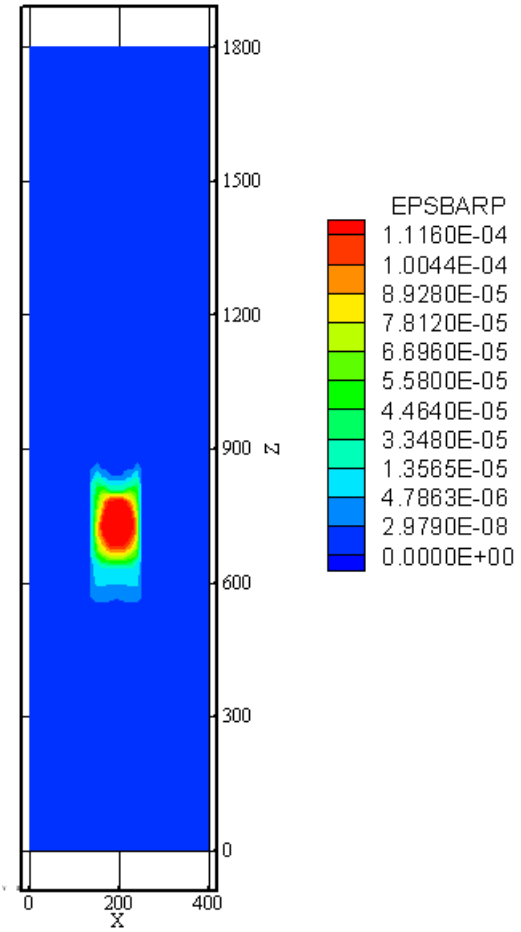

Figure 5.28 Equivalent plastic strain, $\overline{\varepsilon}_{plastic}$ indicating the developed plastic zone

Practical remarks

According to the aforementioned results obtained using elasto-plastic FE analysis the following points are highlighted:

- It is observed that the determination of the onset of yielding depends strongly on the chosen values for strength parameters of the geomaterials even in the same model with the same yield criterion.

- Elasto-plastic behaviour based on Mohr-Coulomb yield criterion, as one of the most well-known and frequently used yield criteria, is dependent considerably on the amount of cohesion. There are two different methods for approximating this value when the amount of *UTS*, *UCS* and internal friction angle are known for the formation: these are the *UCS*-based and the *UTS*-based approximation procedures. The former gives the upper bound and optimistic results whereas the latter gives the lower bound and pessimistic observation about yielding occurrence in the model. Both of these procedures are ***indirect*** methods and give upper bound and lower bound for cohesion values approximately.

- According to the vital influences of cohesion as well as internal friction angle, the laboratory-based analysis on core samples in order for ***direct*** determination of these two important and influential strength parameters are strongly recommended.

5.4 Summary

In this Chapter a case study was presented in order to investigate the induced stresses and displacements fields in a porous sandstone reservoir. The target sandstone formation is planned to be used for future CO_2 geologic sequestration.

The rock mechanical parameters of the target sandstone formation estimated using a log based analysis were used as input data in this chapter for both analytical as well as numerical models. It was assumed that this sandstone layer is a depleted reservoir and CO_2 injection increases the amount of pore pressure up to 50% of initial reservoir pressure at the centre of Formation X (i.e. approximately 12.0 MPa). In another word the injected pore pressure will increase up to 6.0 MPa in the injected zone.

The results of analytical model predicted the amount of uplift due to CO_2 injection up to 6.0 MPa into Formation X equal to 29.4 cm based on elastic geomechanical properties and thickness of the mentioned formation.

The results of numerical simulations indicated predicted a ground uplift of approximately 7.3 cm. This is much less than the value of 29.4 cm obtained using analytical model. The main reason for this discrepancy stems in one of the initial assumptions in the development of the analytical model. It is assumed that the porous reservoir as well as injected zone extends infinitely in horizontal directions, which is in contrast to the geometry of the injected zone considered in this finite element model. The result of elasto-plastic simulation showed that no plastic zone is expected to develop due to an injection of up to 50% pore pressure (at initial pore pressure) into Formation X. This indicates the feasibility of this formation as being a potential formation for CO_2 injection site.

6 Conclusions and recommendations

In this thesis a three-dimensional linear and non-linear finite element program was developed in order to study the effects of injection into porous reservoirs. The developed code includes several sub programs for pre-processing, main-processing (FEM) and post-processing.

In this Chapter the major conclusions made from this study and recommendations for future studies are highlighted.

6.1 Isotropic linear elastic finite element simulations

From linear elastic analysis based on the three dimensional finite element simulations of injection or production the following conclusions were drawn.

6.1.1 Simulation of injection into a horizontal porous zone

- The vertical and horizontal stresses resulted from gravitational consolidation are two principle stresses since the shear stress in this plane is negligible.
- Injection results in increasing the effective *vertical* stress inside the porous reservoir as well as decreasing the effective stress in immediate overburden and underburden considering tensile stresses as positive stresses.
- Injection results in increasing the effective *horizontal* stress inside the porous reservoir as well as decreasing effective stress in immediate sideburden.
- A remarkable shear stress zone near to injected zone shows that the vertical and horizontal stresses near this zone are no longer principle stresses or in another word, injection makes the principle stress direction to rotate around the injected zone.

- Injection induces a tensile vertical stresses inside the porous formation as well as its sideburden. It also induces compressive vertical stresses in immediate overburden and underburden.

- The injection induces a tensile horizontal stresses inside the porous formation as well as in immediate overburden and underburden and induces compressive stresses within the sideburden.

- Increasing the vertical compressive stresses in overburden could create a compaction zone above the injected horizon which has vital importance in collapse of casing.

- Decreasing the horizontal compressive stresses in overburden will decrease the shear strength and even activate the near vertical sliding surfaces since for this type of discontinuity the horizontal stresses act as normal stress.

- Shear stress zone development and rotation of principle directions near to injected zone can decrease the shear stability and even activate the inclined sliding surfaces.

6.1.2 Simulation of injection into a non-horizontal porous zone

The simulation results were presented for three structures subjected to gas injection. One horizontal layer with two anticline shape formations with different slopes was modelled to study the stress redistribution due to gas injection. The following results were obtained from various simulation analyses:

- In the case of the anticline structure with large slopes it was seen that the magnitude of the shear stress component (σ_{zx}) increases at the corners when the structure deviates from being horizontal. This result is expected due to stress concentration at sharp corners. However, the more important conclusion was the development of the shear stress zone at the flank area of the anticline structures.

- The latter result may be attributed to the curvature of the structure but not to stress concentration due to sharp corners.

- This conclusion suggests avoiding drilling wellbores at the flank areas in curved structures such as anticlines as the possibility of interbeds movement and

reactivation of any existing fracture plane is high due to large shear stresses applied in these zones.

6.1.3 Simulation of depletion induced stresses in a coal layer

As the final example, we simulated gas depletion from a coal layer in a Coalbed Methane (CBM) to investigate the subsequent changes in stress and deformations. The main results obtained are listed below:

- After gravitational consolidation it was seen that the ratio of horizontal to vertical stresses was increased within the coal seam due to a higher Poisson's ratio of the coal comparing to the surrounding rocks.

- In order to see the importance of subsidence due to depleting the coal layer, the reservoir pressure increased up to the initial reservoir pressure and then it was reduced in three unloading steps of 75, 50, and 25 % of the initial value. Due to the depletion of the reservoir, the subsidence occurred in overburden and especially at the ground surface.

- In order to highlight the effect of coal seam depletion the effect of gravitational consolidation was discarded and the result of downward movement in overburden was shown. The linear nature of subsidence, as was observed, is due to the linear elastic analysis used for this study.

- The other interesting point which is to be highlighted is the fact that the amount of depletion-induced downward movement is the same in entire overburden zone from above the coal seam to top of the model.

- The main reason for such a result is that in the model presented here the coal seam was assumed to have an infinite lateral extension: this resulted in no arching and sideburden effects and therefore the model behaved unidirectional in vertical direction, similar to the behaviour of a column of rock.

6.2 Elasto-plastic finite element simulations

Based on the elaso-plastic analysis which presented in Chapter 4 the following conclusions were made.

- Validation examples showed that the main finite element program could model successfully the Von Mises, Mohr-Coulomb and Dracker-Prager behaviour in three-dimensional finite element models.

- The elasto-plastic three-dimensional model of the injected reservoir indicated that with increasing the cohesion of the geomaterial, the plastic zone development decreases and vice versa.

- With cohesion values of less than a threshold (300 KPa for injected horizontal reservoir) the model could not converge, i.e. the model was unstable for these low cohesion values.

- The elasto-plastic analysis of the injected reservoir indicated the nucleation of tow plastic zones which increased in volume with decreasing the amount of cohesion of the geomaterial.

- For the lower value of cohesion these tow plastic zones intersected each other and developed a larger plastic zone which extended in overburden and underburden.

- From practical point of view the presence of plastic zone in overburden has a great importance on the caprock sealing integrity and drilling efforts in this area.

6.3 Case study results

In Chapter 5 a case was studied in order to investigate induced stresses and displacements fields in a porous sandstone reservoir referred to as Formation X.

The rock mechanical parameters of this formation, estimated using a log based analysis, were used as input data in Chapter 5 for both analytical as well as numerical models.

In addition, it was assumed that this sandstone layer is a depleted reservoir and CO_2 injection increases the amount of pore pressure up to 50% of initial reservoir pressure at the centre of Formation X (i.e. approximately 12.0 MPa). In another word the injected pore pressure will increase up to 6.0 MPa in the injected zone.

In order to study the effects and influences of CO_2 two main analyses were carried out in this research: analytical model analysis and three-dimensional finite element analysis. The main conclusions are listed below:

- With respect to horizontal stresses CO_2 injection developed a tensile stress zone inside the injected zone and induced tensile stress relaxation in sideburdens. However, it compressed immediate overburden and underburden rocks.

- With respect to horizontal stresses CO_2 injection developed a tensile stress zone inside the injected zone and induced tensile stress relaxation in overburden and underburden formations. However, it resulted in a compressive stress in the immediate sideburden rocks.

- Nucleation of remarkable shear stress near to injected zone showed that the vertical and horizontal stresses near this zone are no longer principle stresses, i.e. injection resulted in the principle stress direction to rotate around the injected zone.

- A large height for the injected zone (660 m along *Z* direction) comparing to its limited width (i.e. 100 m along X direction) resulted in a response similar to unidirectional behavior in horizontal direction at points near to the center of the injected zone.

- The finite element simulation results showed a ground uplift of approximately 7.3 cm. This is much less than the value of 29.4 cm obtained using analytical model. The main reason for this discrepancy was explained to be due to the assumption that in the analytical formulae the porous reservoir, as well as the injected zone, extends infinitely in horizontal directions which are in contrast to the geometry of the injected zone considered in this finite element model.

- The result of elasto-plastic simulation predicted that no plastic zone is expected to develop due to an injection of up to 50% pore pressure (at initial pore pressure) into Formation X.

6.4 Recommendation for future studies

As a continuation of this research study the following analyses would be recommended to understand further aspects of this research topic.

- Improve the current developed FE program by adding the ability for parallel programming in order to decrease the run time of the program or capability of modelling larger structures. This is particularly important when performing loops (or nested loops) as it would be faster in the case of multi core processing.

- Improve the current developed FE program by adding the constitutive models obtained based on critical state concept of plasticity theory and performing analysis with them.

- Improve the current developed FE program by adding constitutive models which has been newly developed for geomaterials and are capable of modelling both compaction and dilation such as Drucker-Prager cap plasticity model.

- Development of the current program towards modelling the visco-elastic and visco-plastic behaviour of the geomaterial since in many instances the geomaterial exhibits such behaviour like in salt beds or shales.

- Performing coupled analysis in conjunction with reservoir simulator results in order to investigate two-way analysis.

- Performing more real case studies and compare the simulation results versus real field data.

References

Abdulraheem A., Zaman M., Roegiers J. C. (1994); A Finite-Element Model for Ekofisk Field Subsidence. Journal of Petroleum Science and Engineering 10 , pp. 299-310

Bathe K.-J. (1996); Finite Element Procedure. Prentice-Hall, Inc., New Jersey.

Baud P., Meredith C. (1997); Damage Accumulation During Triaxial Creep of Darley Dale Sandstone from Pore Volumetry and Acoustic Emission. Int. J. Rock Mech. & Min. Sci. Vol. 34, No. 3-4,

Becker A.A., (1992); The Boundary Element Method in Engineering: A complete course. McGraw-Hill International (UK) Limited.

Besson J., Cailletaud G., Chaboche J.L., Forest S. (2010); Non-linear Mechanics of Materials. Springer Science+Business Media B. V. 2010

Chan A. (2004); Production-Induced Reservoir Compaction, Permeability Loss and Land Subsidence, PhD Dissertation, Stanford Univesity

*Chang C.,Moos D., Zoback M.D.(*1997); Anelasticity and Dispersion in Dry Unconsolidated Sands. Int. J. Rock Mech. Min. Sci., 34,paper no. 48.

Chang C., Zoback M. (1998); Viscous Rheology and State of Stress in Unconsolidated Sands. The 1998 SPE/ISRM Eurock '98', Trondheim, Norway, 8-10 July 1998, pp. 465-473.

Chang C., Zoback M. (2008); Creep in Unconsolidated Shale and its Implication on Rock Physical Properties. The 42nd US Rock Mechanics Symposium and 2nd U.S.-Canada Rock Mechanics Symposium, San Francisco, June 29- July 2, 2008.

Chang C., Zoback M. (2009); Viscous Creep in Room-dried Unconsolidated Gulf of Mexico Shale (I): Experimental Results. Journal of Petroleum Science and Engineering 69, pp. 239–246

Chang C., Zoback M. (2010); Viscous Creep in Room-dried Unconsolidated Gulf of Mexico Shale (II): Development of a Viscoplasticity Model. Journal of Petroleum Science and Engineering xxx (2010) xxx–xxx

Chase C.A., Dietrich J.K. (1989); Compaction Within the South Belridge Diatomite. SPE REservoir Engineering, November 1989, pp. 422-428.

Chin L.Y., Boade R.R., Nagel N.B., Landa G.H. (1994); Numerical Simulation of Ekofisk Reservoir Compaction and Subsidence: Treating the Mechanical Behavior of the Overburden and Reservoir. SPE/ISRM Rock Mechanics in Petroleum Engineering Conference, Delft, The Netherlands, 29-31 August 1994, pp. 787-794.

Coelho L., Soares A., Ebecken N., Alves J., Landau L. (2006); Modelling mechanical behaviour of limestone under reservoir conditions. International Journal for Numerical and Analytical Methods in Geomechanics, 30, pp. 1477-1500

Collin F., Cui Y., Schroeder Ch., Charlier R. (2002); Mechanical behaviour of Lixhe chalk partly saturated by oil and water : experiment and modeling. International Journal for Numerical and Analytical Methods in Geomechanics, 26, pp. 897-924.

Cormeau I., (1975); Numerical Stability in Quasi-Static Elasto/Viscoplasticity. International Journal for Numerical Methods in Engineering, 9, pp. 109-127.

Coulomb, C. A. (1776); Essai sur une application des regles des maximis et minimis a quelquels problemesde statique relatifs, a la architecture. Mem. Acad. Roy. Div. Sav., vol. 7, pp. 343–387.

Cristescu N. (1989); Rock Rheology. Kluwer Academic Publisher. printed in Netherlands.

Cristescu N. (1994); A Procedure to Determine Nonassociated Constitutive Equations for Geomaterials. International Journal of Plasticity, 10, no. 2, pp. 103-131

Cyr N.A., Teter R.D. (1973); Finite Element Elastic-Plastic-Creep Analysis of Two-Dimensional Continuum with Temperature Dependent Material Properties. Computers & Structures, 3, pp. 849-863.

David C., Le Ravalec-Dupin M. (2007);Rock Physics and Geomechanics in the Study of Reservoirs and Repositories. Geological Society, London, Special Publications. Vol. 284; pp. 1-14

Davidson, M. (2009); Underground gas storage project at Welton oilfield, Lincolnshire: Local perspectives and responses to planning, environmental and community safety issues. In: Evans, D.J. and Chadwick, R.A. (eds), Underground Gas Storage: Worldwide Experiences and Future Development in the UK and Europe. Geological Society, London, Special Publications, 313, 149–62.

Dreyer W. (1973); The Science of Rock Mechanics, Part 1. Trans. Tech. Pub., Clausthal-Zellerfeld.

Dudley J.W., Myers M.T., Shew R.D., Arasteh M.M. (1998); Measuring Compaction and Compressibilities in Unconsolidated Reservoir Materials by Time-Scaling Creep. SPE Reservoir Evaluation & Engineering, October 1998, pp. 430-437

Eiksund G., Svano G., Nagel N.B. (1995); Creep related subsidence caused by oil and gas extraction. Land Subsidence (Proceedings of the Fifth International Symposium on Land Subsidence, The Hague, October 1995.

Evans, D.J. (2009); A review of underground fuel storage events and putting risk into perspective with other areas of the energy supply chain. In: Evans, D.J. and Chadwick, R.A. (eds), Underground Gas Storage: Worldwide Experiences and Future Development in the UK and Europe. Geological Society, London, Special Publications, 313, 173–216.

Fjaer J, Holt RM, Horsrud P, Raaen AM, Risenes R. (2008); Petroleum Related Rock Mechanics 2nd Edition. Developments in petroleum science 53.

Fossum, A.F. and Fredrich, J.T. (2000); Cap Plasticity Models and Dilatant and Compactive Pre-Failure Deformation. Proc. 4th North American Rock Mechanics Symp., 1169-1176, Seattle, WA, July 31-August 3, A.A. Balkema, Rotterdam.

Frantziskonis G. N., Abdulraheem A. (1992); Mechanics o f Reservoir Rocks, Theory and Verification. Society of Petroleum Engineers, paper no. 24474, pp. 50

Fredrich J.T., Deitrick G.L., Arguello J G., de Rouffignac E.P. (2000); Geomechanical Modeling of Reservoir Compaction, Surface Subsidence, and Casing Damage at the Belridge Diatomite Field. SPE Res. Eval. & Eng., 3, 348-359.

Fredrich J. T., Fossum A. F. (2002); Large-Scale Three-Dimensional Geomechanical Modeling of Reservoirs: Examples from California and the Deepwater Gulf of Mexico. Oil & Gas Science and Technology – Rev. IFP, 57, no. 5, pp. 423-441

Hagin P.N. (2003); Application of Viscoplelastic, Viscoplastic, and Rate-and-State friction Constitutive Laws to the Deformation of Unconsolidated Sands. PhD Dissertation, Stanford University.

Hagin P.N., Zoback M.D. (2007); Predicting and Monitoring Long-term Compaction in Unconsolidated Reservoir Sands Using a Dual Power Law Model. Geophysics, 72, no. 5, pp. E165–E173.

Hamilton J. M., Shafer J. L. (1991); Measurement of Pore Compressibility Characteristics in Rock Exhibiting "Pore Collapse" and Volumetric Creep. SCA Conference, Paper Number 9124.

Hansen K.S., Prats M., Chan C.K. (1995); Modeling of Reservoir Compaction and Surface Subsidence at South Belridge. SPE Production & Facilities, August 1995, pp. 134-143

Harrison, J. and Hudson (2000); Engineering rock mechanics:part 2-Illustrative worked examples, Pergamon Press, 506 p

Havard, J. and French, R. (2009); The importance of gas storage to the UK: The DECC perspective. In: Evans, D.J. and Chadwick, R.A. (eds), Underground Gas Storage: Worldwide Experiences and Future Development in the UK and Europe. Geological Society, London, Special Publications, 313, 13–16.

He W., Hajash A., Sparks D. (2002); A model for porosity evolution during creep compaction of sandstones. Earth and Planetary Science Letters,197, 237-244

Hettema M.H.H., Schutjens P. M.T.M., Verboom B.J.M., Gussinklo H.J. (1998); Production-Induced Compaction of Sandstone Reservoirs: The Strong Influence of Field Stress. The 1998 SPE/ISRM Eurock '98', Trondheim, Norway, 8-10 July 1998, pp.547-554

Hettema M.H.H., Schutjens P. M.T.M., Verboom B.J.M., Gussinklo H.J. (2000); Production-Induced Compaction of a Sandstone Reservoir: The Strong Influence of Stress Path. SPE Reservoir Evaluation. & Engineering, 3 (4), August 2000, pp. 342-347

Hill R. (1950); The Mathematical Theory of Plasticity. Clarendon Press, Oxford.

Holland, J.R. and Applegate, J.K., (2008); Recent Coalbed Methane Exploration in The Galilee Basin, Queensland, Australia. 2008 International Coalbed and Shale Gas Symposium, Tuscaloosa, Alabama, 19–23 May, #0807.

Hughes T.J.R., Taylor R.L. (1978); Unconditionally Stable Algorithms for Quasi-Static Elasto/Visco-Plastic Finite Element Analysis. Computers & Structures, 8, pp. 169-173.

Hunsche, Hample (1999); Rock salt — the mechanical properties of the host rock material for a radioactive waste repository, Engineering Geology 52, pp. 271–291.

Itasca Consulting Group (2000); Fast Lagrangian Analysis of Continua (FLAC) User's Guide - Version 4.0. Itasca Consulting Group, Inc. Minneapolis, Minnesota 55415 USA

Johnson J.P., Rhett D.W., Siemers W.T. (1988); Rock Mechanics of the Ekofisk Reservoir in the Evaluation of Subsidence. The 20th Annual Offshore Technology Conference, Houston, Texas, May 2-5, 1988., pp. 39-50

Kanchi M.B., Zienkiewicz O.C., Owen D.R.J. (1978); The Visco-Plastic Approach to Problems of Plasticity and Creep Involving Geometric Non-Linear Effects. International Journal for Numerical Methods in Engineering, 12, pp. 169-181.

Landau L.D., Lufshitz E.M. (1970); Theory of Elasticity. Second Edition, Pergamon Press.

Langer (1979); Reological behavior of rock masses, Proc. 4th Int. Congr. on Rock Mechanics, Balkema, Rotterdam, 13, pp. 29-62.

Lewis R.W., Schrefler B.A. (1998); The Finite Element Method in the Static and Dynamic Deformation and Consolidation of Porous Media, Second Edition. Wiley, New York.

Longuemare P., Mainguy M., Lemonnier P., Onaisi P., Gérard C., Koutsabeloulis N. (2002); Geomechanics in Reservoir Simulation:Overview of Coupling Methods and Field Case Study. Oil & Gas Science and Technology – Rev. IFP, 57 , no. 5, pp. 471-483

Minkoff S.E., Stone C.M., Bryant J., Peszynska M., Wheeler M. (2003); Coupled Fluid Flow and Geomechanical Deformation Modeling. Journal of Petroleum Science and Engineering, 38, pp. 37– 56

Minkoff S. E., Stone C. S., Bryant S., Peszynska M. (2004); Coupled Geomechanics and Flow Simulation for Time-Lapse Seismic Modeling. Geophysics, 69, no. 1 , pp. 200–211

Neto E., Peric D., Owen D.R.J. (2008);Computational Methods for Plasticity: Theory and Applications. John Wiley & Sons Ltd

Obert L., Duval W. (1967); Rock MEchanics and The Design of Structure in Rock. J. Wiley & Sons, Inc. USA

Owen D.R.J., Hinton E. (1980); Finite Elements in Plasticity: Theory and Practice. Swansea: Pineridge Press.

Pande G.N., Owen D.R.J., Zienkiewicz O.C. (1977); Overlay Models in Time-Dependent Non-linear Material Analysis. Computers & Structures, 7, pp. 435-443.

Perzyna P. (1966). Fundamental Problems in Viscoplasticity. Advances in Applied Mechanics, vol. 9. New York: Academic Press. pp. 243–377

Pettersen (2008) ; Using relations between stress and fluid pressure for improved compaction modelling in flow simulation and increased efficiency in coupled rock mechanics simulation. Petroleum Geoscience, Vol. 14, pp. 399-409

Plaat, H. (2009); Underground gas storage—why and how. In: Evans, D.J. and Chadwick, R.A. (eds), Underground Gas Storage: Worldwide Experiences and Future Development in the UK and Europe. Geological Society, London, Special Publications, 313, 25–37.

Prager W. (1955); The Theory of Plasticity- A Survey of Recent Achievements. Proceeding of Institute Mechanical Engineering, London, 3-19.

Rhett D.W. (1998); Ekofisk Revisited: A New Model of Ekofisk Reservoir Geomechanical Behavior. The 1998 SPE/ISRM Eurock '98', Trondheim, Norway, 8-10 July 1998, pp. 367-375.

Rice J.R. (1975); On the Stability of Dilatant Hardening for Saturated Rock Masses. J. Geophysics. Res., 80, no. 11, 1531-1537.

Ruddy I., Andersen M.A., Pattillo P.D., Bishlwal M., Foged N. (1988); Rock Compressibility, Compaction, and Subsidence in a High-Porosity Chalk Reservoir: A Case Study of Valhall Field. The 1988 SPE Annual Technical Conference and Exhibition, Houston, October 2-5 1988

Sadd M.H. (2005); Elasticity: Theory, Applications, and Numerics. Elsevier Inc., Butterworth-Heinemann, USA

Salencon, J. (1969); Contraction Quasi-Statique D'une Cavité a Symétrie Sphérique Ou Cylindrique Dans Un Milieu Elastoplastique, Annales Des Ponts Et Chaussées, 4, 231-236.

Schofield A., Wroth P. (1968); Critical State Solid Mechanics. McGraw-Hill, London, UK.

Schutjens P. M.T.M., Blanton T.L., Martin J.W. , Lehr B.C., Baaijens M.N. (1998); Depletion-induced compaction of an overpressured reservoir sandstone: An experimental approach. The SPE/lSRM Euro '98', Tronheim, Norway, 8-10 July 1998, pp. 53-61

Senseny, Hansen, Russell, Carter, and Handin (1992); Mechanical behavior of rock salt: Phenomenology and Micromechanisms", Int. J. Rock Mech. Min. Sci. & Geomech. Abstr., 29, 4, pp 363-378.

Settari A., Mourits F.M. (1998); A Coupled Reservoir and Geomechanical Simulation System. SPE Journal, 219-226.

Settari A, Walters D.A. (2001); Advances in Coupled Geomechanical and Reservoir Modeling with Applications to Reservoir Compaction. Society of Petroleum Engineers Journal, pp. 334-342

Settari A., Sen V. (2008); Geomechanics in Integrated Reservoir Modeling. 2008 Offshore Technology Conference, Houston, Texas, USA, 5–8 May 2008

Smlts R.M., Waal J.A. (1988); A Comparison Between the Pressure-Lag Model and the Rate-Type Model for the Prediction of Reservoir Compaction and Surface Subsidence. SPE Formation Evaluation, June 1988, pp. 357-363.

Teatinia P., Gambolatia G., Ferronatoa M., Settari A. T., Walters D. (2011); Land uplift due to subsurface fluid injection. Journal of Geodynamics 51, pp. 1–16

Vogler & Blum (1990); Micromechanical modeling of creep in terms of the composite model, Proc. 4th Int. Conf. on creep and fracture of engineering materials and structures, London, pp. 65-19.

Waal J.A., Smlts R.M. (1988); Prediction of Reservoir Compaction and Surface Subsidence: Field Application of a New Model. SPE Formulation Evaluation, June 1988, pp. 347-356.

Weaver W., Johnston P. (1984); Finite elemenet for structural analysis. Prentice-Hall, INC, Englewood Cliffs, New Jersey

Xie S. Y., Shao J. F. (2006); Elastoplastic Deformation of a Porous Rock and Water Interaction. International Journal of Plasticity 22, pp. 2195–2225

Yale D.P. (2002); Coupled Geomechanical-Fluid Flow Modeling: Effects of Plasticity and Permeability Alteration. The SPE/ISRM Rock MEchanics Conference, Irvin, Texas, 20-23 October 2002.

Yin, S., Dusseault M., Rothenburg, L. (2007); Coupled multiphase poroelastic analysis of reservoir depletion including surrounding strata. Int. J. of Rock Mechanics& Mining Science, **44**, 758-766

Yu H.-S., (2006); Plasticity and Geotechnics. Springer Science+Business Medi, LLC, USA

Ziegler H. (1959); A Modification of Prager's Hardening Rule. Quaterley Applied Mathematics, 17, 55.

Zienkiewicz, O.C. (1982); Basic formulation of static and dynamic behaviours of soil and other porous media. Applied Mathematics and Mechanics, 3 (4), 457–68.

Zienkiewicz O.C., Cormeau I.C. (1974); Visco-plasticity – Plasticity and Creep in Elastic Solids - A Unified Numerical Solution Approach. International Journal of Numerical Methods in Engineering, 8, 821–845.

Zienkiewicz, O.C and Shiomi, T. (1984); Dynamic behavior of saturated porous media: the generalized Biot formulation and its numerical solution. International Journal of Numererical and Analystical Methods in Geomechanics, 8, 71–96.

Zienkiewicz O.C., Taylor R.L. (2000); The Finite Element Method. Volume I: The Basis. 5th edn. Butterworth–Heinemann.